ERDC/CERL CR-18-2

US Army Corps
of Engineers®
Engineer Research and
Development Center

ERDC
INNOVATIVE SOLUTIONS
for a safer, better world

Measurement of Blast Waveforms with Condenser Microphones

Measurement Interpretation and Correction

Thomas B. Gabrielson

July 2018

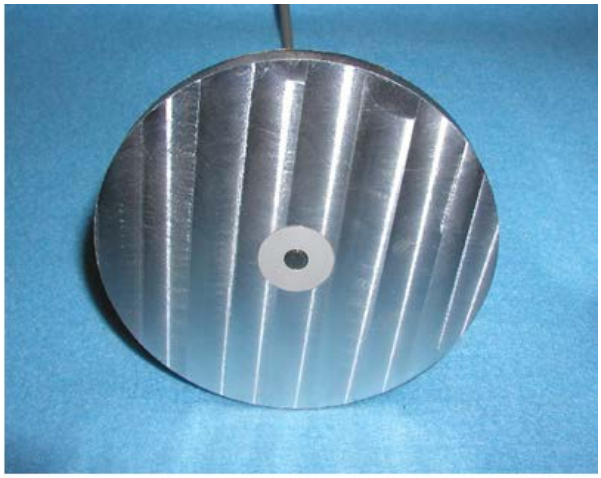

Construction Engineering
Research Laboratory

The U.S. Army Engineer Research and Development Center (ERDC) solves the nation's toughest engineering and environmental challenges. ERDC develops innovative solutions in civil and military engineering, geospatial sciences, water resources, and environmental sciences for the Army, the Department of Defense, civilian agencies, and our nation's public good. Find out more at www.erdc.usace.army.mil.

To search for other technical reports published by ERDC, visit the ERDC online library at http://acwc.sdp.sirsi.net/client/default.

ERDC/CERL CR-18-2
July 2018

Measurement of Blast Waveforms with Condenser Microphones

Measurement Interpretation and Correction

Thomas B. Gabrielson

The Pennsylvania State University
Graduate Program in Acoustics
Applied Research Laboratory
PO Box 30
North Atherton St.
State College, PA 16804

Final Report

Prepared for U.S. Army Public Health Command
Aberdeen Proving Ground, MD 21012-5403

Under Physics Models Environmental Quality Technology Program,
Project 622720D048

Abstract

This work evaluated the accuracy of blast-wave measurements using commercial measurement-grade condenser microphones. The principal advantages of measurement microphones are their ease of calibration and wide acceptance as measurement standards in acoustics. A number of special techniques are discussed for improving the results obtained with these microphones. Of particular importance are: (1) the desired resolutions for the measured parameters (peak pressure, rise time, time to zero-crossing, peak under-pressure); (2) the sensors and data-acquisition equipment used; (3) post-measurement corrections and digital correction filters; and, (4) laboratory evaluation compared to field measurements.

Executive Summary

This work considers the accuracy of blast-wave measurements using commercial measurement-grade condenser microphones. The principal advantages of measurement microphones are their ease of calibration and wide acceptance as measurement standards in acoustics. While selection and use of these microphones might seem simple, a number of special techniques are available for improving the data obtained with such systems. Of particular importance are:

- the desired resolutions for the measured parameters (peak pressure, rise time, time to zero-crossing, peak under-pressure)
- the sensors and data-acquisition equipment used
- post-measurement corrections and digital correction filters
- laboratory evaluation compared to field measurements.

Measurements of blast waves are demanding. Accurate waveform measurement for a standard (0.57 kg) C4 explosion at 50 m may require a sensor and data acquisition system with a bandwidth from 1 Hz to 1 MHz and a peak-pressure capability of 2000 Pa or more. Commercially available measurement microphones and the associated amplifiers can accommodate peak pressures of 2000 Pa or more, but are bandwidth limited to from several hertz to somewhat over 100 kHz. With correction filters, these measurements can be extended to below 1 Hz on the low-frequency end. The fastest rise time achievable with off-the-shelf measurement-microphone hardware is 3 microseconds, and that response can only be obtained with care in the measurement setup, acquisition, and post-processing. The actual shock-front rise time may be a microsecond or less depending on peak pressure and atmospheric turbulence.

Figure ES-1 shows a typical blast-wave measurement. The issues that have the most influence on the design of a data-acquisition system are: (1) the expected peak pressure, and (2) the required rise-time resolution. A clean record of the rise and initial decay can often be captured, but subsequent features may be obscured by the ground-reflected path, secondary reflections, or reverberation. Consequently, estimation of the time to zero-crossing or the peak under-pressure may be difficult. If these featured are important, the early portion of the waveform can be fit with an analytical function and the latter portion of the analytical function used to estimate the zero-crossing or the characteristics of the negative phase.

Figure ES-1. Typical measured pressure waveform from an explosion of 1.25 lb (0.57 kg; a "full stick") of C4 at 50 m. The measured pressure is the irregular blue curve. The smooth black curve is an analytical function, which, when replicated and delayed to simulate the ground reflection, produces the dotted red curve. Critical points are: (A) peak pressure, (B) rise time, (C) time to zero-crossing, and (D)) peak negative pressure. The area under the curve from the leading edge to the zero-crossing (A to C) is the "positive impulse"; the area under the curve from the zero-crossing and beyond is the "negative impulse."

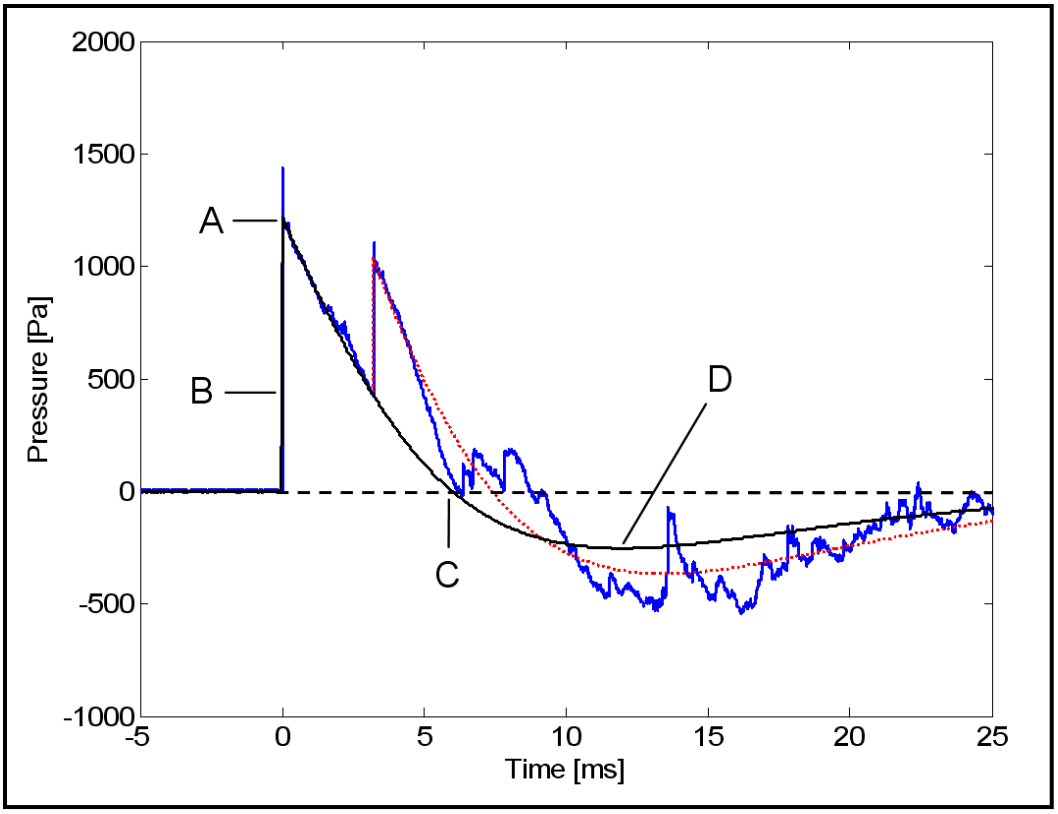

Desired parameter resolution

Peak pressure

If the expected peak pressures are below 2000 Pa, it is likely that ¼-in. or ⅛-in. measurement microphones can be used without significant distortion. The commonly cited "3 percent distortion" pressure is not a reliable metric for determining limiting pressures for blast-wave measurement; noticeable distortion may occur for peak pressures of half the 3 percent equivalent pressure.

Rise time

If the pressure rise time of the initial shock is not expected to be faster than 20 microseconds, use of standard measurement microphones is straightforward. With special techniques, measurement to 3 microseconds

are practical. Below 3 microseconds, the bandwidth of even the fastest measurement microphone is insufficient so a special wideband microphone would be required. As a rule of thumb, the rise time in microseconds based on absorption losses is no less than $200/P_{shock}$, where P_{shock} is the peak pressure of the shock in pascals. Atmospheric turbulence may slow the pressure rise considerably; however, at a distance of 50 m for C4 explosions (P_{shock} of the order of 1000 Pa), the rise times are typically less than 3 microseconds.

Time to zero-crossing

In practice, measurement of the time to zero-crossing is difficult because of interfering ground reflections. Fitting the measurement with a model pulse (with direct and ground reflection components) may be useful for estimating this value. Here, the low-frequency response of the measurement system is important. Fortunately, there are procedures for correcting inadequate low-frequency response. Recovery of the low-frequency components of the signature is simpler than overcoming bandwidth limitations for rise-time estimation.

Peak under-pressure

As with the time to zero-crossing, estimation of the peak under-pressure is difficult in the presence of ground reverberation and reflection and the low-frequency response of the measurement system is important. As with the time to zero-crossing, fitting with a model function may lead to consistent estimates for peak negative pressure. (See Figure ES-2.)

Example systems

The most suitable commercial measurement microphones* are the ⅛-in. pressure microphone (B&K 4138; GRAS 40DP), the ¼-in. free-field microphone (B&K 4135; GRAS 40BF), and the ¼-in. pressure microphone (B&K 4938; GRAS 40BP). The so-called “free-field” microphones are often advocated, but there are advantages to using “pressure” microphones for these measurements. For example, the commercial measurement microphone with the widest available bandwidth, the ⅛-in. microphone, is not available as a free-field microphone.

* Throughout this report, specific products are mentioned. This does not constitute an endorsement of those products; other manufacturers may have equivalent products available.

Figure ES-2. Application of correction filters to a blast waveform (0.57 kg of C4 at 50 m) recorded with a ¼-in. pressure microphone pointed directly at the blast. The raw recorded waveform is the blue curve (sampled at 200,000 samples per second) . The black curve is the result of applying the Butterworth transient-correction filter; the positive peak that remains is the result of microphone diffraction. The red curve is the result of applying the diffraction-correction filter. The red curve shows the step-like change in pressure characteristic of the leading edge of a shock wave.

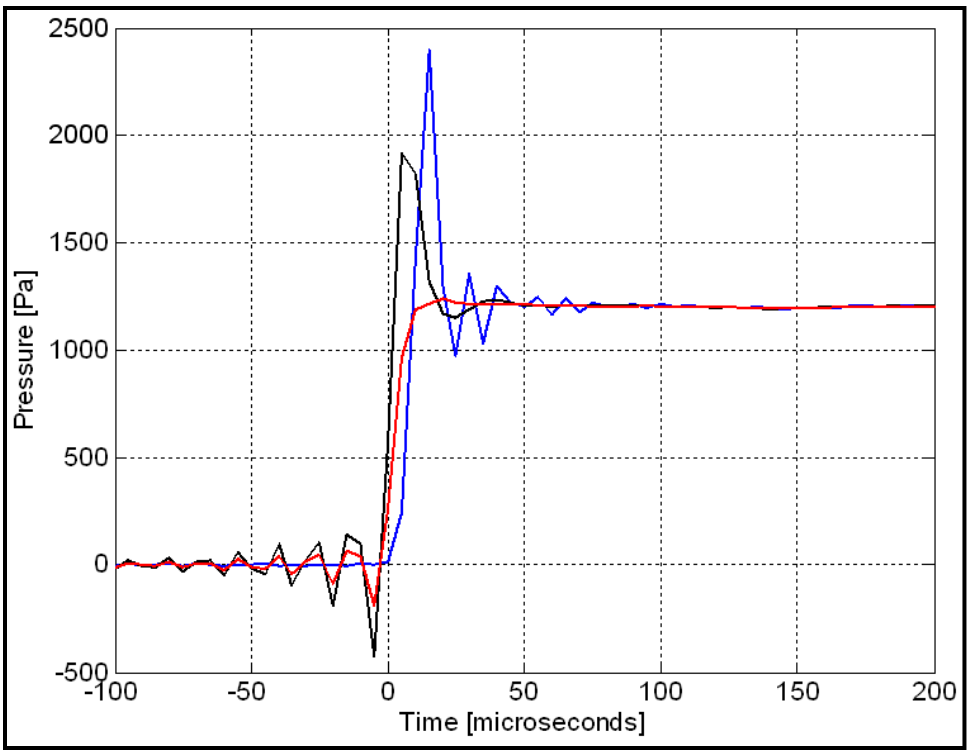

Microphone orientation

Orientation of the microphone with respect to the incoming shock front has a strong effect on the time-domain response. This orientation is described by the angle of the microphone axis with respect to the direction of shock propagation. In the zero-degree orientation, the microphone is pointed directly at the explosion; in the 90-degree orientation, the microphone axis is perpendicular to the direction of arrival of the wave front. In practice, there are three useful configurations:

- Free-field microphone at zero degrees (¼-in. only); potential rise-time resolution of 8 μs.
- Pressure microphone at 90 degrees (¼- or ⅛-in.); potential rise-time resolution of 5 μs for the ⅛-in. microphone and 10 μs for the ¼-in. mi-

crophone. Note that this orientation is the same as for the sense element in a blast pencil*; however, the ½-in. element of the blast pencil limits the rise-time resolution to no better than 26 μs. (The blast pencil's utility is its far higher peak pressure range.)

- Pressure microphone at zero degrees with diffraction correction (¼- or ⅛-in.); potential rise-time resolution of 3 μs for the ⅛-in. microphone and 8 μs for the ¼-in. microphone.

A fourth variation is the "baffled" microphone. Baffle is a term used in acoustics to describe an acoustically rigid wall in which a sensor is flush mounted. The diffraction correction mentioned for the pressure microphone at zero degrees is necessary because of interference between the direct wave incident on the microphone and the wave that is scattered by the edge of the microphone element. Inserting a microphone into a flat plate delays this edge-scattered wave. Until the time of arrival of the edge-diffracted wave, the pressure on the sensor face is twice the free-field pressure.† A sufficiently large baffle would eliminate the requirement for either a free-field microphone or for diffraction correction. For a 10-cm (4-in.) diameter, circular baffle plate, the edge-diffracted wave arrives about 150 μs after the direct wave. For C4 explosions, this is not far beyond the leading edge of the pressure waveform. To achieve clean reproduction for 10 ms, the baffle edges would have to be more than 3 m away from the sensor. This would rarely be practical; however, if only peak pressure and rise time are important a small baffle can be used to eliminate the need for diffraction correction.

Data acquisition

The bandwidth of preamplifiers and conditioning electronics and the sampling rate also determine the achievable performance particularly for determination of the rise time. Example systems include:

- Instrumentation recorders with standard "high" rate sampling – 192 or 200 kilosamples per second (kS/s). Potential rise-time resolution of 5-10 microseconds. Recommendation: turn off the internal anti-aliasing

* The *body* of the blast pencil is pointed toward the explosion; however, the sense element is flush mounted in the side of the body.

† i.e., twice the pressure in the limit of linear acoustics.

filter* and substitute an external analog Bessel filter to minimize peak-pressure estimation errors. At these sample rates, the data acquisition system limits the rise time resolution so a ⅛-in. microphone at 90 degrees (with the protection grid left in place) would be an effective sensor choice.

- Digitizing oscilloscopes with sample rates of at least 500 kS/s. Rise-time resolution is then limited by microphone response and signal-conditioning electronics. With the extended-band option for the B&K NEXUS conditioning amplifier and the B&K 4138 (or equivalent) ⅛-in. microphone, potential rise-time resolution is 3 microseconds. Note that, for peak pressure and rise time measurement, the stored record length need only be a fraction of a millisecond; for characterization of the overall pulse shape, the minimum record length would be 20 ms (10,000 samples at 500 kS/s) for charge weights up to a kilogram of C4. For these higher sampling rates, the ideal microphone assembly may be a ⅛-in. microphone in a small baffle at zero degrees augmented by a separate ⅛-in. unbaffled microphone at 90 degrees. The baffled microphone would give good resolution of the rise phase (down to 4 or 5 microseconds) and peak pressure while the unbaffled microphone would record subsequent features accurately. Alternately, a ⅛-in. unbaffled microphone at zero degrees with subsequent diffraction correction would be suitable (although the protection grid would have to be removed either with or without the baffle in the zero degrees orientation).
- High-resolution ("24-bit") instrumentation recorders with a sampling rate of 96 kS/s. The extra amplitude resolution† may be useful in circumstances in which the expected peak pressure is not known and adjustments to the levels cannot be made once the measurements are started. At this sample rate, the minimum rise-time resolution would be roughly 20 microseconds so either a ⅛- or ¼-in. microphone at 9 zero degrees would be suitable with the ¼-in. microphone being the less expensive option.

* In a system that uses a sigma-delta analog-to-digital converter, it is usually not possible to turn off the critical anti-aliasing filter since that filter is built in to the sigma-delta processing algorithm. The first stage analog filter in front of a sigma-delta converter has little effect on the transient performance of the sigma-delta system.

† Keep in mind that the true resolution may be significantly less than that implied by the "label" for the digitizer. At 96 kS/s, most "24-bit" digitizers generate results with 16 bits (or less) effective resolution. At high sample rates, the lower-order bits are uncorrelated noise.

Corrections and correction filters

Response limitations and measurement artifacts can be minimized by proper selection and orientation of sensors; however, post-measurement correction filters can be used either to extend further the useful range of a measurement or to remove artifacts:

- A microphone in the zero degree orientation, in which the shock front strikes the diaphragm head-on, produces a significant change in the acoustic field by its presence. This is often called "microphone diffraction." A free-field microphone is internally over-damped to compensate, but the effect on a pressure microphone is straightforward to model and an effective digital diffraction-correction filter can be applied in software to make the output of a pressure microphone equivalent to a free-field measurement.
- The most common variety of anti-aliasing filter used in commercial data-acquisition systems* is the Butterworth low-pass filter. This filter has a fast roll-off in magnitude above the "cut-off" frequency; however, it introduces a significant (10 to 20 percent) overshoot in amplitude for sudden changes in pressure. Many acquisition systems allow turning off the anti-aliasing filter; if this is an option, then an external analog Bessel filter can be substituted. If use of a Butterworth filter is unavoidable, a time-reversed digital filter can be used to move the Butterworth overshoot and ringing to the portion of the waveform prior to the shock. The effect on rise time is small (roughly a 10 percent degradation in minimum rise-time resolution) while the peak pressure estimate is much improved.
- Measurement microphones designed for high-frequency, fast rise-time signals usually have low-frequency response roll-off frequencies of several hertz. While the spectral peak for typical C4 explosions is above 20 Hz, a low-frequency response roll-off below 2 or 3 Hz will affect estimation of the duration of the positive phase and the negative peak pressure in the explosion waveform. For the microphones considered here, the estimation error introduced is likely to be no more than 10 percent; however, the low-frequency response can be corrected with relatively simple filters.

* As mentioned earlier, the critical anti-aliasing filter in a sigma-delta analog-to-digital converter is normally implemented as an integral part of the converter chip set and would probably not be a Butterworth filter. The transient performance of an elliptic filter, for example, is somewhat better than that of a Butterworth filter; however, a converter of this type should be tested for transient response.

As an example of the effectiveness of post-measurement corrections, Figure ES-2 shows an uncorrected recording of the leading edge of a C4 explosion waveform along with the results of two corrections. The dominant artifacts near the shock-front pressure rise are: (1) the ringing that results from the Butterworth anti-aliasing filter, and (2) the overshoot caused by the physical presence of the microphone in the acoustic field. The first correction filter (blue to black) moves the ringing artifact from the positive-pressure peak to the region before the onset of the shock. The second filter (black to red) removes the diffraction artifact. The corrected waveform shows the fast rise (limited by the anti-aliasing filter's response) to the peak pressure behind the shock front with a smooth transition from the rise phase to the decay phase. On the time scale shown, the pressure variation appears as a step function.

Laboratory evaluation

Set up and execution of measurements with C4 charges require special facilities and considerable expense. Fortunately, some aspects of explosion-shock measurement can be evaluated in the laboratory with simple equipment:

- Freely propagating shocks with rise times as fast or faster than field-measured C4 shocks can be generated with an "explosive" source and a 2- to 3-m length of pipe open at both ends. If a small balloon is inflated to burst or a blank-firing pistol is fired inside one end of the pipe, the strong nonlinearity in propagation through the pipe forms a strong, leading-edge shock that exits the other end. Once leaving the pipe, the shock propagates as a free-field shock and is usable from 0.5 to 10 m from the pipe end.
- Peak pressures from 20 to 1000 Pa can be achieved with balloon pops; peak pressures greater than 2000 Pa can be achieved with a .38 caliber, blank-firing pistol. Rise times at the higher pressures are tenths of a microsecond.
- These laboratory-produced shocks differ from the field C4 shocks in one important way – they have far less energy, which means that the time series are much shorter. This is helpful in obtaining clean recordings of the negative phase; however, nonlinearity in the measurement system would be expected to have significantly different effects for two waveforms with the same peak pressure but different total energy.
- A relatively inexpensive custom microphone using a thin piezoelectric element in the thickness mode is capable of resolving sub-microsecond

rise times. With laboratory-generated (indoor) shocks and the wide-band microphone, the theoretical minimum rise times are nearly reached and the theoretical relationship that the product of rise time and peak pressure is constant has been verified from 20 to 500 Pa (10 to 0.4 microseconds).

Table of Contents

List of Figures

Figure **Page**

Figure **Page**

Figure **Page**

Figure **Page**

Figure **Page**

Figure **Page**

Figure **Page**

Figure **Page**

Preface

This study was conducted for the U.S. Army Public Health Command (USAPHC) as part of the Operational Noise Discrete Events: Physics Models Environmental Quality Technology (EQT) Program under Project D048, "Industrial Operations & Pollution Control Technology," The technical monitor was Ms. Catherine Stewart, MCHB-IP-EON.

The work was completed by the Ecological Processes Branch (CNN) of the Installations Division (CN), Construction Engineering Research Laboratory (CERL). The work was performed by Pennsylvania State University under Contract No. W9132T-07-2-0011. The CERL Contracting Officer's Technical Representative (COTR) was Dr. Larry L. Pater. At the time of publication, Dr. Chris C. Rewerts was Chief, CEERD-CNN, and Mr. Donald K. Hicks was Chief, CEERD-CN. The associated Technical Director was Mr. Alan B. Anderson. The Deputy Director of ERDC-CERL was Dr. Kirankumar V. Topudurti and the Director was Dr. Lance D. Hansen.

COL Bryan S. Green was Commander of ERDC, and Dr. David W. Pittman was the Director.

1 Introduction

1.1 Background

Blast waveforms are challenging to record: pressure rise times associated with the shock wave can, in some conditions, be of the order of a microsecond and the peak pressures can exceed 1000 Pa (1% of atmospheric pressure) for even small explosions. These characteristics require high-bandwidth, low-distortion measurement systems. In addition, because the time-domain waveform is important, aspects of the data collection system that are not normally considered in other acoustic measurements can have significance. This work was undertaken to evaluate the accuracy of commercial, measurement-grade microphones in the recording of pressure waveforms from explosive blasts.

1.2 Objectives

The objective of this work was to assess various methods for accurate recording of pressure waveforms from explosive blasts using commercial measurement-grade microphones.

1.3 Approach

This work was accomplished in the following steps:

1. Commercially available measurement microphones were investigated, and the microphones most suitable for testing were identified.
2. Orientation of the microphone with respect to the incoming shock front was investigated.
3. "Baffled" microphones were investigated.
4. Some aspects of explosion-shock measurement were evaluated in the laboratory with simple equipment.
5. Results were analyzed, and conclusions were drawn regarding the appropriate use of condenser microphones to measure blast waveforms.

2 Measurements

2.1 The problem

Perhaps the two most demanding measurements of the explosion pressure signature are the peak free-field pressure and the initial pressure rise time. Consider, for example, the waveform measurement shown in Figure 3. The blue trace is the waveform measured at 50 m from the explosion of a "full stick" (0.57 kg) of C4. At time zero, the measurement indicates a rapid rise in pressure to about 1400 Pa followed by a slower decay. At 3 milliseconds, a ground reflection of similar shape arrives. Beyond 6 milliseconds, the waveform increases in complexity from secondary reflections and reverberation. The dotted red curve represents an analytical function and a delayed copy that replicates the ground reflection. The analytical function follows the exponential decay from the initial pressure peak through zero to the negative-pressure phase. (Appendix A includes more examples of waveforms from C4 explosions.)

Figure 3. Typical measured pressure waveform from explosion of 1.25 lb (0.57 kg; a "full stick") of C4 at 52 m. This measurement was made using a B&K 4138 ⅛-in. condenser microphone oriented at 90 degrees to the shock front. The dotted red curve is an analytical curve fit that captures the direct arrival, the ground reflection, and the negative-pressure phase.

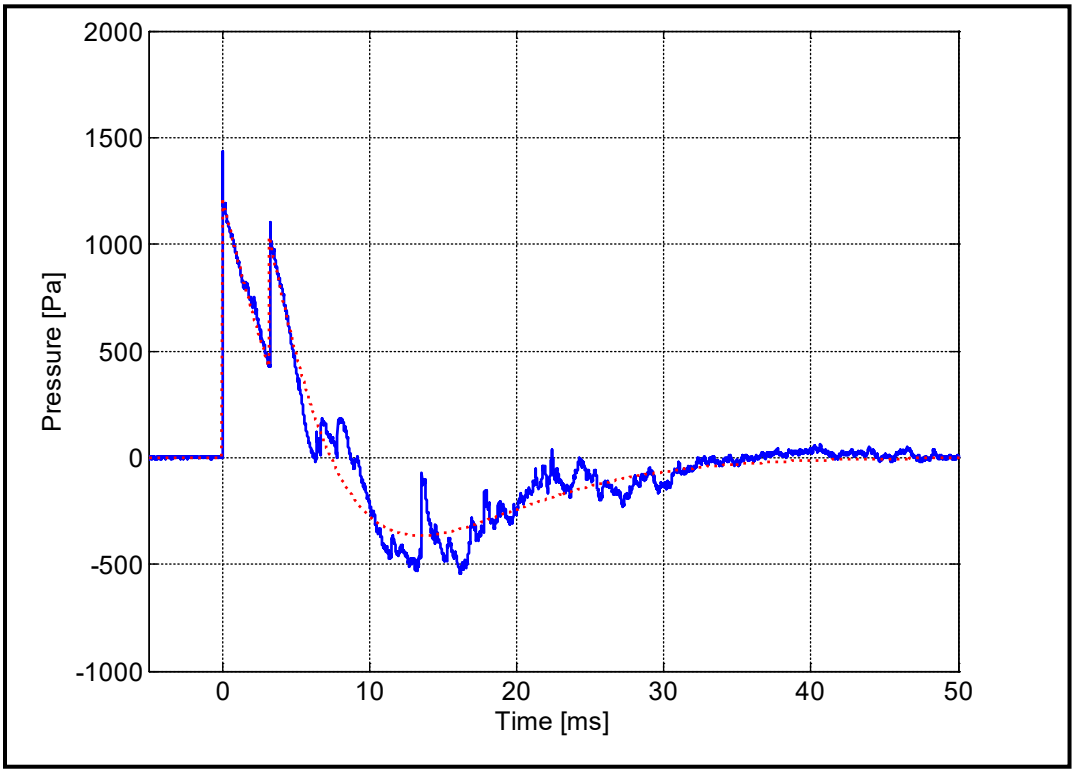

The general shape of the pressure decay after the initial shock front suggests that the actual peak pressure may be significantly below the value of the spike in the waveform. In fact, the actual acoustic pressure peak is just over 1200 Pa; the spike to 1400 Pa is an artifact of the data collection system.

To more closely explore the rise time associated with the initial shock front, one would expand the time scale as shown in Figure 2. The measurement (blue curve) might be interpreted to indicate that the 10- to 90-percent rise time was on the order of 10 microseconds. The value of the peak pressure is ambiguous, but the expanded time scale shows behavior that appears to be a "ringing" artifact. A simple test shows that this rise time estimate is a characteristic of the electronics rather than of the shock front. For the measurement shown in Figures 3 and 4, the microphone signal was anti-alias filtered at 80 kHz with an 8th order Butterworth low-pass filter prior to digitization at 200,000 samples per second. If this same filter were used on an ideal step function in pressure, its behavior would appear almost identical to the recorded waveform. Both the rise time and the ringing artifact are associated with the anti-aliasing filter, not with the acoustic pressure.

Figure 4. Pressure rise associated with the shock front of the explosion recorded in Fig. 3. The blue curve is the measurement. The red curve is generated by filtering an ideal step function by a filter equivalent to the anti-aliasing filter (8th order Butterworth low-pass filter at 80 kHz) in the data acquisition recorder used for the blue curve. The sampling rate is 200,000 samples per second or one sample every 5 microseconds.

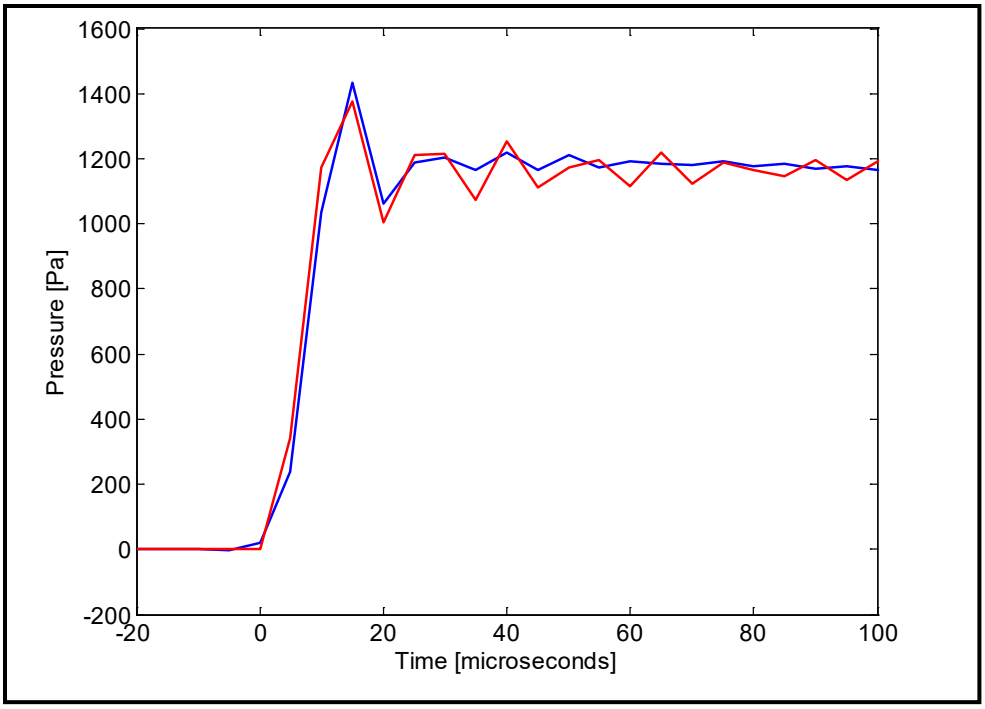

The point of this short introduction is that the measurement system can introduce artifacts or mask the actual acoustical behavior especially when trying to assess peak pressure or rise time associated with explosive shock fronts. Fortunately, there are measurement techniques that avoid some of these problems and there are methods to remove artifacts.

The portion of the waveform after the initial rise is somewhat easier to record accurately. If the objective is to approximate the wave shape with a model waveform, determination of the exponential-decay time constant and the peak under-pressure would be important. Another useful metric is the total energy in the pulse. Most of the discussion in this report relates to measurement of the peak pressure and the leading-edge rise time as these features are the most challenging to measure accurately.

2.2 The measurement problem

If the pressure signature from an explosion could be measured free from reflections and measurement artifacts and at a distance sufficient for complete shock formation, the waveform would look something like that shown in Figure 3.

Figure 5. Idealized pressure signature from a full stick (0.57 kg) of C4 at a distance of 50 m. When the leading edge of the explosion shock arrives, the pressure jumps almost discontinuously to 1200 Pa, then drops through zero acoustic pressure to a smooth, negative-pressure peak, after which the pressure returns asymptotically to zero. With reference to Equation 2, p_0 = 1200 Pa, t_0 = 6 ms, and α = 1.33. The positive phase extends from 0 to t_0 and p_0 is the peak pressure.

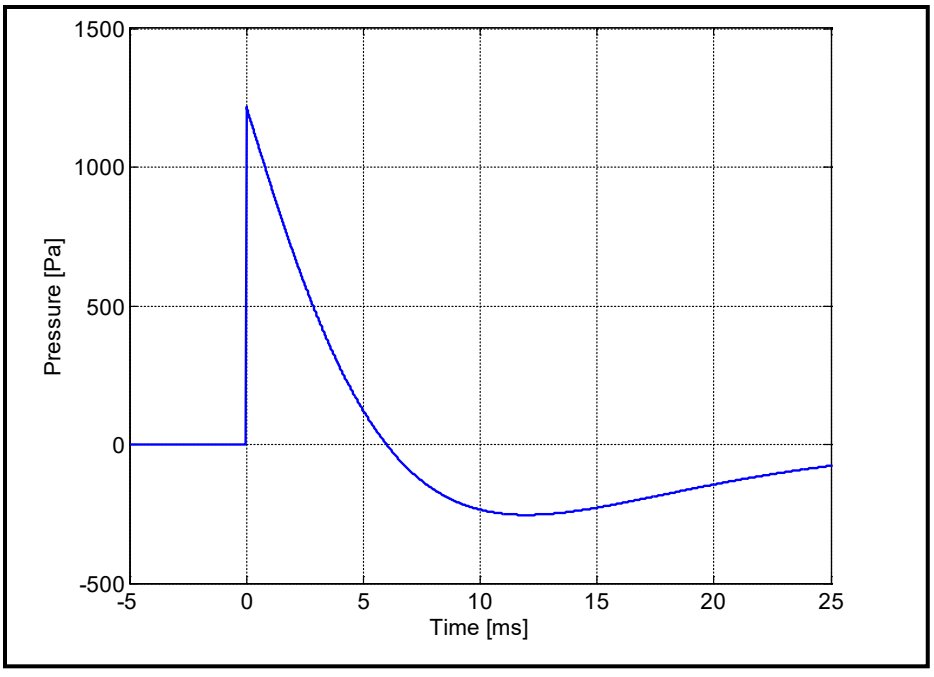

The model pressure function used here is a variation on the modified Friedlander pulse. The modified Friedlander pulse:

$$p_F(t) = p_0 \left[1 - t/t_0\right] e^{-\alpha t/t_0} \quad (1)$$

is often used to describe the pressure from an explosion (e.g., Ford, et al. 1993, or Ismail and Murray 1993). The peak pressure is p_0, the function crosses zero at $t = t_0$, and α is an adjustable parameter. While this function produces both a positive phase and a negative phase, the fit to the actual negative phase is often poor. In an attempt to maintain the two-parameter simplicity of the Friedlander function while improving the fit to measured negative phases, the following variation, the "*F2*" function (see Appendix B), was used:

$$p_{F2}(t) = p_0 \left[1 - \left(t/t_0\right)^2\right] e^{-\alpha t/t_0} \quad (2)$$

For the C4 measurements reported here, this function fits both the positive and negative phases reasonably well. As in the ordinary modified Friedlander pulse, the peak pressure is p_0 and the pressure crosses the zero-pressure axis at $t = t_0$. The parameter, α, can be viewed either as an adjustment to fit the peak negative pressure or an adjustment to fit the time of the negative-pressure peak. The negative-pressure peak in the *F2* function occurs at:

$$t = \left(t_0/\alpha\right)\left[1 + \sqrt{1 + \alpha}\right] \quad (3)$$

Measured waveforms are more complicated. Unless the propagation distance is short and both the source and sensor are high off the ground, the duration of the positive phase of the pressure pulse is generally longer than the separation between the direct arrival and the ground-reflected arrival so the two arrivals overlap. (See Figure 4.)

Furthermore, the measurement system may not have a sufficiently fast response to capture the initial pressure rise rate and often introduces artifacts like amplitude overshoot. Even the idealized waveform produces a more complicated trace after filtering and adding a reflection (Figure 4). What is not obvious on the time scale shown in Figure 4 is that the nearly step-like change in pressure at the beginning of the shock has been rounded by the filtering and the resultant rise time reflects the filter characteristics rather than the explosion characteristics.

Figure 6. The idealized pressure signature from Fig. 3 is shown as a blue dashed line. Addition of a single ground reflection 3 ms after the direct arrival and simple filtering as would be done by an anti-aliasing filter (at 80 kHz) produces the trace shown in red. The filter overshoot of about 20% is visible at the pressure peak and the second arrival changes the appearance of the negative phase significantly.

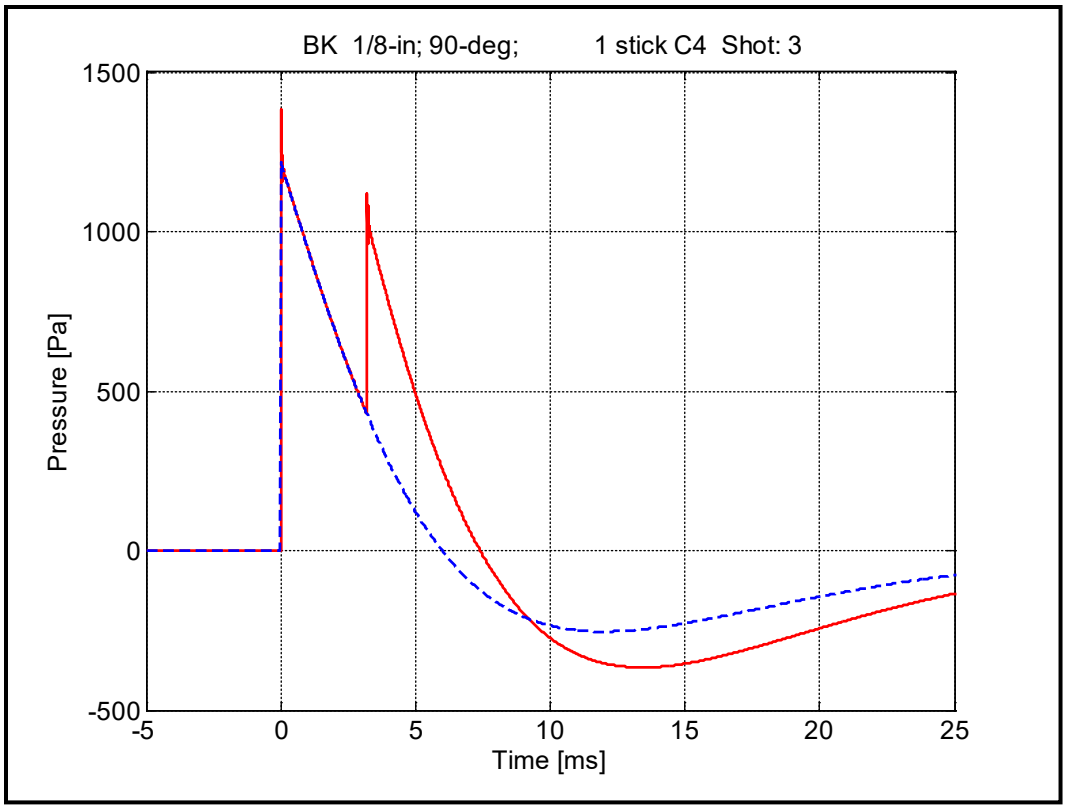

While the direct-plus-ground-reflection model is reasonably representative, a real measurement is complicated still further by reverberation from the ground, secondary reflections, and, to a lesser degree, atmospheric turbulence. Figure 5 shows one of the actual C4-explosion measurements along with the model pulse.

The frequency distribution of energy (Figure 6) shows the general character of an explosion spectrum: a peak at a frequency roughly equal to the reciprocal of the pulse duration* with f^2 dependence in energy below the peak and f^{-2} dependence in energy above the peak. The *F2* model function fits the spectrum reasonably well. (The ordinary modified Friedlander function fits the spectral roll-off above the peak, but, unlike the *F2* function, rolls off too slowly below the peak.)

* The duration of the model pulse is infinite but, from Figure 5, virtually all of the energy is in the first 40milliseconds.

Figure 7. Measured blast pressure (blue curve) of a full stick of C4 (0.57 kg) at a distance of 52 m. The source is 4.7 m above the ground; the receiver is 8.1 m above the ground. The model curve from the previous figure (red dotted line) fits the overall pulse shape reasonably well and the first 6 ms very well. Beyond 6 ms, ground reverberation and secondary reflections complicate the trace. The rms values of the data and of the model are within 4% (0.3 dB).

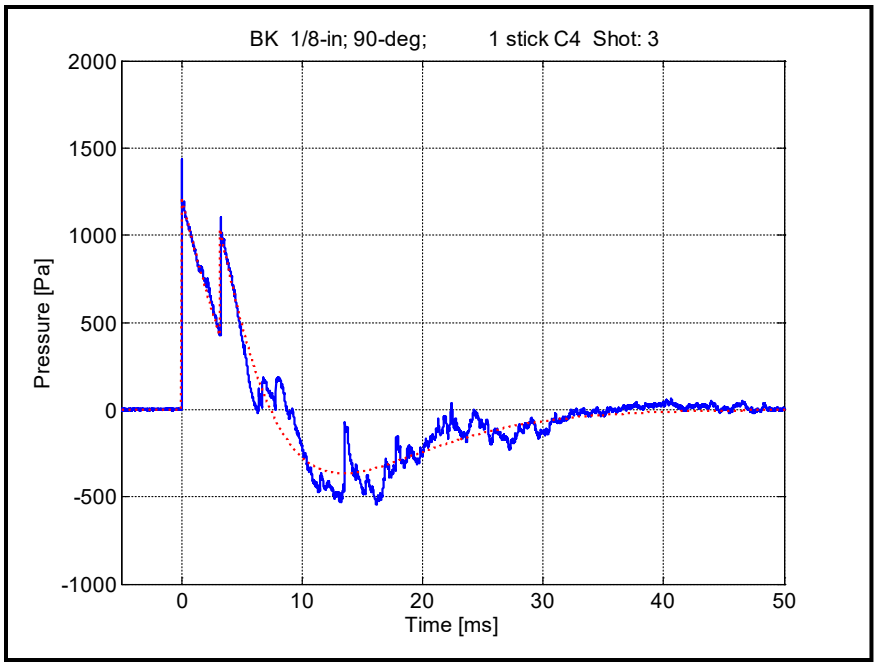

Figure 8. Energy spectral density (ESD) for the time series in Fig. 5. (The "energy" here is the square of the linear pressure spectrum with units of Pa^2s^2 or, equivalently, Pa^2s/Hz.) The ESD for the measurement is shown in blue; the ESD for the model pulse is shown in red. The general character – the peak near 25 Hz and the roll off above and below – is well represented by the direct-plus-ground-reflection model pulse. The two-path interference pattern (dips near 200, 500, and so on) can be seen in both the model and the measurement.

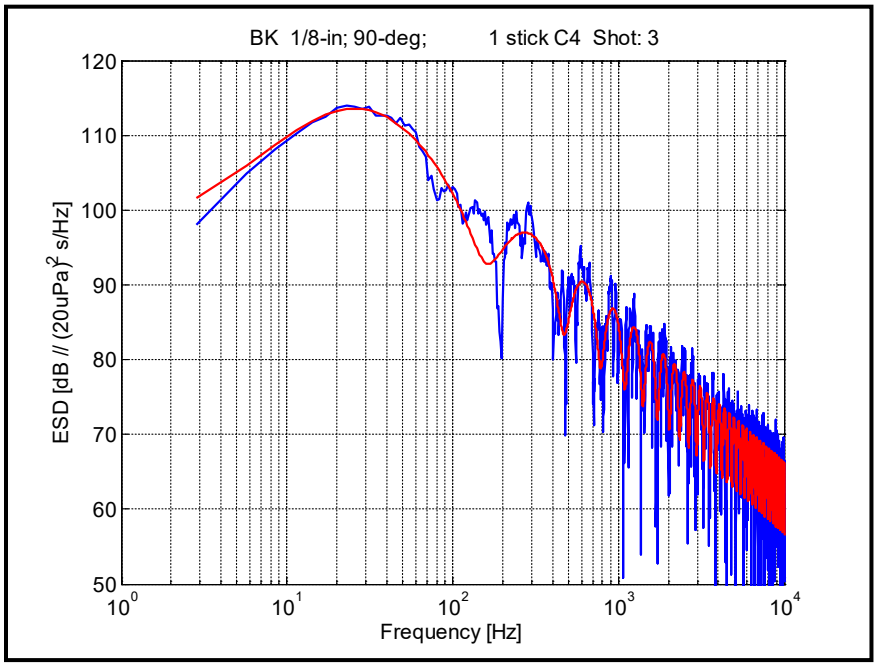

While characterization of the negative-pressure phase is interesting, the critically important parameters for this investigation are the peak pressure and initial rise time.* These parameters are challenging to measure as they require a large measurement bandwidth and freedom from measurement-system artifacts. The measurements of C4 explosions examined here were made at a distance of about 50 m. This distance is far enough for the explosion shock to be fully developed, but not so far that atmospheric turbulence has an overwhelming influence. Previous measurements (Loubeau 2006, Loubeau et al. 2006) indicated that the rise time would be near a minimum at this range so 50 m represents a particular measurement challenge. Theoretical predictions for rise times suggest values of the order of a microsecond for these peak pressures and propagation distances.

The two most influential parameters with regard to planning a measurement system are: (1) the expected peak pressures, and (2) the required resolution for rise time. For example, for C4 charges on the order of a kilogram, the peak pressures at 50 m are within the nominal amplitude range† of ¼-in. or ⅛-in. condenser measurement microphones; however, the ⅛-in. microphone, which has the highest bandwidth of commercial measurement microphones, cannot resolve rise times faster than 3 microseconds. (See Appendix C for C4 model parameters.)

In practice, resolution of rise times faster than 3 microseconds requires a sensor with a wider bandwidth than any commercially available condenser measurement microphone; whereas, resolution of rise times slower than 20 microseconds is straightforward with commercial microphones and electronics. Between 3 and 20 microseconds, measurements can be made with condenser measurement microphones with careful setup and careful analysis.

With respect to measurement of the negative phase, the only significant instrumentation issue is that of the low-frequency system response. Commercial ⅛-in. microphone systems have the poorest low-frequency response of the standard measurement microphones. As discussed later in this report, the error in estimation of peak negative pressure and negative

* This work uses the conventional definition of rise time: the time from 10 percent of peak amplitude to 90 percent of peak amplitude along the initial rise phase. Much of the subsequent discussion addresses the impact of processing artifacts on this measurement.

† There is little if any guidance from manufacturers with regard to handling peak pressure in short-time events. There is some discussion of the issue of sensor nonlinearity later in this report, but it seems likely that, for peak pressures below 2000 Pa, the ¼- or ⅛-in. measurement microphones may have acceptably small nonlinear distortion.

impulse are small, but not negligible; however, correction of the low-frequency response is straightforward. (See Appendix D.) Perhaps the more pressing practical issue is the difficulty in arranging the measurement geometry for sufficient separation of the direct and ground reflection to produce a clean negative phase. In many cases, the characteristics of the negative phase can be extracted indirectly by using the best-fit model curve (including a ground reflection replica). The positive phase at least through the ground-reflection arrival is often sufficiently clean to permit constructing the model-curve fit.

2.3 The measurement system

As context for the subsequent discussion, Figure 7 shows the components of a typical measurement system. Consideration is given to each element in such a system and its influence on the measurement of acoustic waveforms from explosions.

Figure 9. Components of a measurement system for explosive waveforms. For orientation, the incident shock front is shown in blue. Three microphones are shown: each microphone is shown as a cylinder with two parts: at the front is the microphone cartridge; the longer cylinder behind is the preamplifier. There are several choices for microphone orientation. The upper microphone is oriented at 90 degrees to the direction of propagation of the incident shock front. This orientation minimizes the measurement artifacts for a "pressure" microphone. The middle microphone is oriented at zero degrees (as a "free-field" microphone would normally be). The lower assembly includes a "baffle", which can be used to improve the accuracy of rise time and peak pressure measurements. Beyond the microphones are: the conditioning amplifier (CA), the data acquisition recorder (DAQ), and any post-processing (PP). Interconnection cables can also influence the system characteristics.

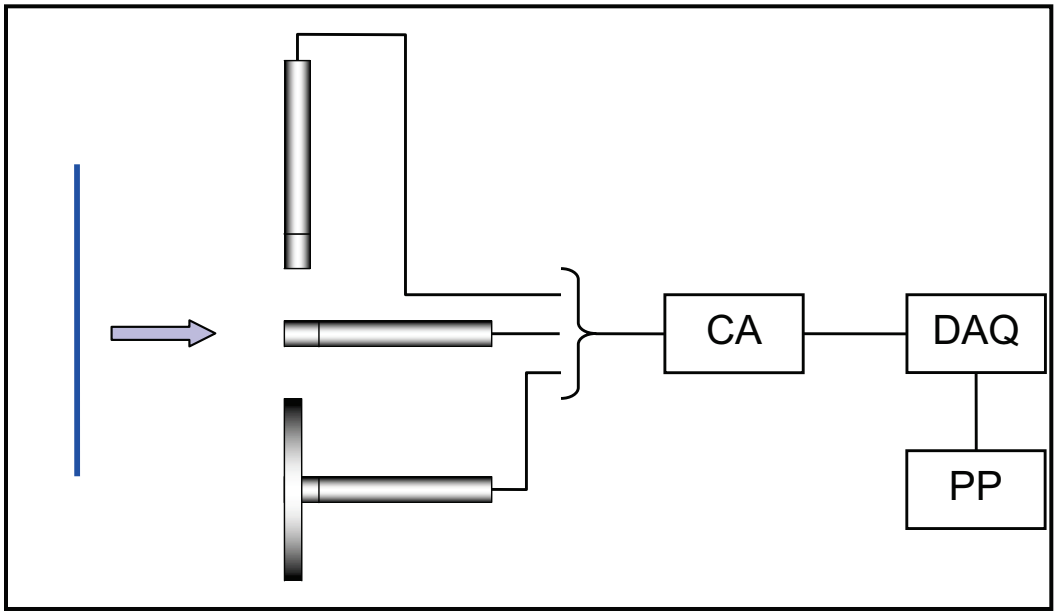

One way to organize the discussion is to consider the following categories of effects. First, the presence of the sensor in the acoustic field alters the field. Consequently, the size, shape, and orientation of the sense element affect the measured waveform. Second, the basic transduction response of the sensor introduces additional limits to both low- and high-frequency response and to system linearity. And, third, any subsequent stage of electronics (including cabling) can introduce high- and low-frequency roll-offs, nonlinearity, and time-domain artifacts (like ringing and overshoot).

2.4 Measurements

The analysis in this report is based on two types of measurements. Field measurements of the acoustic waveforms of C4-explosion blasts were made on 13 September 2007 at the U.S. Army Aberdeen Test Center (Aberdeen Proving Grounds, Aberdeen, MD) Trench Warfare Firing Pad 1. These were followed by a series of laboratory measurements in Spring 2008. The laboratory source produced freely propagating shock pulses at 1 to 10 m range that replicated the peak pressures and shock rise times of the C4 measurements (at 50 m range); however, the total energy of the laboratory pulses was far smaller so the pressure decay from the peak value was faster in the laboratory measurements.

2.4.1 Field measurements of C4

Previous measurements (Loubeau 2006) indicated that the rise time for C4 explosions in air would be shorter at 50 m from the explosion than either 20 or 100 m. At the shorter distances, the waveform has not had sufficient propagation distance to fully shock; at the longer distances, the cumulative effects of atmospheric turbulence start to broaden the shock. Consequently, the C4 measurements for this study were made at 50 m. Five charge weights were used based on fractions of a standard 0.57 kg (1.25 lb) "stick" of C4: ⅛-stick, ¼-stick, ½-stick, full stick, and double stick.

For the field measurements, 10 microphones were used: two ⅛-in. B&K 4138 pressure microphones, four ¼-in. B&K 4938 pressure microphones, three ½-in. GRAS 40AE free-field microphones, and one custom-built wideband microphone. The three ½-in. microphones were included to exaggerate the effects of sensor nonlinearity.

Peak pressures at 50 m ranged from 500 to 2000 Pa. (See Appendix A for typical waveforms.) Shock-front rise times were at least as fast as the minimum

rise-time resolution (3 microseconds) of the condenser-microphone measurement system. The roughly exponential decay in pressure behind the shock front* had a range of exponential time constants from 2 to 4 milliseconds.

2.4.2 Laboratory measurements

A number of measurements in the laboratory were made using free-field propagating shocks generated by an open-ended shock tube. In a conventional shock tube, a bursting diaphragm generates a large pressure step that propagates down the tube; however, replacement of the expendable diaphragm is inconvenient when many shocks are required. The pressure waveform produced by bursting a balloon or firing a blank pistol cartridge is not usable if fired in the open, but, if fired inside one end of a pipe that is 2 or 3 m long, the high-amplitude acoustic wave that propagates down the tube (with little loss) shocks up rapidly. Furthermore, the wave that exits the pipe is effectively high-pass filtered by the reflection coefficient at the end of the pipe. In this way, freely propagating shocks of more than 1000 Pa peak pressure and sub-microsecond rise time can be generated a few meters beyond the pipe exit. Both the peak pressure and the shock rise rate of an outdoor C4 explosion can be matched or exceeded in the lab – the difference is in the total energy in the pressure pulse. The energy in the laboratory pulse is much lower than the energy in the C4 explosion; consequently, there is considerably more low-frequency energy in the outdoor C4 explosions.

The pressure pulses were produced either by inflating a small balloon until it burst or by firing a .38 caliber blank-firing pistol inside one end of a 3-m length of 6-in.† schedule 40 polyvinyl chloride (PVC) pipe. A clean shock forms as the pulse travels down the pipe and leaves the pipe as a freely-propagating shock. Measurements were made at distances from 1 to 10 m from the exit end of the pipe. Peak pressures ranged from 20 to 2000 Pa. (Appendixes E and F show models for balloon bursts and for .38 caliber blanks.) Shock-front rise times were a few tenths of a microsecond. faster than the minimum rise-time resolution (3 microseconds) of the condenser-microphone measurement system with a fast digitizer. (Appendix G describes rise-time models and wideband measurements.) The roughly exponential decay in pressure behind the shock front had a range of exponential time constants from 50 to 200 microseconds.

* Appendix C includes a more complete model for the C4 pressure history.

† Metric units are used in this report except when the "units" are actually labels for products, e.g., "6-in. PVC pipe" and "¼-in. condenser microphone."

3 Sensors and Sampling

3.1 Sensor selection

The widest bandwidth available in commercial measurement microphones is the 140 kHz bandwidth of the ⅛-in. condenser microphone. This microphone is only available as a pressure microphone.* Commercial ¼-in. condenser microphones are available with bandwidths† to 70 kHz as pressure‡ microphones or to 100 kHz as free-field§ microphones. Microphone orientation is also critical as illustrated in Figure 8.

Figure 10. Time-domain performance of a pressure microphone with a shock incident at zero degrees (bottom) and at 90 degrees (top). The zero degrees orientation produces a large pressure overshoot at the shock front. The smaller artifact in the upper trace is the result of subsequent electronic low-pass filtering. The 90-degree orientation produces a more accurate peak pressure; however, the rise time is somewhat slower (not apparent on these scales). In contrast, a free-field microphone has its response overdamped to reduce the diffraction overshoot in the zero degrees orientation (consequently a free-field microphone shows a much slower rise time if used in the 90-degree orientation).

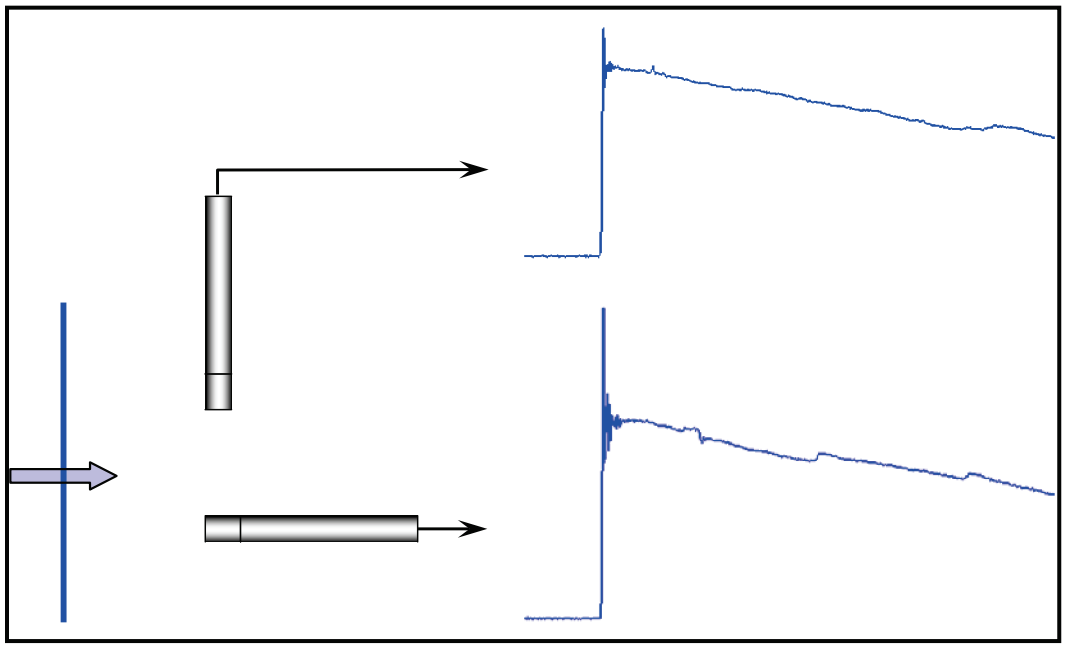

* For example, the B&K 4138 or the GRAS 40DP.

† One must be careful in interpreting advertised bandwidth. For example, when a pressure microphone is used in the zero-degree orientation (with subsequent diffraction correction), the effective bandwidth is higher than the advertised bandwidth. Conversely, the effective bandwidth for a free-field microphone is considerably less than advertised if it is used in the 90-degree orientation.

‡ For example, the B&K 4938 or the GRAS 40BP.

§ For example, the B&K 4135 or the GRAS 40BF.

3.2 Data acquisition recorder sampling

Two data acquisition recorders were used for the field measurements of C4 explosions: (1) a TEAC GX-1 instrumentation recorder at its maximum sampling rate of 200,000 samples per second (16-bit A/D; 12 bits effective), and (2) a Tektronix TDS3014 digital oscilloscope set to sample at 50,000,000 samples per second (50 MS/s; 9-bit A/D; 8 bits effective). Laboratory measurements of free-field shocks were made with the TDS3014 at sampling rates from 25 MS/s to 1000 MS/s. The TDS3014 only stores 10,000 points per channel so, in some cases, only part of the waveform could be captured.

4 Response

4.1 Anti-aliasing filter response

The TEAC GX-1 has internal anti-aliasing filters that can be enabled on each input channel. These filters are 8th order Butterworth low-pass filters. The 80 kHz setting was used for the field measurements of C4. The combination of sampling rate and anti-aliasing filter sets a lower limit on the apparent rise time. This was illustrated earlier in Figure 4 – waveform rise times faster than 5-10 microseconds cannot be resolved. In addition, the anti-aliasing filter introduces a 15 to 20% overshoot, which would have to be accounted in a peak-pressure measurement.

The overshoot can be effectively eliminated by turning the internal anti-aliasing filters off and adding external Bessel low-pass filters. (It may, in fact, be possible to record without anti-aliasing filters since the explosion spectrum drops naturally with increasing frequency, but this was not verified.) For this study, an external filter module was constructed with plug-in filter boards for selecting filter cutoff frequency and filter type (Figure 9). Appendix H includes a further description.

Figure 11. External anti-aliasing filter module. This is a two-channel filter box with interchangeable filter boards. An extra plug-in filter board (LTC1563 analog filter IC [integrated circuit]) is shown to the right. The unit is designed for use either in the lab or in the field to replace the internal anti-aliasing filters in the data acquisition recorder.

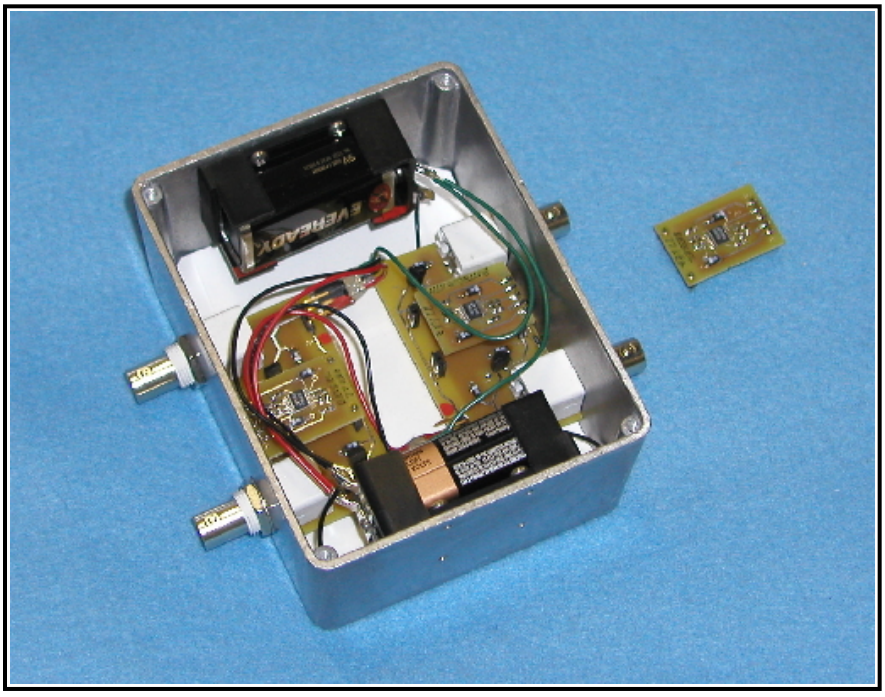

The Bessel and Butterworth filters were first compared using an arbitrary-function generator producing a "falling-exponential" waveform with a time constant (3.5 ms) comparable to the C4 waveforms. The falling-exponential waveform is step-like rise in voltage followed by an exponential decay. This is a reasonable first approximation to the shock front and the initial decay of an explosion pulse. For comparison, Figure 10 shows the time-domain performance of a Butterworth low-pass filter and a Bessel low-pass filter of the same frequency and order. (These are analog filter circuits, not software simulations.)

As is well known, the Butterworth filter introduces an overshoot (of about 10% in this example) and a cycle of ringing just after the pulse leading edge. The Bessel filter has a slightly faster rise time and no discernable overshoot. The Bessel filter is rarely used in commercial data-acquisition systems as an anti-aliasing filter because its high-frequency roll-off in magnitude is considerably slower than a Butterworth filter of the same order; however, the Bessel filter is a better choice when measuring waveforms with sharp transitions like explosion shocks.

Figure 12. Performance of two varieties of anti-aliasing filter for rise time and overshoot. These are analog filter circuits with an input exponential pulse. The sampling frequency is 25,000,000 samples per second. The red curve is the output of a 4th-order Butterworth low-pass filter; the blue curve is the output of a 4th-order Bessel low-pass filter. Both filters have characteristic frequencies of 77 kHz. The Bessel filter has no significant overshoot and a slightly faster rise than the Butterworth filter.

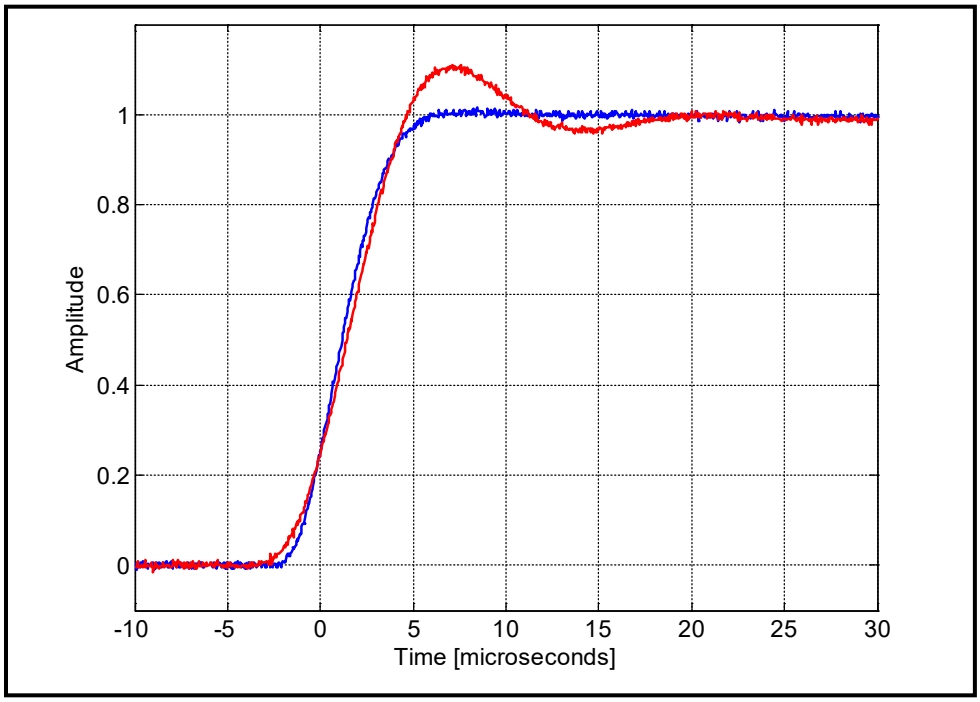

If data has already been recorded using a data acquisition system with Butterworth anti-aliasing filters, the effects of the overshoot can be minimized by post-processing. The success of this technique depends on the group delay characteristics of the Butterworth filter. The group delay, τ_G, is (roughly) the delay time for a *narrowband* pulse passing through the filter. When the group delay is a function of frequency, different frequency components of a *wideband* pulse (like an explosion shock) travel through the filter as different speeds and this leads to distortion – in the Butterworth filter, overshoot and ringing.

The group delay is proportional to the rate of change of phase with frequency:

$$\tau_G = -\frac{1}{2\pi}\frac{d\phi}{df} \tag{4}$$

where:

ϕ is the phase (in radians) of the filter's response at the frequency f.

If the group delay does not depend on frequency, then broadband pulses (like explosion waveforms) will be passed through the filter without distortion. The overshoot observed in the Butterworth filter is a consequence of the particular frequency dependence of the group delay.

The TEAC GX-1 instrumentation recorder used in the field C4 measurements implements an 8th-order Butterworth low-pass filter with a characteristic frequency* of 85 kHz. Figure 11 shows the magnitude and phase of the frequency response of this filter and Figure 12 shows the group delay as a function of frequency.

Since the transfer function of the Butterworth filter is known, it would be tempting to construct an exact inverse filter to remove the overshoot, but inversion of the high-frequency response leads to a noisy, unstable filter. Also, it is preferable to find a technique that does not need to be matched to the specific characteristics of each channel of the instrumentation recorder. Instead of removing the overshoot, a filter can be designed to manipulate the group delay to move the overshoot to the region of the waveform before the leading edge of the shock. Then the overshoot will not interfere with an estimate of the peak pressure.

* Nominally 80 kHz, but measured at 85 kHz.

Figure 13. Magnitude and phase response of an 8th-order Butterworth low-pass filter with a characteristic frequency of 85 kHz.

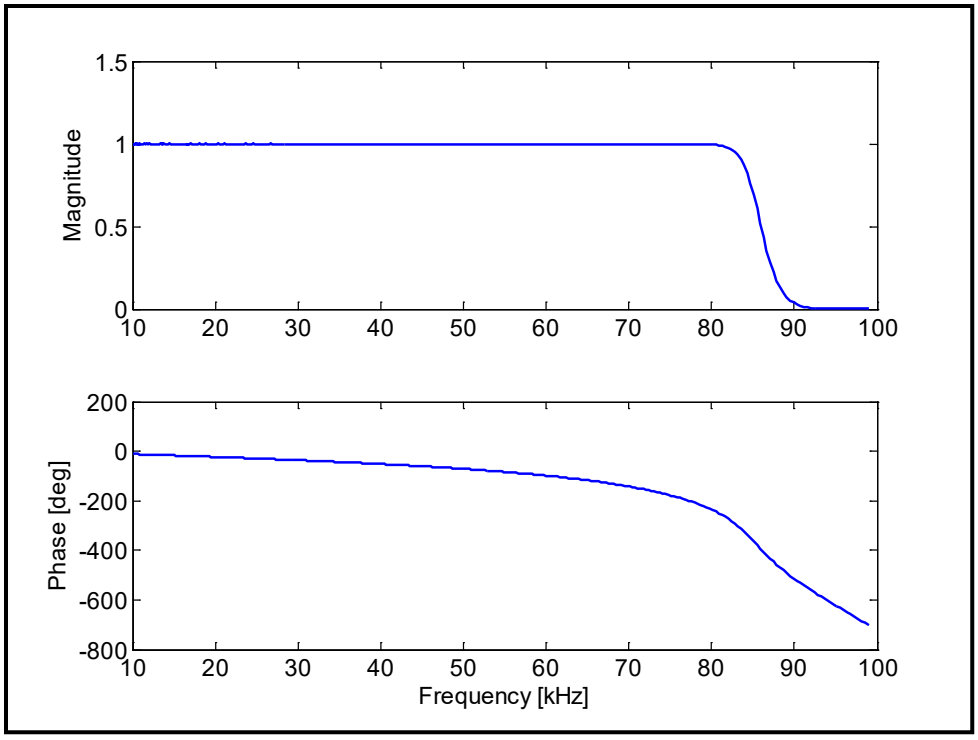

Figure 14. Group delay of the 85 kHz Butterworth filter (blue curve) shown in Fig. 13. Signal content above 60 kHz lags behind that of lower frequencies with a sharp peak at the filter's characteristic frequency. The red curve is the total group delay of an 85-kHz filter followed by a time-reversed 75-kHz filter of the same order. For the red curve, the delays up to 80 kHz are negative, which moves the first filter's ringing to before the shock front.

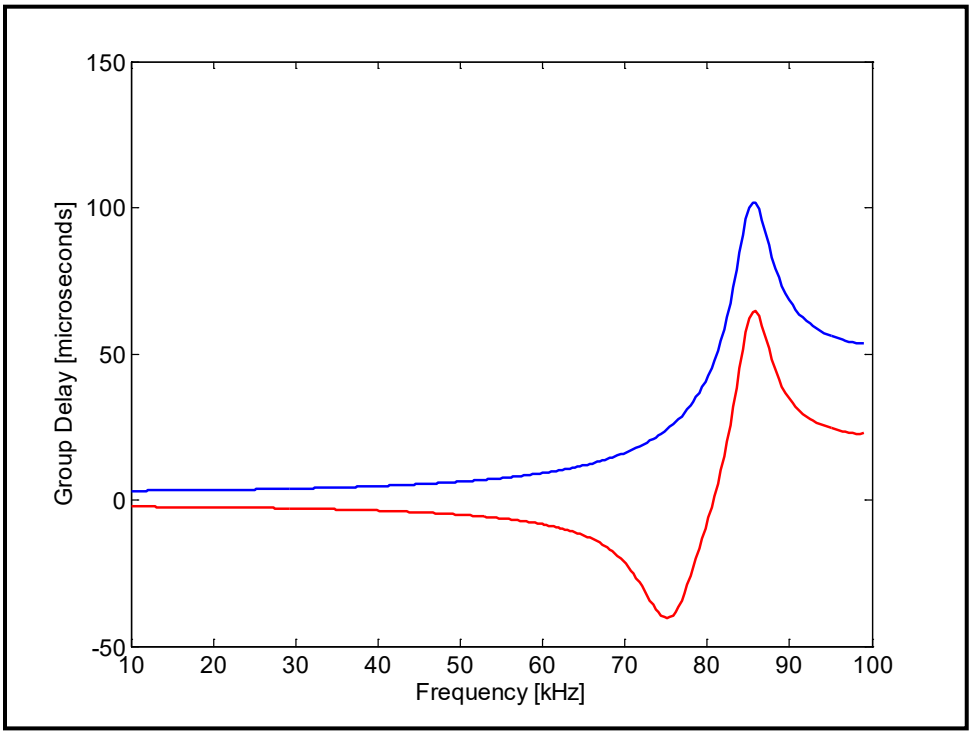

Since this implies anticipatory behavior, this technique cannot be applied in real time, but that is not a significant disadvantage when measuring individual shock events. If the time series of a signal is reversed and passed through a filter, the group delay is, in effect, reversed. In principle, the group delay can be canceled completely, but this is ineffective: the overshoot is only reduced to about half its original amplitude and the ringing is split symmetrically around the shock front.

A more effective strategy is to design the post-processing filter to have a characteristic frequency about 10% lower than the original filter. When this new filter is applied to the time-reversed data, the overshoot is moved to the zero-pressure portion of the waveform just prior to the leading edge and the rise time is only lengthened slightly. Figure 13 shows the total group delay of the time-reversed filter combined with the original filter. Figure 14 shows an example of this compensation filter. The ringing and overshoot are still present; however, they appear prior to the pressure rise. Since the acoustic pressure prior to the rise is zero, ringing and overshoot there do not influence the rise time or peak pressure estimate.*

Figure 15 shows a longer portion of the time series. The shape and amplitude of the waveform is preserved everywhere, but in the immediate vicinity of the shocks. While it is preferable to use Bessel filters for anti-alias filtering when recording shocks, many commercial data acquisition systems are equipped with Butterworth filters. When overshoot artifacts appear in such recordings, the time-reversed filtering described above can limit the impact. A sample implementation of this filtering in MatLab is given in Appendix I.

4.2 Preamplifier and conditioning amplifier response

The sharpest cutoff filter in the signal chain is normally the anti-aliasing filter prior to analog-to-digital conversion; however, the high-frequency roll-off in preamplifiers and conditioning amplifiers can also have an effect on estimation of peak pressure and rise time.

* An appropriate strategy would be to start with the peak pressure, then search backwards in time down the leading-edge to locate the 90 percent point and then the 10 percent point. The location of the 10-percent point may still be influenced by the compensation filter so it might be even more reliable to start from the pressure peak and search backwards in time to find the point of maximum slope (rather than the 10- to 90-percent criterion).

Figure 15. Overshoot compensation filter applied to a C4 explosion waveform recording. The blue curve shows the shock front and the anti-aliasing filter induced overshoot and ringing. After time reversing, passing through an 8th-order Butterworth low-pass filter with a characteristic frequency 10% lower than the actual anti-aliasing filter, and then reversing to normal time (the red curve), the overshoot and ringing has been moved almost entirely to the region before the shock. This simplifies estimation of peak pressure and rise time. The sampling frequency is 200,000 samples per second.

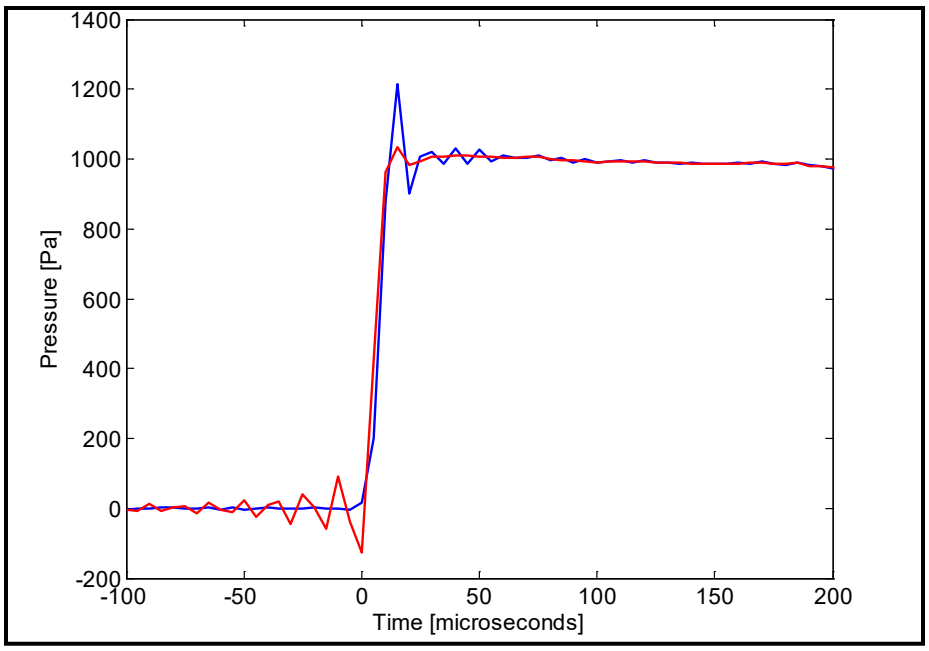

Figure 16. Overshoot compensation filter applied to a C4 explosion waveform recording. The blue curve shows the shock front and the anti-aliasing filter induced overshoot and ringing. After time reversing, passing through an 8th-order Butterworth low-pass filter with a characteristic frequency 10% lower than the actual anti-aliasing filter, and then reversing to normal time (the red curve), the overshoot and ringing has been almost entirely moved before the shock. This makes the peak pressure and rise time measurements simpler.

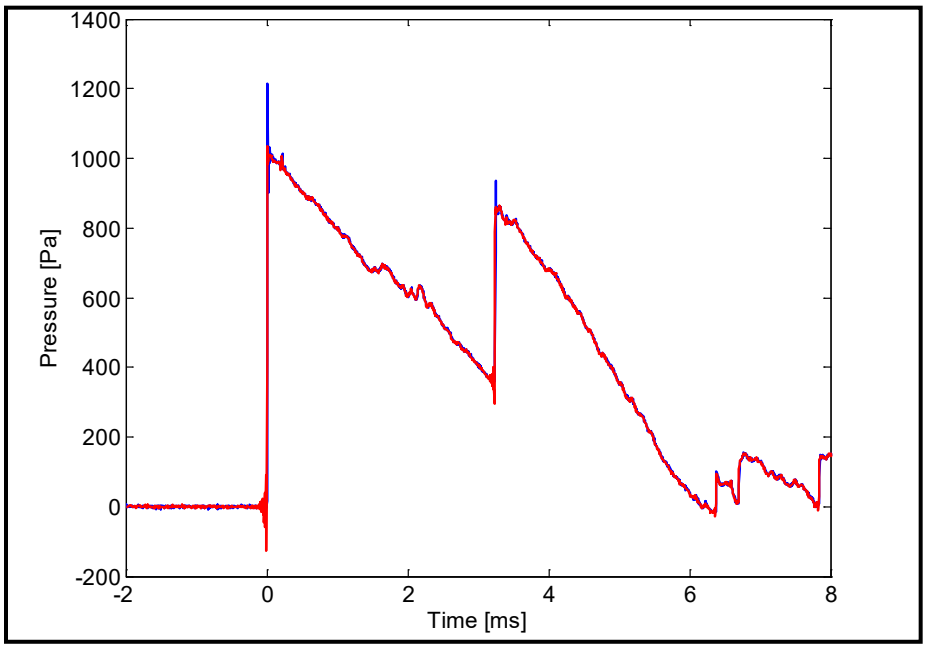

Figure 17. Response of a B&K 2670 preamplifier and 2690A conditioning amplifier to an exponential pulse. The input pulse waveform is shown in blue; the output in red. The overshoot and well-damped ringing is similar to that of a 2nd-order Butterworth low-pass filter (but the filter type is not described in the equipment data sheets). The 2690A used here is the 200 kHz extended-frequency version; the normal 2690A shows similar behavior except that the overshoot peak is about twice as wide.

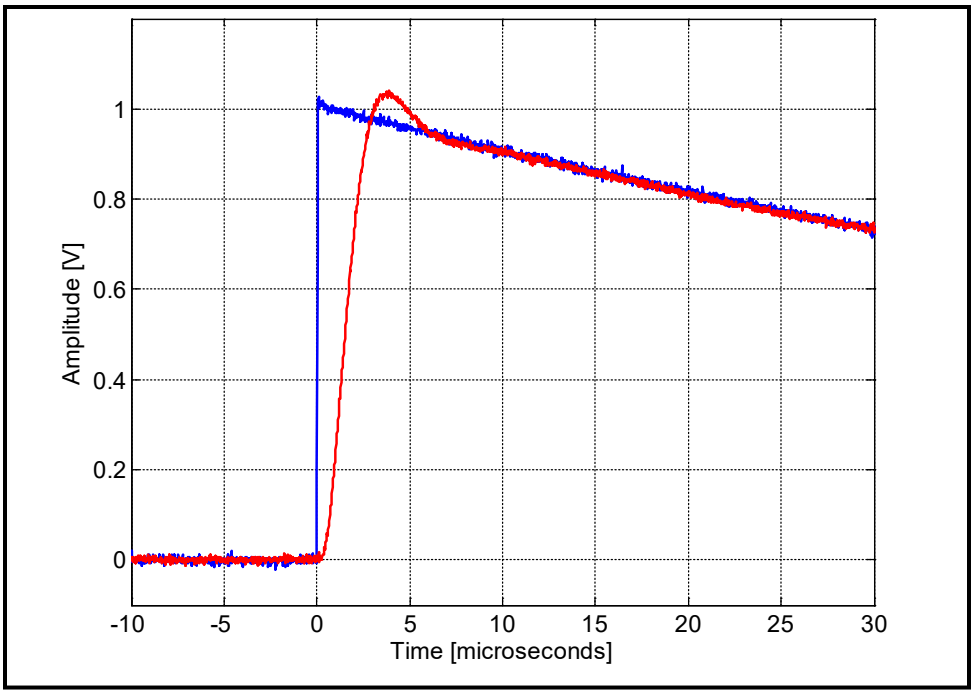

To isolate these effects from the response of the microphone cartridge, an input adapter* is used in place of the cartridge. The input adapter loads the preamplifier with an appropriate capacitance while permitting connection of an external signal. With the input adapter, an electronic waveform can be passed through the preamplifier. For these tests, the preamplifier and conditioning amplifier were tested together and the output of the conditioning amplifier was recorded using the Tektronix TDS3014 digital oscilloscope.

The C4 measurements using ¼-in. and ⅛-in. microphones were made with B&K 2670 preamplifiers and either of two B&K 2690A (NEXUS) conditioning amplifiers, one with the extended-bandwidth option (WH3219). Feeding an exponential pulse (from an arbitrary-function generator) through the input adaptor, the 2670 preamplifier, and the 2690 extended-band conditioning amplifier (set for maximum bandwidth and 3.16 mV/Pa), produces the output shown in Figure 15.

* For example, GRAS RA0080 6 pF input adapter for ¼-in. microphone preamplifiers.

As in the case of the anti-aliasing filter, the overshoot can be minimized with a post-processing filter. A two-pole low-pass filter with simple poles at 200 kHz reduces the overshoot substantially though with some slowing of the rise response. The frequency-domain response, $H(f)$, of this correction filter is:

$$H(f) = \left(\frac{1}{1 + jf/f_0}\right)\left(\frac{1}{1 + jf/f_0}\right) \tag{5}$$

with a corresponding s-domain response:

$$H(s) = \frac{1}{1 + 2s/\omega_0 + s^2/\omega_0^2} \tag{6}$$

from which digital filter coefficients can be determined from the bilinear transformation. The bilinear transformation can be done by hand to write closed-form expressions for the time-domain filter coefficients. Define the following:

$$\begin{aligned} d_s &= f_s/\pi f_0 \\ d_0 &= 1 + 2d_s + d_s^2 \\ d_1 &= 2 - 2d_s^2 \\ d_2 &= 1 - 2d_s + d_s^2 \end{aligned} \tag{7}$$

where f_s is the sampling frequency. Then the time-domain filter coefficients can be written (in MatLab vector form) as:

$$\begin{aligned} A &= [d_0,\ d_1,\ d_2]/d_0; \\ B &= [1,\ 2,\ 1]/d_0; \end{aligned} \tag{8}$$

and applied using the *filter* function:

$$y_{filtered} = \text{filter}(B, A, y); \tag{9}$$

Figure 16 shows an example application of this correction filter to the amplifier output. This correction filter is useful if the data acquisition recorder samples at least as fast as 500,000 samples per second. The C4 measurements using the TEAC GX-1 were sampled at 200,000 samples per second. In this case, the high-frequency cut-off of the anti-aliasing filter is below the high-frequency cut-off of the conditioning amplifier and the lower cut-off masks the preamplifier/amplifier overshoot.

Figure 18. Reduction of overshoot with two-pole correction filter. The black curve is the result of filtering the amplifier output (red curve) with the correction filter. This measurement was made with the extended-band 2690A and a correction-filter f_0 = 200 kHz. (For the normal 2690A, use f_0 = 100 kHz.) Little of the overshoot remains; the rise time has increased from about 2 microseconds to about 3 microseconds. The peak pressure seems to be better estimated from the uncorrected (red) curve, but this is coincidental; in this example, the decay rate after the leading edge nearly matches the overshoot error. A more reliable estimate of the peak pressure would result from finding the decay rate after the leading-edge transient, then extrapolating backward in time to the time of the leading edge.

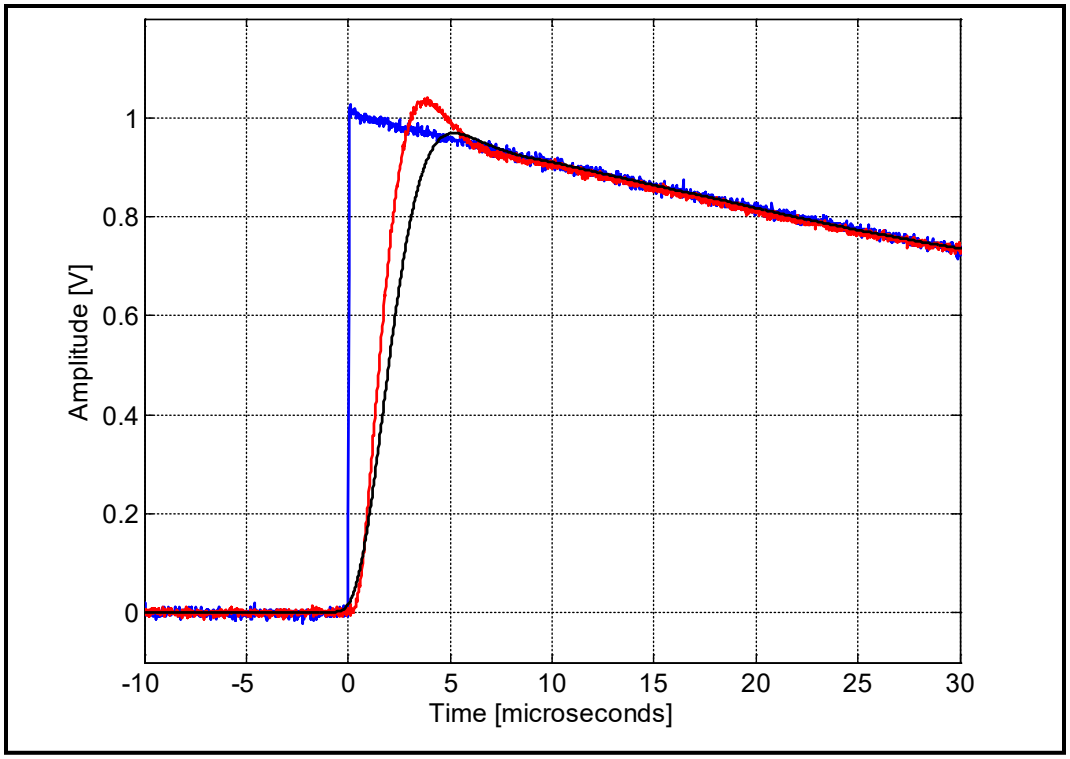

5 Microphone Effects and Baffles

5.1 Microphone shape effects

Insertion of a microphone into the acoustic field changes the acoustic field. If the microphone dimensions are much smaller than an acoustic wavelength, the influence of the microphone body on the field can often be neglected. However, the actual acoustic pressure on the microphone diaphragm may be two to four times higher than the free-field pressure when the wavelength approaches the microphone diameter. The effect depends on microphone orientation with the strongest effect when the wave front strikes the diaphragm directly from the front (the zero degrees orientation shown in Figure 17).

Microphone manufacturers often supply curves of the magnitude of the frequency response as it relates to microphone orientation; however, predicting the effects on time-domain signals requires the phase response as well. Figure 18 shows measured signals for four different orientations and a laboratory-generated free-field shock with a peak pressure of about 500 Pa.

Figure 19. Orientation of microphone with respect to incoming wave. In the zero degrees orientation, the axis of the microphone points directly toward the incoming wave front; in the 90-degree orientation, the microphone axis is parallel to the wave front. The zero degrees orientation is the normal orientation for a "free-field" microphone; the 90-degree orientation gives practically free-field performance with "pressure" microphones.

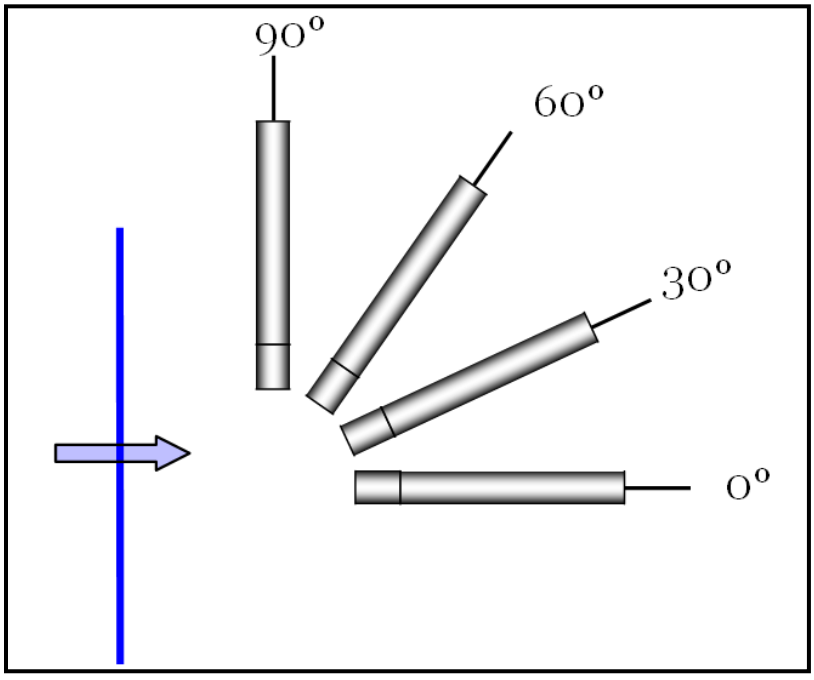

Figure 20. Measured time-domain response of a ¼-in. "pressure" microphone (B&K 4938) to a shock wave for the four microphone orientations shown in the previous figure. In this case, the true peak pressure is about 500 Pa. The highest overshoot is for the zero degrees orientation (blue). Also shown are 30 degrees (red), 60 degrees (green), and 90 degrees (black).

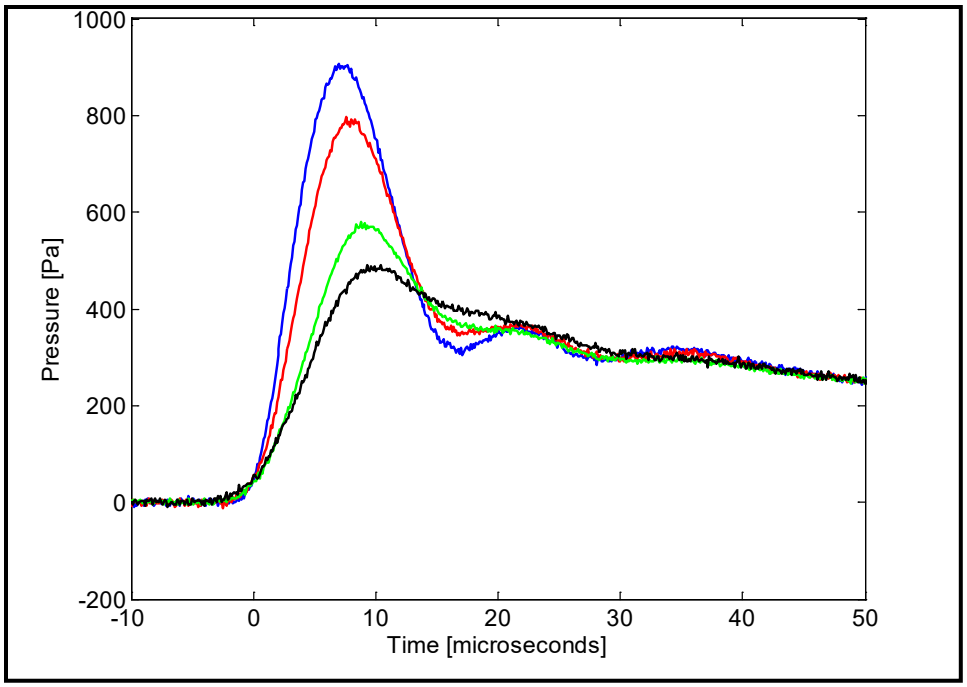

For a "pressure" microphone (in contrast to a "free-field" microphone), an orientation of 90 degrees produces a relatively artifact-free record of the acoustic pressure waveform (Figure 18). In addition, effects of the microphone's protection grid are much smaller in the 90-degree orientation. The measurements discussed here were all taken with the protection grids removed, but an earlier study (Gabrielson et al. 2005) examined the artifacts introduced by the protection grids. For a free-field microphone in the zero degrees orientation, the protection grid should be removed as the grid introduces significant artifacts. For field deployment in conditions under which the membrane might be damaged if the protection grid is removed, a pressure microphone at 90 degrees with the grid in place will produce signatures almost as clean as a free-field microphone at zero degrees with the grid removed.

The large overshoot shown for the zero-degree orientation shown in Figure 18 is a direct result of diffraction from the microphone face. (A free-field microphone has added damping to counteract the pressure rise associated with the diffraction-response peak. Because of the compensation damping in a free-field microphone, if the free-field microphone is used in the 90-degree orientation, an octave or more in high-frequency response is

lost.) This diffraction-response peak occurs when the non-dimensional frequency, *ka*, equals 2.5. The non-dimensional frequency, *ka*, equals $2\pi fa/c$ where *c* is the sound speed, *a* is the microphone radius, and *f* is the ordinary acoustic frequency. This peak occurs at about 45 kHz for a ¼-in. microphone and at about 90 kHz for a ⅛-in. microphone.

The effects of diffraction at the end of a circular rod can be calculated* and the results of this calculation can be used to generate a correction filter. Such a correction filter can be used to remove the diffraction overshoot from a pressure microphone in the zero-degree orientation (and, in a modified form, the filter can be used in conjunction with circular baffles).

The pressure on the surface of the microphone diaphragm (in the zero-degree orientation) as a function of radial distance can be expressed as a series:

$$p_{face}(r) = 2 + \sum_{m=0}^{N} g_m \frac{J_0(j_{1m}\, r/a)}{J_0(j_{1m})} \tag{10}$$

where:

a is the microphone radius
J_0 is the zero-order Bessel function
j_{1m} are the zeros of the J_1 function.

Evaluation of the series coefficients, g_m, which are functions of frequency, follows Jones (1955); MatLab code for this calculation is included in Appendix J. The average pressure on the microphone can be found by integrating this pressure distribution over the active face of the diaphragm. If the entire circular face were active with uniform response, the integration can be done in closed form with the result:

$$p_{eff} = 2 + g_0 \tag{11}$$

However, for a condenser microphone, the active area is somewhat less than the total microphone face area; furthermore, the diaphragm responds more to pressure near the center than near the edge. To represent these effects, Bessel weighting is used to taper the diaphragm response down to zero at the edge of the active region. When this is done, the pressure distribution function must be integrated numerically to find the effective diaphragm pressure, p_{eff}.

* See Jones (1955). As with many studies, Jones calculates only the magnitude of the diffraction response. To reconstruct (or remove) the effects of diffraction on pulses in the time domain, it is essential to know the phase of the response as well.

This calculation can be used to determine the effective frequency response that results from diffraction at the microphone face (still considering the zero degrees orientation only). Figure 19 shows this response as a function of frequency for a ¼-in. microphone and for a ⅛-in. microphone. From this calculation, both the magnitude and phase are determined; consequently, an inverse filter can be developed to remove the diffraction response from a measured waveform. The inverse of the full diffraction solution can be used as a frequency-domain correction filter. (Appendix K includes MatLab code.) However, a relatively simple approximate representation can also be used to develop a fast, time-domain correction filter.

Figure 21. Effective frequency response resulting from microphone diffraction in the zero-degree orientation. The magnitude and phase for a ¼-in. microphone (blue) and a ⅛-in. microphone (red) are shown. At low frequency, there is little influence – the response magnitude is near unity and the phase is near zero. At high frequency, the effective response corresponds to the simple pressure doubling expected at a hard surface. In normalized frequency, the transition region extends from $ka = 0.5$ to $ka = 4$. The response magnitude is $\sqrt{2}$ (3-dB above unity) at $ka = 1$ and the magnitude peak occurs at $ka = 2.5$ (45 kHz for the ¼-in.; 90 kHz for the ⅛-in.).

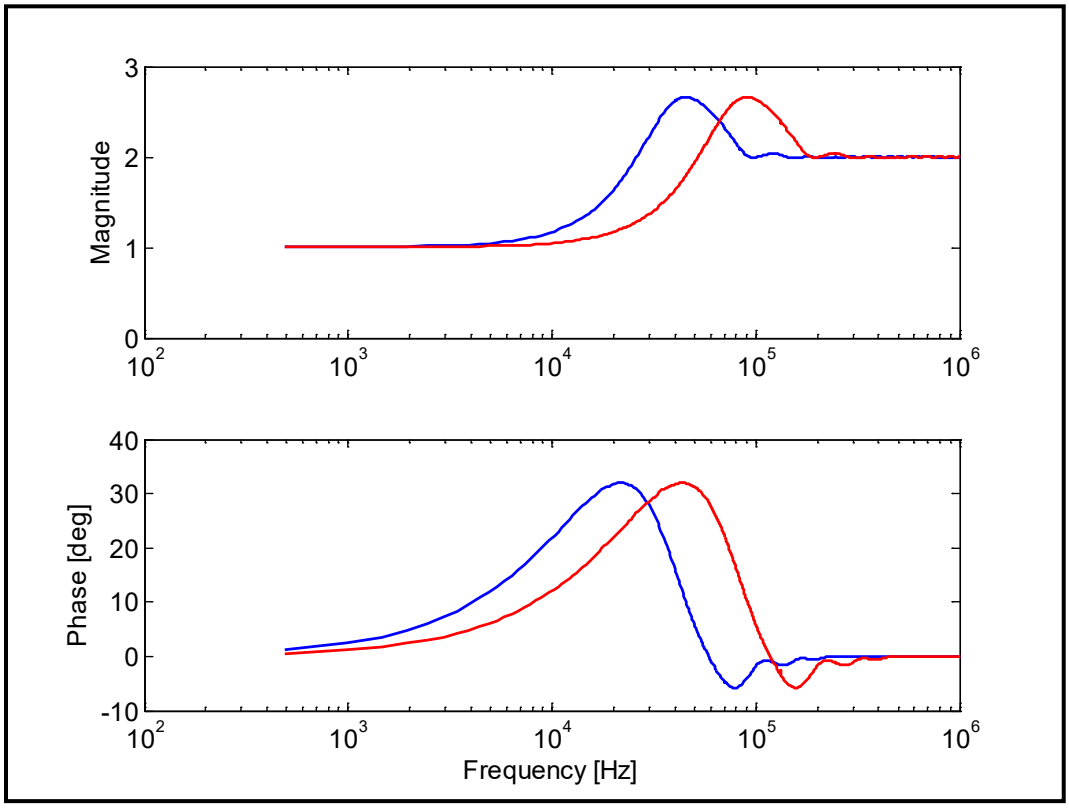

Calculation of the series solution is complicated; fortunately, the diffraction response is fairly well approximated by a filter with two factors:

$$H(f) = \left(A_1 \frac{f_1 + jf}{f_2 + jf} \right) \left(1 + \frac{A_2 \, jf/(Q f_3)}{1 - (f/f_3)^2 + jf/(Q f_3)} \right) \tag{12}$$

where

$$\begin{aligned} f_2 &= 2 f_1 = \sqrt{2} f_0 \; ; \; f_3 = 2.5 f_0 \\ A_1 &= 2 \; ; \; A_2 = 0.5 \; ; \; Q = 1.0 \end{aligned} \tag{13}$$

and f_0 is the frequency for which $ka = 1$.

The first factor in parentheses represents a smooth transition between one and two – at low frequencies, the influence of the microphone is negligible so the apparent pressure is equal to the actual free-field pressure; at high frequencies, the surface of the microphone produces pressure doubling. The second factor in parentheses adds a peak to the response at the location of the actual diffraction peak (at $ka = 2.5$). For comparison, Figure 20 shows the effective response from the series ("exact") solution to the response of the approximate filter function.

Figure 22. Comparison between series solution (blue) and approximate solution (red dashed) for the effective diffraction response of a ¼-in. microphone.

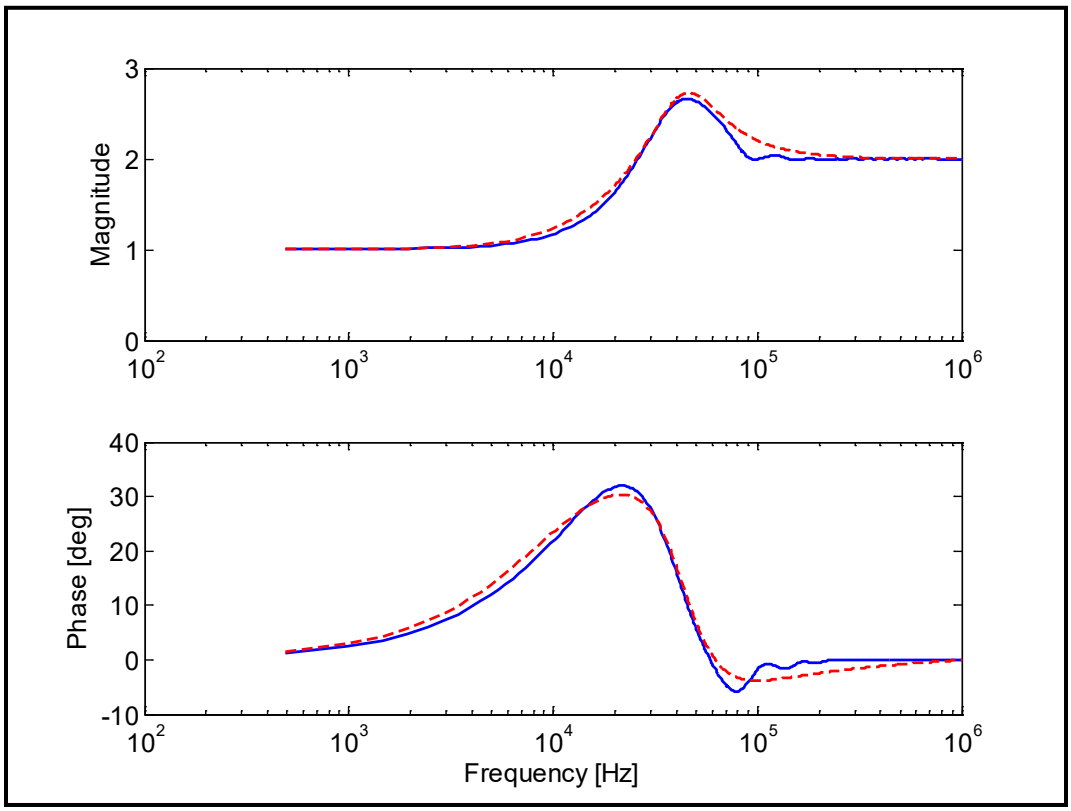

A more complex approximation would improve the correspondence with the series solution; however, the performance of the simple approximation given above is reasonably good. That approximation can be rewritten in the s-domain by the substitution, $s = j2\pi f$, then manipulated into a numerator polynomial in s divided by a denominator polynomial in s. From this form, the bilinear transformation can be used to find z-domain coefficients for a time-domain filter. Appendix L includes a MatLab routine for implementing this approximate inverse filter.

The time-domain filter must be applied with some care. If the sampling frequency is too low, the filter output can be erratic. This filter should not be used for correction of ⅛-in. microphone data if the sampling rate is below 192 kS/s and should not be used for correction of ¼-in. microphone data if the sampling rate is below 96 kS/s.

The diffraction-correction filters were evaluated both in the laboratory and on the field-measured C4 data. In Figure 21, the correction filter has been applied to a laboratory measurement (blue trace) with a ⅛-in. microphone (B&K 4138) oriented at zero degrees to the incoming shock. While the measured waveform peaks at almost 1000 Pa, the actual acoustic peak pressure is only a bit more than half that value. The red and black curves show the waveform after passing through the diffraction-correction filters. The red curve is the output of the frequency-domain filter (the "exact" solution) and the black curve is the output of the simplified time-domain filter. There is little difference between the two filter outputs; both remove the diffraction overshoot and reproduced the fast rise and exponential decay expected for the shock.

For comparison, Figure 22 shows the diffraction-correction results for the output directly from the microphone preamplifier/amplifier (left plot) to the diffraction-correction results for the output after the output was filtered with a 4th-order Bessel low-pass filter (at 77 kHz). A model exponential fit is also drawn in each figure to show the consistency in the results with respect to estimation of peak pressure and exponential decay rate. Of particular interest is the apparent rise time for the measurement shown on the left. By expanding the time scale, the 10-to-90-percent rise time after diffraction correction can be estimated as approximately 3 microseconds. This is the theoretical limit for apparent rise time for this microphone and electronics combination – the fastest rise time achievable with a standard condenser measurement microphone and factory electronics.

Figure 23. Pressure waveform (blue) recorded with a ⅛-in. pressure microphone (B&K 4138) oriented at zero degrees to an incoming shock showing the diffraction-induced overshoot to almost 1000 Pa. Passing this waveform through the frequency-domain diffraction-correction filter produces the red curve; passing this waveform through the time-domain approximate diffraction-correction filter produces the black curve. (The residual ripple with a period of about 5 microseconds results from the preamplifier/amplifier low-pass filtering discussed earlier.)

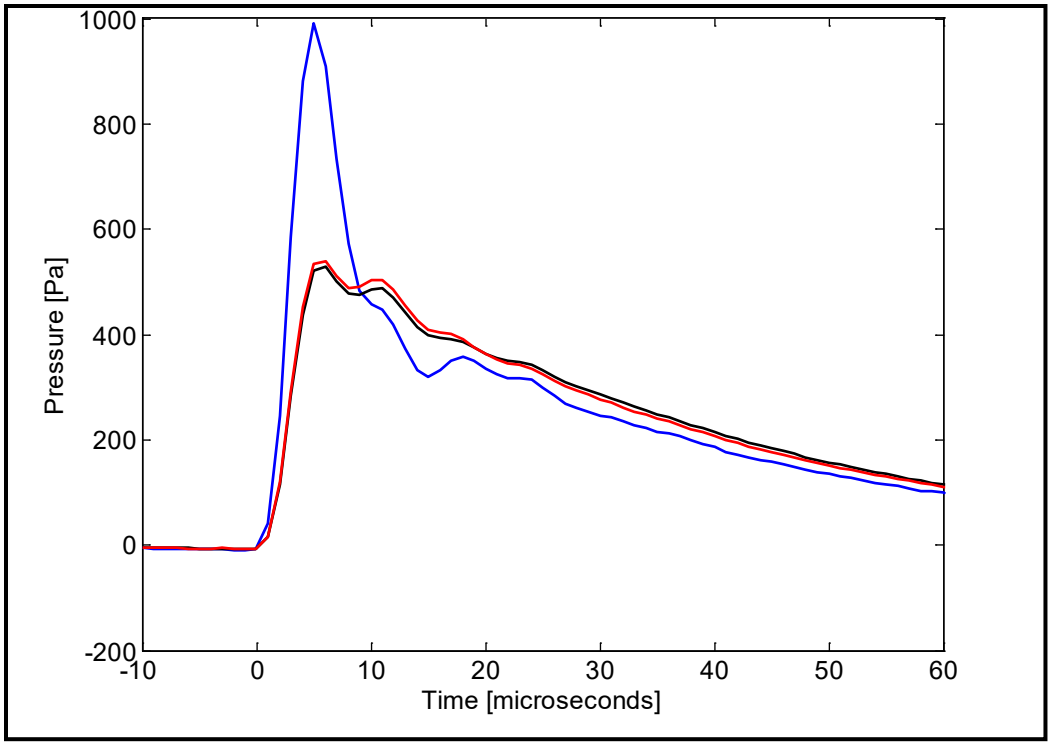

Figure 24. The plot on the left is a reproduction of the previous figure with a model exponential (black, dashed) included to fit the exponential decay and pulse start time. The model exponential has a pressure peak of 650 Pa and an exponential time constant of 35 microseconds. The plot on the right shows the microphone output after passing through a 4th-order Bessel low-pass filter at 77 kHz (blue curve) and then after application of the frequency-domain diffraction-correction filter (red curve). The same model exponential is also included. Except for a longer rise time and a slightly lower apparent peak pressure, the corrected (red) curve on the right is consistent with the corrected (red) curve on the left.

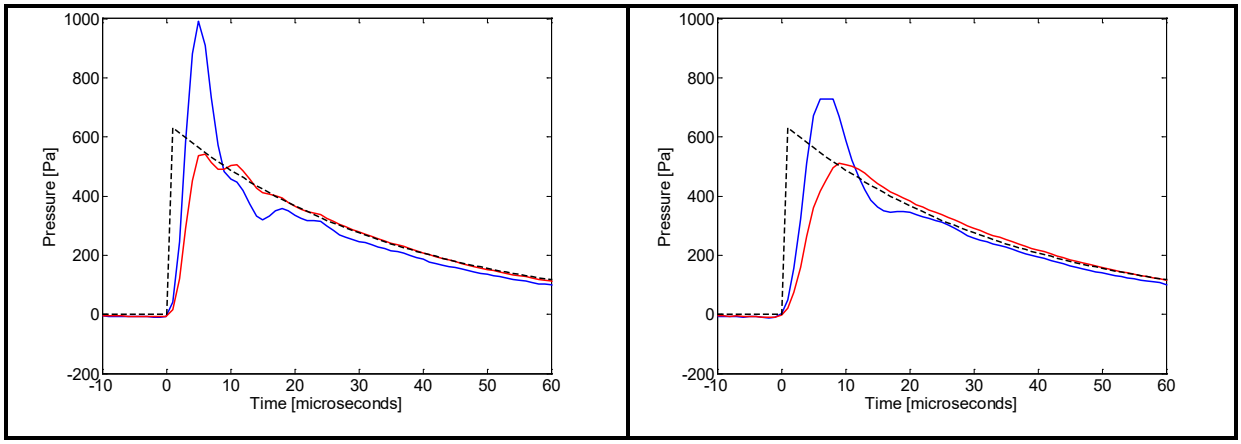

For the parameters of this test, the theoretical rise time of the shock is less than a microsecond (Appendix G). The results shown are dominated by the characteristics of the measurement equipment. Waveforms from field measurements of C4 explosions are not as clean as the laboratory-generated shock waveforms and comparison sensors were spaced several meters apart in contrast to the centimeter-separation in the lab. Nevertheless, the field measurements are representative of practical measurements and the corrections described above can be applied with reasonable success to these C4 measurements.

Figure 23 shows the recorded waveform from a full stick (0.57 kg; 1.25 lbs) of C4 at 52 m from a ⅛-in. microphone oriented at zero degrees to the incoming shock front. The direct-arrival shock appears at zero seconds and the ground-reflected shock appears at 3 milliseconds. The shock arrivals are each accompanied by the expected diffraction overshoot (significantly higher in amplitude than the overshoot caused by the anti-aliasing filter). Although the overshoot on the direct arrival reaches almost 2000 Pa, it appears that the actual peak pressure is between 1200 and 1300 Pa.

Figure 25. Pressure waveform recorded with a ⅛-in. (B&K 4138) microphone oriented at zero degrees to the incoming shock from a 0.57 kg C4 charge at 52 m. The direct (t = 0) and ground-reflected (t = 3 ms) arrivals are clearly visible as is the diffraction-induced overshoot in the pressure record.

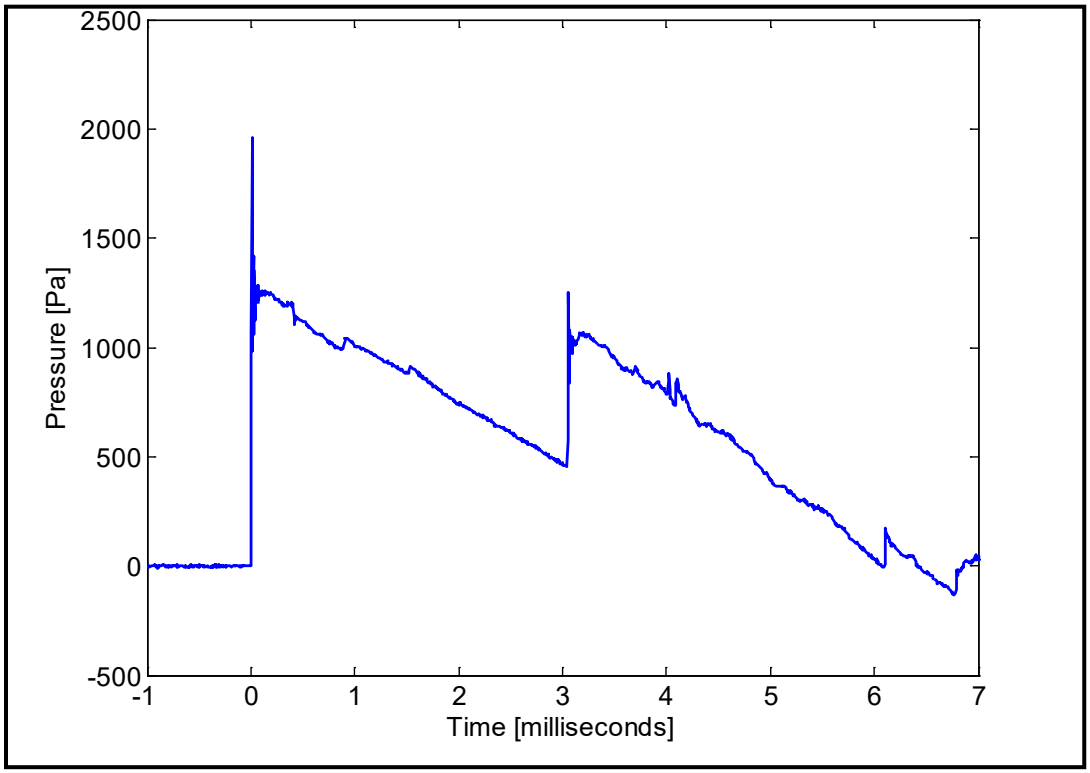

To examine more closely the pressure rise in the vicinity of the shock front, both of the interfering artifacts may be removed. The anti-aliasing filter introduces ringing at the shock front and the presence of the microphone in the acoustic field introduces the large diffraction overshoot. In Figure 24, the time-reversed Butterworth correction filter moves the filter ringing from the top of the pressure rise (blue curve) to the region before the shock (black curve). Subsequent application of the diffraction-correction filter eliminates the diffraction overshoot (red curve). The time scale is expanded in this figure to show details in the vicinity of the shock front more clearly.

For comparison, the fully corrected waveform from Figure 24 is shown in Figure 25 along with the waveforms from the ¼-in. and ⅛-in. microphones in the 90-degree orientation. Both of these 90-degree microphone waveforms have been corrected for the ripple introduced by Butterworth anti-aliasing filter.

Figure 26. Waveform behavior in the vicinity of the shock front from 0.57 kg of C4 at 52 m. The waveform was recorded with a ⅛-in. (B&K 4138) microphone oriented at zero degrees. The raw waveform is the blue curve (sampled at 200,000 samples per second). The black curve is the result of applying the Butterworth transient-correction filter; the positive peak that remains is the result of microphone diffraction. The red curve is the result of applying the diffraction-correction filter. The red curve shows the step-like change in pressure characteristic of the leading edge of a shock wave.

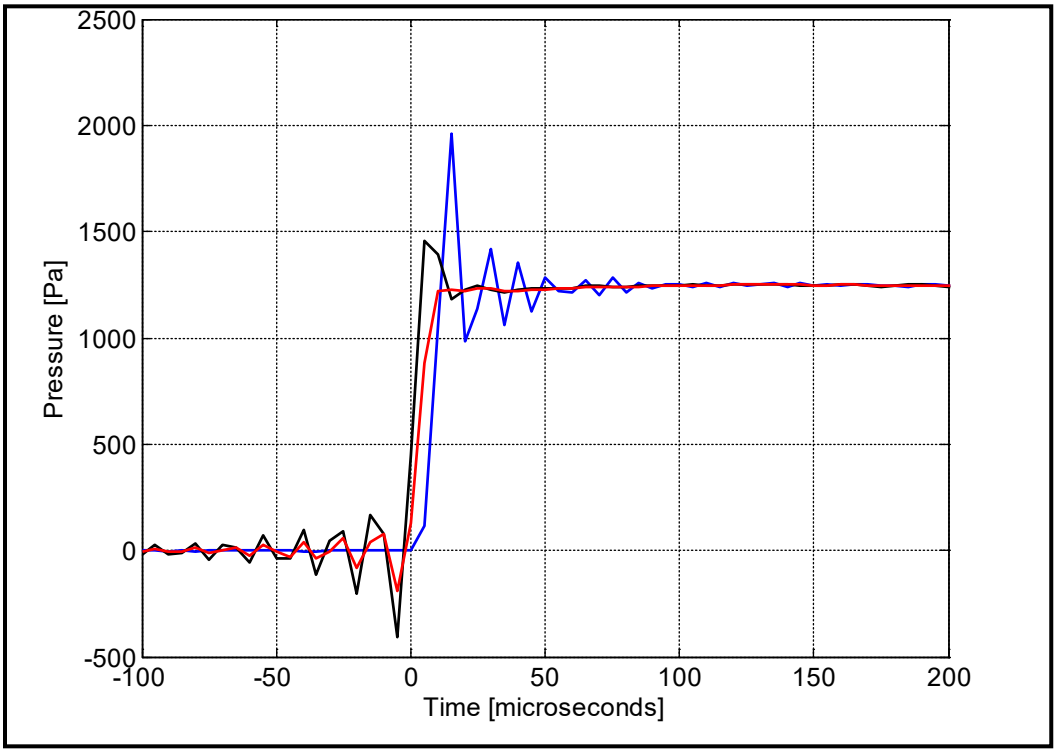

Figure 27. The diffraction-corrected waveform from the previous figure is shown here in red. The blue curve is the output of the ¼-in. microphone in the 90-degree orientation; the black curve is the output of the ⅛-in. microphone in the 90-degree orientation. These latter two curves have been corrected for the anti-aliasing filter ripple. The rise time indicated here is between 5 and 10 microseconds, which is the limiting rise time for this data acquisition system.

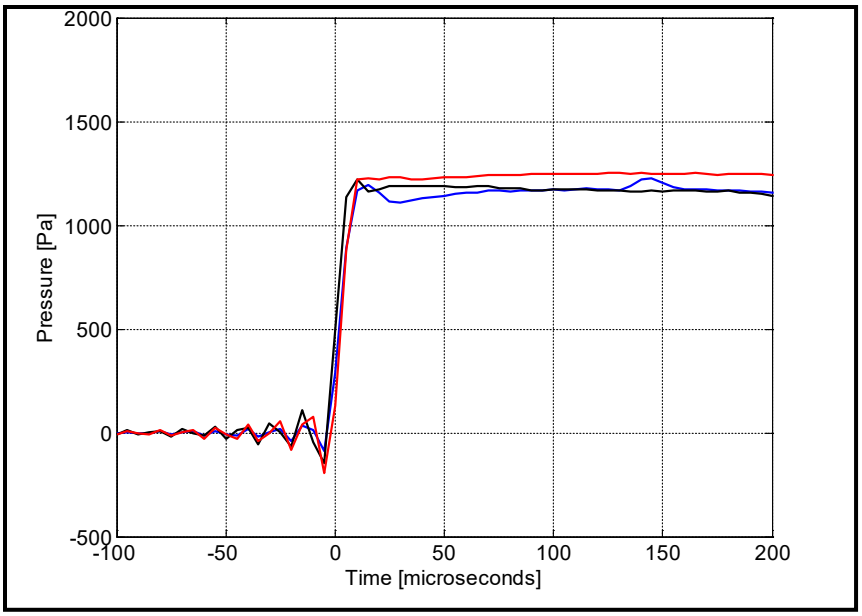

The ¼-in. microphone in the zero-degree orientation shows a considerably higher diffraction overshoot as shown in the Figure 26. Keep in mind that the diffraction overshoot is a narrow peak in time so the appearance of this peak depends on the location of the sample points with respect to the actual peak; at 200 kS/s, the sample points are 5 microseconds apart. Also, the diffraction peak near 90 kHz for the ⅛-in. microphone is above the anti-aliasing filter roll-off so the overshoot is suppressed compared to that of the ¼-in. microphone. The consistency of the corrected results between Figures 24 and 26 serves to illustrate the tolerance of the diffraction-correction algorithm to relatively sparse sampling.

Overall, the diffraction and ripple corrections are successful with respect to representation of the pressure rise in the vicinity of the shock front, which is the most challenging part of the waveform to record accurately. For comparison, Figures 27 and 28 show the corrected waveforms from four sensors (¼-in. at zero degrees, ⅛-in. at zero degrees, ⅛-in. at 90 degrees, and ¼-in., in a 10-cm baffle) for a single shot. The output of the baffled microphone is corrected for ripple, but then simply divided by two. (The following section discusses baffling). Figure 27 shows enough of the waveform to include the pressure drop in the baffled-microphone waveform and Figure 28 expands the plot in the vicinity of the arrival of the shock front.

Figure 28. Diffraction and ripple corrections applied to the waveform from a ¼-in. (B&K 4938) microphone oriented at zero degrees. The raw waveform is the blue curve. The black curve is the result of applying the Butterworth transient-correction filter; the positive peak that remains is the result of microphone diffraction. The red curve is the result of applying the diffraction-correction filter. The result is similar to that for the ⅛-in. microphone except that the rise time is slower here commensurate with the reduced bandwidth of the ¼-in. microphone.

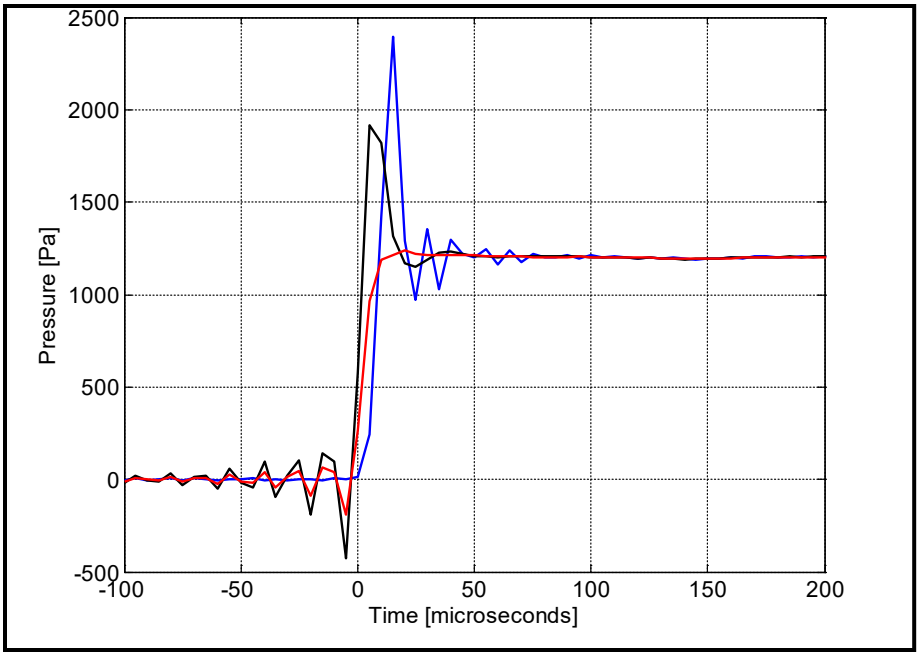

Figure 29. Comparison of the corrected outputs from four sensors for the same C4 blast. Shown are the ¼-in. microphone at zero degrees (blue), the ⅛-in. microphone at zero degrees (red), the ⅛-in. microphone at 90 degrees (black), and the ¼-in. microphone in a 10-cm baffle (dashed red). All of the outputs have been corrected for anti-alias filter ripple; the zero-degree microphones have also been corrected for diffraction. The output of the baffled microphone was not diffraction corrected; that output was divided by two.

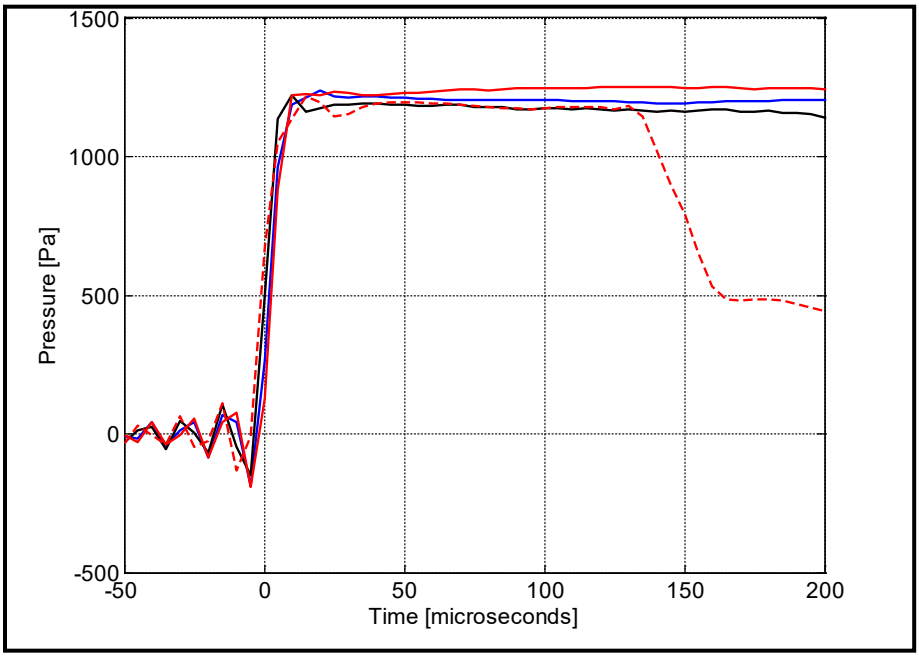

Figure 30. Corrected waveforms from Fig. 27 plotted on an expanded time scale to show the rise-time detail. Shown are the ¼-in. microphone at zero degrees (blue), the ⅛-in. microphone at zero degrees (red), the ⅛-in. microphone at 90 degrees (black), and the ¼-in. microphone in a 10-cm baffle (dashed red). The rise time is, in all cases, limited by the data-acquisition system response.

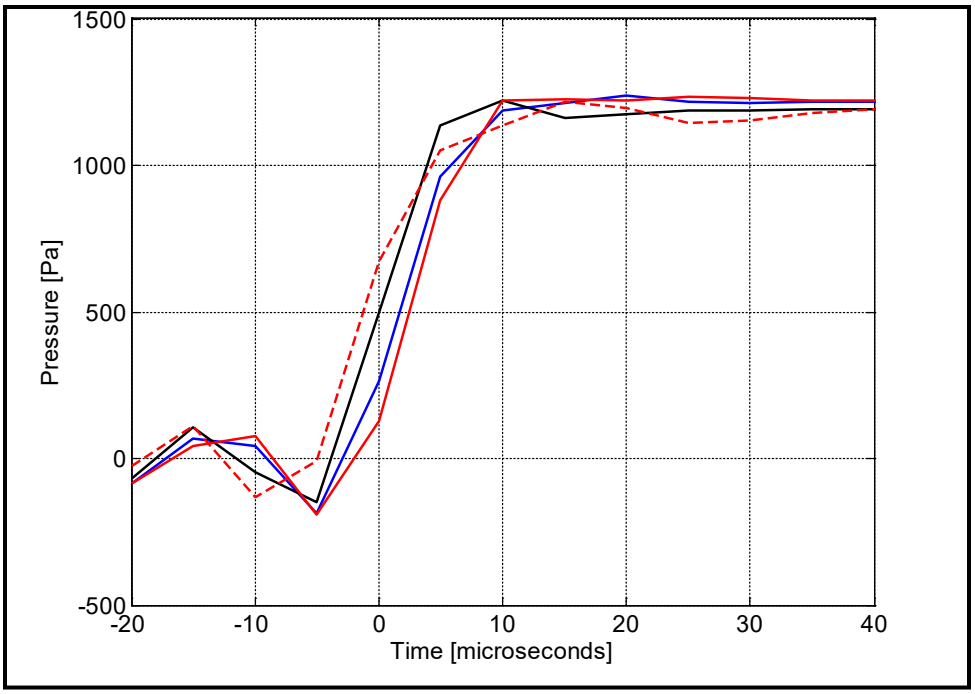

After correction, all of the waveforms are similar in their representation of the pressure rise at and after passage of the shock front. The peak-pressure estimates are reasonably close even though the sensors are several meters apart (but roughly in a plane perpendicular to the direction to the blast so the ranges are similar). The expanded-scale plot in Figure 28 shows agreement in rise time although, in all cases, the rise time is limited by the data-acquisition system.

Since the 90-degree orientation does not produce the large diffraction overshoot, it is natural to consider the 90-degree orientation for all measurements of shocks if pressure microphones are used.* In some respects, 90-degree orientation of a pressure microphone is preferable to zero-degree orientation of a free-field microphone. For example, the microphone protection grid can be left on in the 90-degree orientation with relatively little waveform disruption, whereas, leaving the protection grid on a free-field microphone in the zero-degree case generates substantial artifacts in

* In principle, a "free-field" microphone allows operation in the zero-degree orientation without diffraction overshoot; however, the widest bandwidth measurement microphone commercially available is the ⅛-inch microphone, which is not available in a free-field model. If the bandwidth of a ¼-in. microphone is acceptable then the free-field version can be used to advantage (although, in the zero-degree orientation, the protection grid must be removed to avoid artifacts).

the waveform. If diffraction were the only consideration, there would be little reason to use free-field microphones for these measurements; however, the 90-degree orientation introduces a geometrical effect on the apparent rise time. In the 90-degree orientation, the shock front passes along the surface of the microphone diaphragm; this passage takes time. Figure 29 shows the effective pressure produced by the passage of a pressure step.

Translating this transit time to effective rise times shows that, in the 90-degree orientation, the rise time estimate would be no shorter than 5 microseconds for a ⅛-in. microphone, 10 microseconds for a ¼-in. microphone, and 20 microseconds for a ½-in. microphone. The minimum rise time for the ½-in.-diameter sense element in a blast pencil would be 26 microseconds. Notice that, for the TEAC GX-1 instrumentation recorder running at its maximum sample rate (200,000 samples per second) and an 80-kHz anti-aliasing filter, rise times shorter than 5 microseconds cannot be distinguished so the ⅛-in. microphone in the 90-degree orientation would be acceptable.

Figure 31. Effective acoustic pressure on a sense element oriented at 90 degrees to an incoming step function in pressure as that step sweeps across the sensor face. For a membrane-based transducer (a measurement microphone), the pressure follows the red curve as the pressure step progresses across the circular membrane. The 10 to 90% rise time would equal 1.1 times the radius over the sound speed. For a disk transducer (a piezoelectric blast pencil, for example), the rise is somewhat slower because the disk element is equally sensitive across the entire diameter. In that case, the rise time would be 1.4 times the radius over the sound speed.

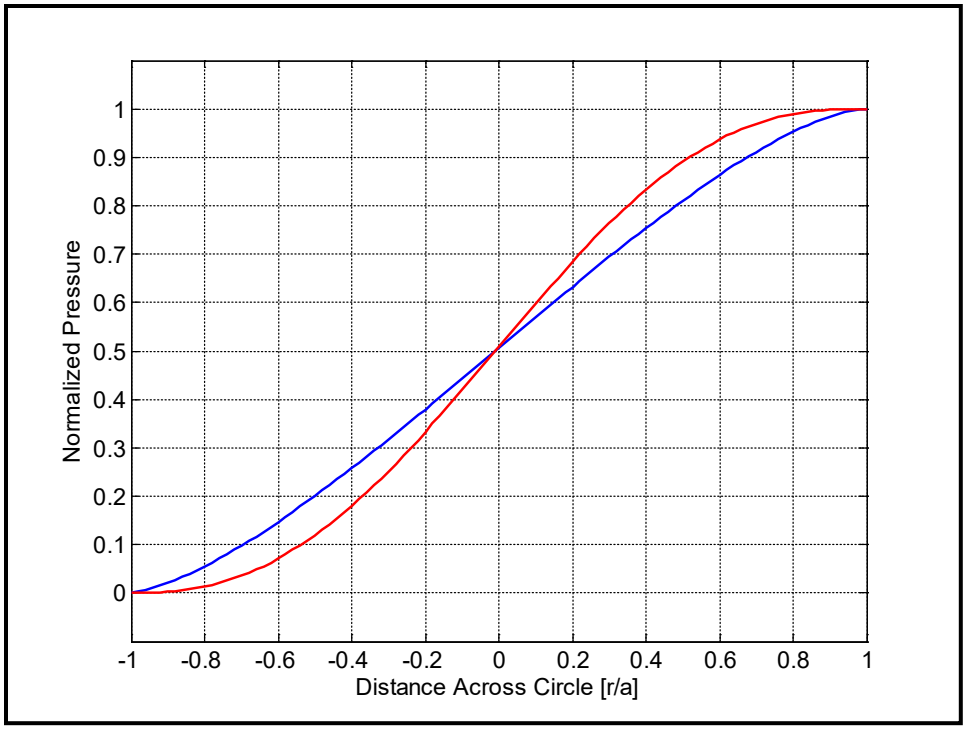

5.2 Baffles

Another approach to accurate measurement of rise time and peak pressure is to augment the microphone with a "baffle." In the acoustical sense, a baffle is a rigid surface into which the sense element is inserted. A baffle of infinite extent would produce twice the free-field pressure* independent of frequency. A sensor in a very large baffle oriented at zero degrees would not show any diffraction artifacts (except for simple pressure doubling). There are practical limits to the size of useful baffles. Particularly for outdoor measurements (often elevated meters above the ground), one must account for the wind force exerted on a large flat surface and the large total weight in mounting the sensor to a tower and in securing the tower.

For a baffle of finite dimensions, the pressure doubling is effective until the wave diffracted from the edge of the baffle reaches the sense element. If, for example, a small-diameter microphone is mounted at the center of a 10-cm (4-in.) circular disk, then the edge-diffracted wave reaches the microphone about 150 microseconds after the direct wave. The first 100 or so microseconds of the waveform will simply show a doubling in effective acoustic pressure, but at about 150 microseconds the waveform may depart dramatically from the free-field waveform. If one were only interested in the rise time and peak pressure, this corruption of the waveform after the edge wave arrives may be of little consequence.

It is often suggested that, by making the shape of the baffle irregular, the edge-wave arrival can be spread out in time thereby minimizing the impact on the waveform. While this has some merit, the irregular baffle boundary does not eliminate the transition from simple pressure doubling to edge-wave interference; the irregular baffle merely smoothes the transition from pre-edge-wave to post-edge-wave. There is still a marked effect on the waveform; the effect is simply more abrupt for the circular baffle (with sense element at the center).

One advantage to the symmetric geometry – a sense element at the center of a circular baffle – is that prediction of the effects is straightforward and, therefore, the effects can be removed with a suitable correction filter. The theory for the circular baffle is virtually identical to that for diffraction by

* For high peak pressures, this pressure doubling might push the microphone far enough into nonlinearity to introduce significant errors into the waveform. Then again the published 3 percent distortion limit for the B&K 4938 ¼-in. pressure microphone is 6 dB higher than it is for the B&K 4135 ¼-in. free-field microphone, which implies that use of a baffle with the pressure microphone would not introduce additional distortion compared to the free-field microphone without a baffle.

the flat end of a cylindrical microphone except that the small active area of the baffle configuration means that very little spatial averaging occurs. Consequently, the diffraction response function for the circular baffle is more complicated. Figure 30 shows the magnitude and phase of the diffraction function for a ¼-in. microphone flush mounted at the center of a 10-cm circular baffle.

The response is similar in appearance to a Fresnel-integral function, which is not surprising since Fresnel-like functions arise in diffraction problems. With increasing frequency, the pressure distribution on a circular disk becomes increasingly complicated. The active region of the sense element, in effect, performs a spatial average of that surface field. For the unbaffled microphone, almost the entire disk area is averaged and that results in a diffraction response with only a single dominant peak. In contrast, for the baffled microphone, the active area is a small portion of the disk area near the center so the degree of spatial averaging is much less. This appears as an increase in complexity – many more peaks in the magnitude – of the diffraction response. The peaks taper slowly as the active region approaches a wavelength in radius.

Figure 32. Magnitude and phase of diffraction response for ¼-in. microphone in a 10-cm (4-in.) circular baffle. The function is considerably more complicated than the diffraction response for the unbaffled microphone. In this case, the baffle produces a complicated pressure field that is only sampled over a small, central region so there is much less spatial averaging than when the active region of the sensor covers most of the diffraction-disk area.

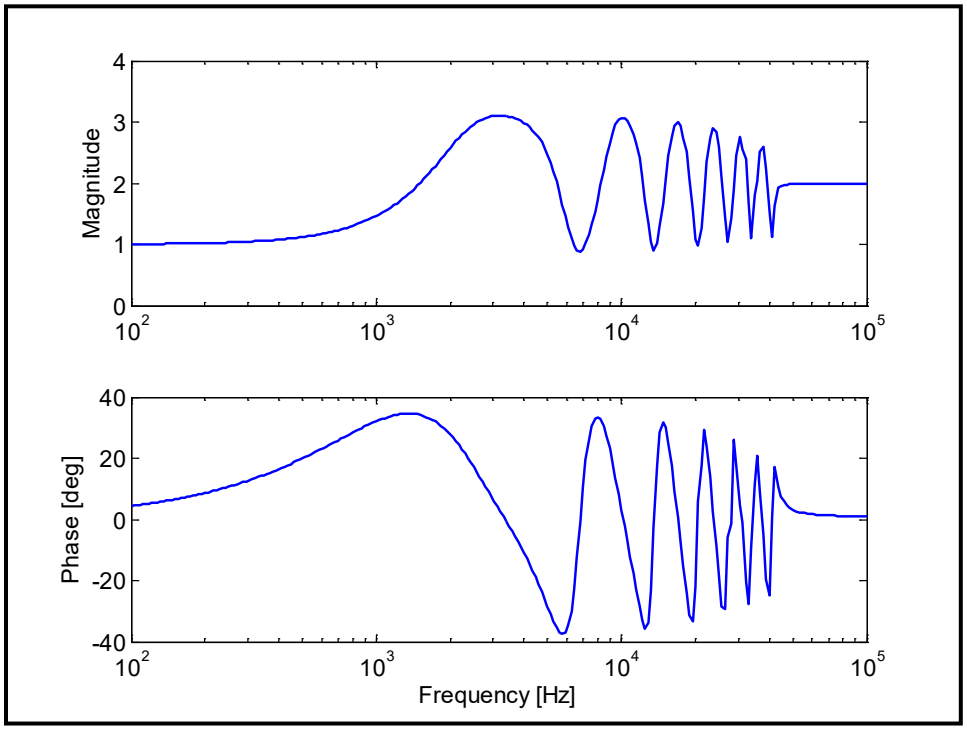

The diffraction response shown in Figure 30 is artificially tapered beyond 45 kHz. The actual oscillations continue to decay at a slower rate, but this contributes little to the accuracy of a correction filter.

As before, the examination of baffle-correction filters is begun using laboratory-generated free-field shocks. The baffle used in this study (Figure 31) can be converted to accept ½-in., ¼-in., or ⅛-in. microphones although only the results from ¼-in. microphones are reported here.

For the laboratory shocks, a ⅛-in. reference microphone oriented at 90 degrees was positioned a few centimeters above the baffle and in the same plane as the front surface of the baffle. Figure 32 shows the results from one test in this configuration. The red curve is the output of the ¼-in. microphone in the baffle. The large negative-pressure peak at about 150 microseconds is the arrival of the edge-diffracted wave at the central microphone position. The 90-degree reference microphone waveform is shown in blue and the result of filtering the red curve with a diffraction-correction filter based on the 10-cm baffle diameter and a 6.3-mm (¼-in.) central active region is shown in black. Removal of the edge-wave effects is almost complete.

Figure 33 shows the same waveforms as in Figure 32, but on an expanded time scale to show the leading-edge details. The diffraction-correction filter removes the diffraction overshoot while preserving the rise time.

Figure 33. Ten-centimeter (4-in.) circular baffle for ¼-in. microphone. The microphone is inserted (with its protection grid removed) into the gray PVC sleeve and secured with its diaphragm flush with the surface of the baffle. The diameter of the exposed portion of PVC on the baffle's front surface is 19 mm.

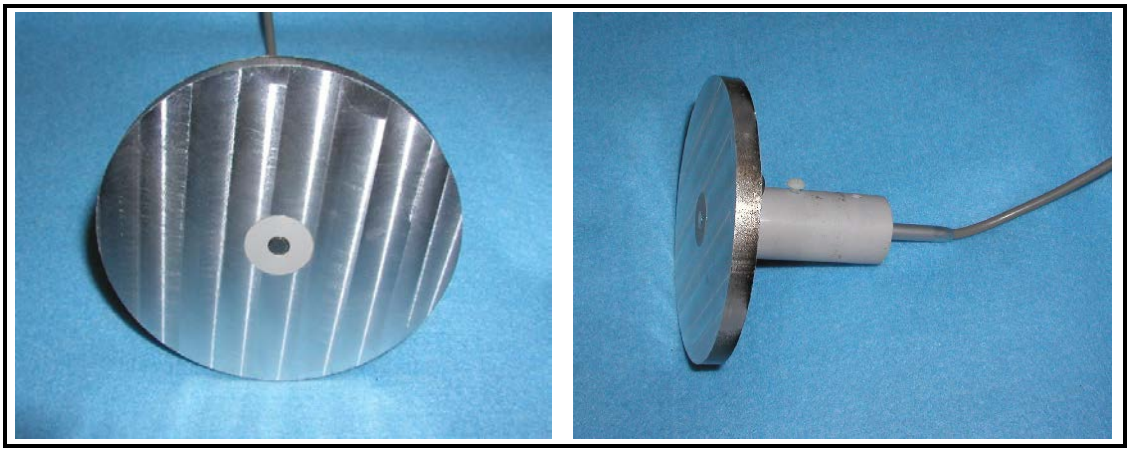

Figure 34. Measurement of a laboratory-generated free-field shock with the 10-cm circular baffle and ¼-in. microphone (red). The blue curve is the waveform from a reference ⅛-in. microphone oriented at 90 degrees. The black curve is the result of a correction filter applied to the waveform from the baffled microphone.

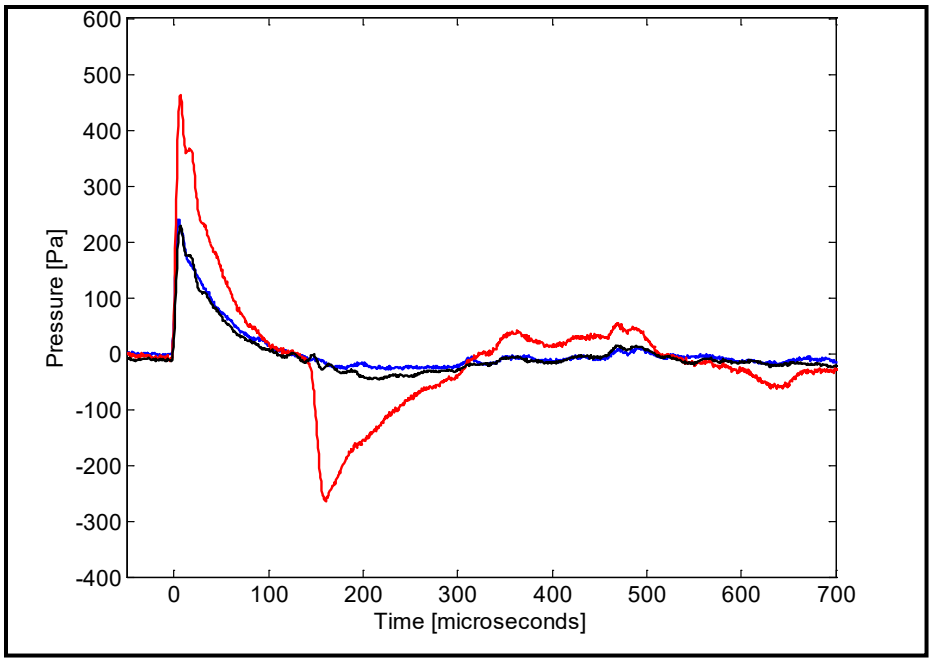

Figure 35. Expanded view of the waveforms from Fig. 30. The corrected, baffled waveform (black) and the 90-degree reference waveform (blue) give consistent estimates for peak pressure. The rise time indicated by the corrected, baffled waveform is slightly longer than that of the 90-degree reference (because the 90-degree reference is a ⅛-in. microphone); however, the 5 microsecond rise time indicated by the baffled ¼-in. microphone is considerably shorter than the theoretical limiting value for the ¼-in. microphone in the 90-degree orientation (about 10 microseconds). The ripple in the baffled-microphone waveform is likely associated with the 19-mm central PVC adapter plug in the baffle.

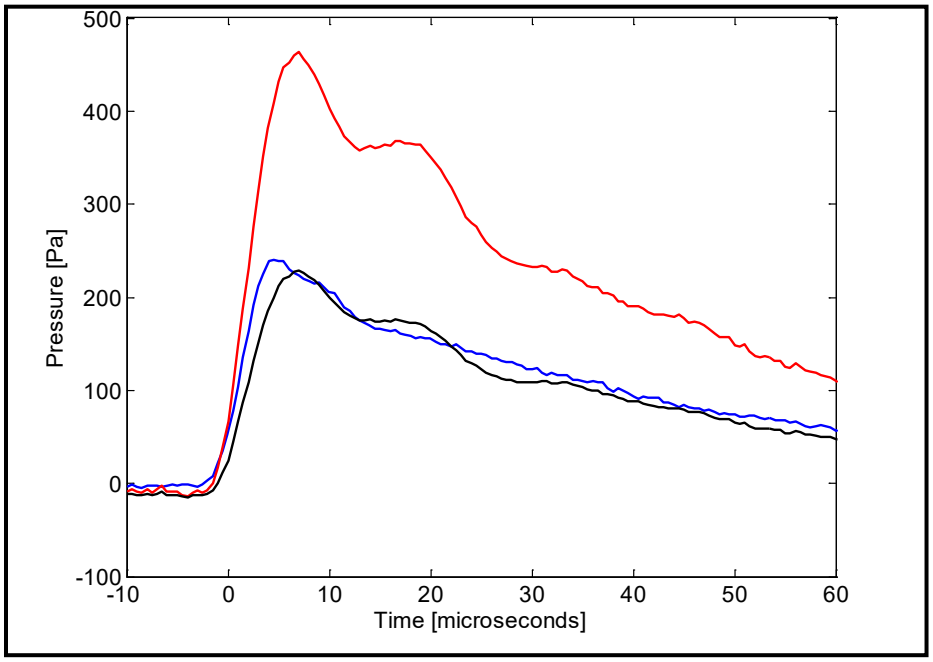

The principal advantage of the baffle is simplicity in interpretation of the waveform for times prior to arrival of the edge wave. This is illustrated in Figure 34, in which the waveform from the baffled microphone is simply divided by two (red) rather than being corrected for diffraction. Compared to the full diffraction correction applied to the baffled waveform (black), the two curves are virtually identical until the edge wave arrives.

The laboratory shocks used above have much lower total energy than the field-measured C4 shocks (even when the peak pressure is the same). Consequently, the laboratory waveforms decay more rapidly after the shock front with exponential time constants ranging from 50 to 200 microseconds – the decay time constants for the C4 shocks range from 2 to 4 milliseconds. The edge wave from the 10-cm circular baffle arrives at the microphone element 150 microseconds behind the direct arrival; consequently, the apparent inverted "reflection" arrival appears in the waveform after the pressure has dropped to near zero in the laboratory measurements. By contrast, for the C4 waveforms, the edge wave arrives before the initial pressure has dropped very far (Figures 34 and 35).

Figure 36. Comparison of two methods of correction of waveforms from a baffled microphone. The black curve is the full diffraction-correction filter applied to the output of the baffled microphone. The red curve is the baffled-microphone output divided by two. The waveforms are virtually identical until 150 microseconds – the time of arrival of the edge-diffracted wave from the baffle. As in Fig. 35, the blue curve is the output of the ⅛-in. reference microphone.

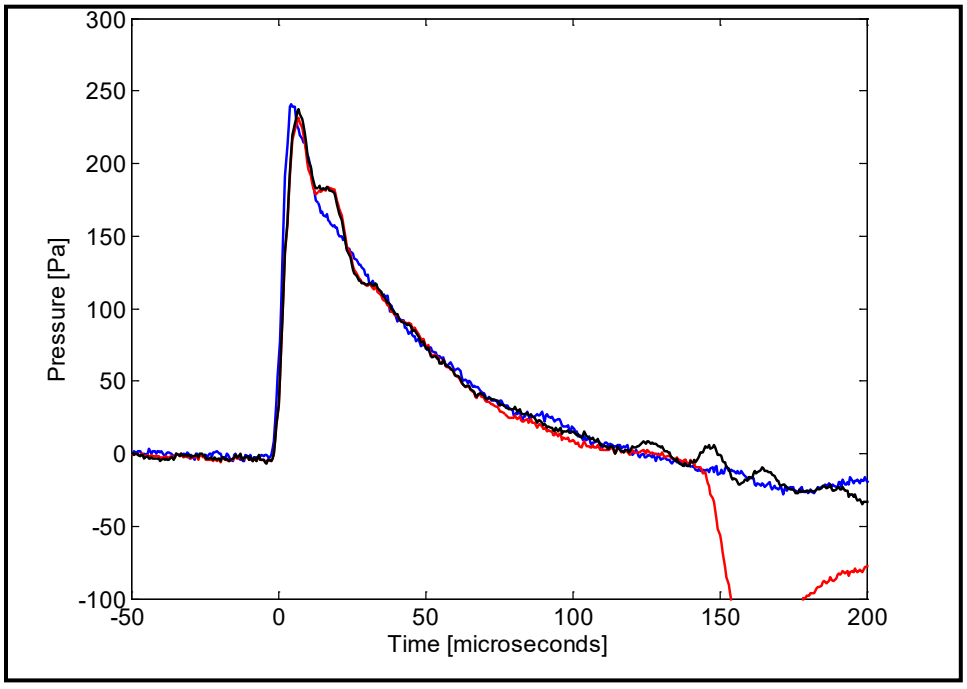

Figure 37. Waveforms from a 0.57 kg C4 explosion at 52 m. The red curve is the output of a ⅛-in. microphone at 90-degree orientation. The blue curve is the output of the baffled ¼-in. microphone divided by two. The ground-reflected arrival appears at about 1.2 milliseconds for the baffled microphone and at about 3.2 milliseconds for the ⅛-in. microphone. (The ⅛-in. microphone was mounted several meters higher than the baffled microphone so the ground-reflected arrival appears later.) The edge wave for the baffled microphone interferes with the direct arrival after about 0.15 milliseconds causing the sharp drop in the apparent pressure for the baffled-microphone output.

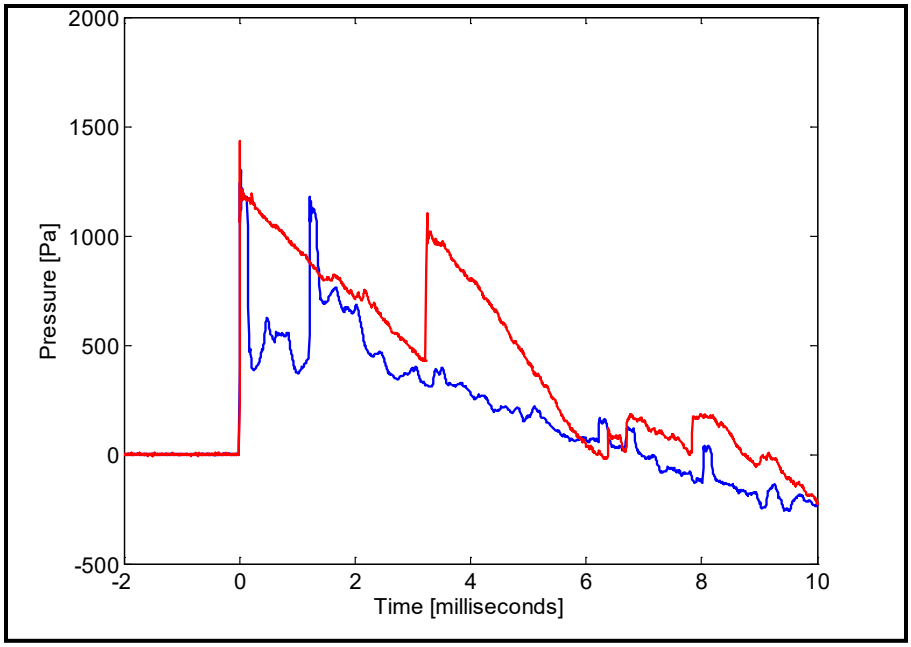

Figure 35 shows the output of the baffled ¼-in. microphone (blue curve) and a 1/8-in. reference microphone (red curve) for a C4 explosion. The baffled output (shown divided by two) only tracks the reference waveform for the first 100 microseconds or so.

Figure 36 shows the result of applying the diffraction-correction filter. The diffraction-corrected waveform is not as clean as the result obtained for the laboratory shocks. There are two factors that may contribute: (1) for the field measurement, another 10-cm baffle was mounted about 10 cm from the first one in the same plane thereby generating additional scattering, and (2) alignment of the baffle perpendicular to the direction of arrival was more difficult on the tower used in the field measurement. Nevertheless, the diffraction-correction filter produces a reasonable approximation of the entire waveform while preserving the rise time and the peak pressure accuracy of the baffled microphone. If the only parameters of interest are the peak pressure and rise time, then the waveform (divided by two) from the baffled pressure microphone presents a simple and accurate solution. As for the unbaffled microphone at zero degrees, the protection grid must be removed to gain acceptable results in the baffle.

Figure 38. Waveforms from the previous figure shown with an expanded time scale. As before, the red curve is the output of a ⅛-in. microphone at 90-degree orientation and the blue curve is the output of the baffled ¼-in. microphone divided by two. The black curve is the result of applying the diffraction-correction filter to the blue curve. (The ringing just after the initial shock front is the anti-aliasing filter artifact discussed earlier.)

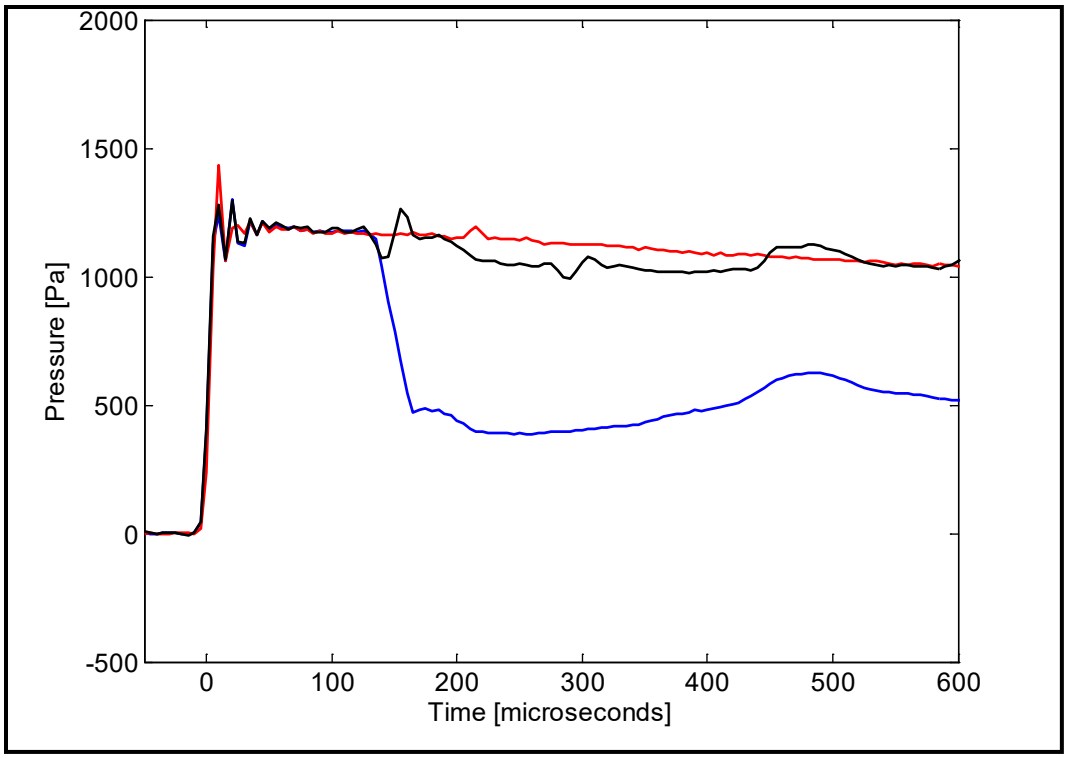

6 Observations and Discussion

6.1 Observations of nonlinearity

Several ½-in. microphones were included in the C4 field measurements to exaggerate the effects of microphone nonlinearity. Peak pressures up to 2000 Pa for the C4 explosions at 50 m do not have obvious nonlinear distortion with either the ¼-in. or the ⅛-in. microphone, but the ½-in. microphone shows significant distortion for peak pressures of more than 100 Pa. Figure 37 shows the nonlinearity in response for the ½-in. condenser microphone for laboratory-generated shocks. The ½-in. free-field microphone (GRAS 40AE) was used with a 20-dB attenuator and the output of the microphone (at zero-degree orientation) was compared to the output of a ¼-in. (B&K 4938) microphone at 90-degree orientation (since the 4938 is a pressure microphone) for a number of peak pressures. Both microphone outputs were low-pass filtered at 9 kHz so that the resultant bandwidths were equivalent. Then the two outputs were plotted after normalizing the pressure by the peak value of the ¼-in. microphone. This assumes that nonlinearity in the ¼-in. microphone can be neglected compared to the nonlinearity in the ½-in. microphone. The results for six different peak pressures (80, 240, 480, 900, 1300, 1750 Pa) are shown below.

The usual specification for microphone nonlinearity is a sound pressure level for 3% distortion. However, this specification does not relate directly to a time-domain waveform. This distortion value is determined by the level of harmonic distortion with a steady sinusoid at the specified level. For example, the 3% distortion level for the GRAS 40AE is 148 dB (relative to 20 micropascals rms) or 500 Pa-rms. In the time-domain comparison above, a level of 480 Pa-peak produces an underestimate of the peak pressure by a few percent compared to the reference ¼-in. microphone, but the distortion becomes noticeable for the 240 Pa case. Of more significance is the observation that the waveform from the ½-in. microphone crosses over the "true" pressure after about 80 μs and remains above the reference waveform. For the 900-Pa example, the ½-in. waveform is 10% low at the peak, but after the crossover, is 20% or more high. If the pressure were to decay more slowly (as for the C4 explosions), then the ½-in. waveform may produce a significant overestimate for peak pressure (and a corresponding overestimate of rise time). This is apparent in Figure 38.

Figure 39. Comparison of ½-in. (with 20 dB attenuator – red curves) and ¼-in. microphones (blue curves) for high peak pressures. The peak pressures are (from left to right, row by row) 80, 240, 480, 900, 1300, 1750 Pa. There is a 10% drop in apparent amplitude for a peak pressure of 900 Pa and a 20% drop in amplitude with considerable waveform distortion for a peak pressure of 1750 Pa.

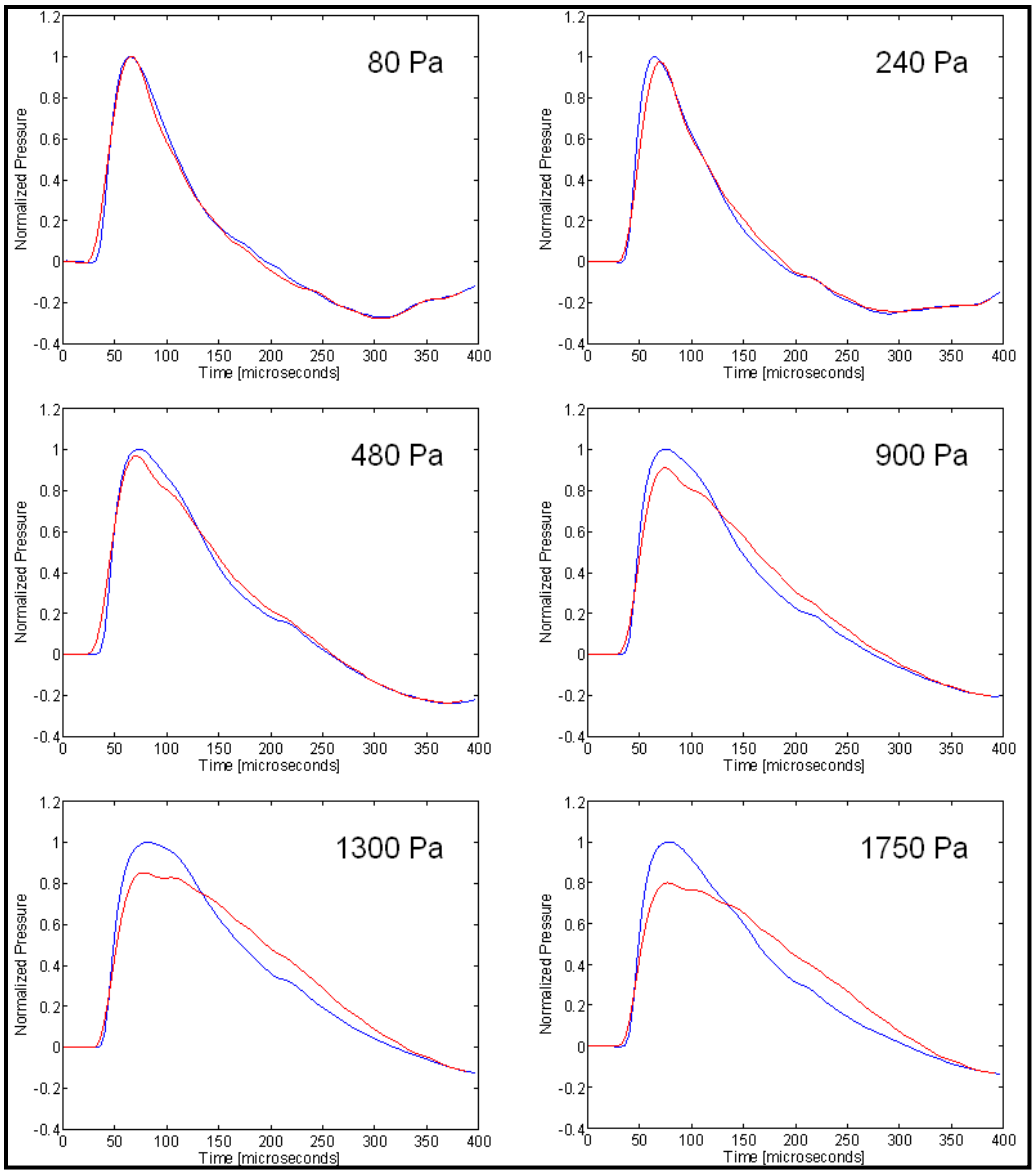

With regard to the nonlinearity in the microphone response, peak pressure is not the only critical parameter, the total energy in the input pulse is important also. Laboratory measurements can replicate the rise time and peak pressure of the C4 explosions, but the laboratory-generated shocks have far less energy so they decay considerably faster. For a peak pressure of about 500 Pa, the amplitude error for a laboratory shock was 10% low. Figure 38 shows the response of the ½-in. microphone in the same configuration (zero-degree orientation; 20 dB attenuator) to a C4 shock (⅛-stick) with a peak pressure of about 500 Pa.

Figure 40. Comparison of ½-in. (with 20 dB attenuator – red curves) and ⅛-in. microphones (blue curves) for high peak pressure from a C4 explosion. The apparent peak of the distorted (red) curve is about 30% higher than the actual peak pressure. The greater energy in this acoustic pulse produces a considerably different distortion than in the previous figure in which the distorted output indicated a peak pressure 10% lower than actual.

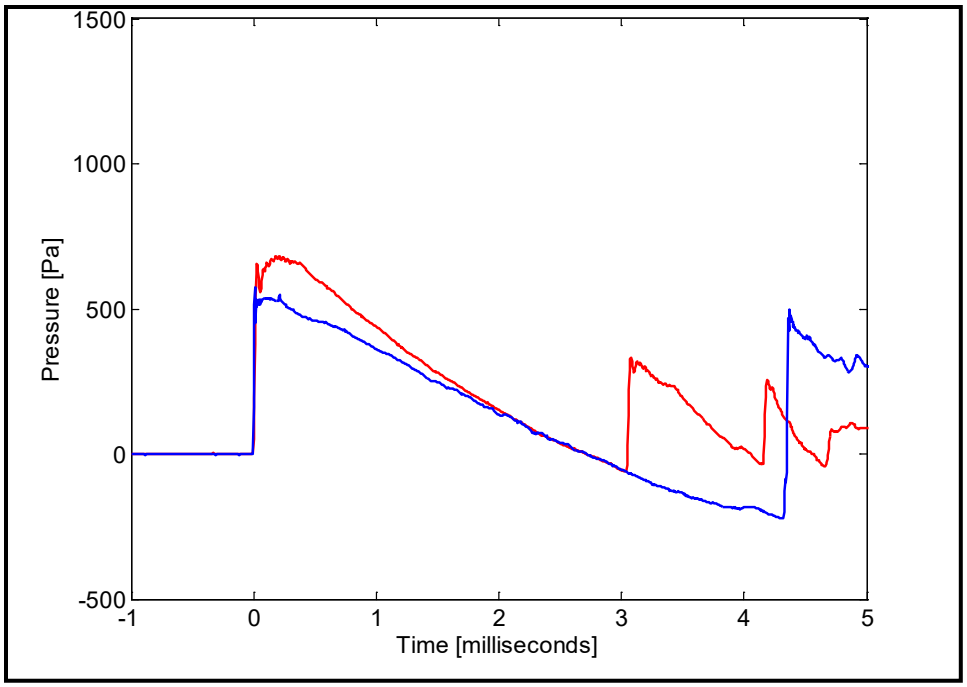

In the above example, the crossover occurs so early in the waveform that it is not apparent on the scale of the figure. The ½-in. record would lead to an *overestimate* of peak pressure of about 30%. Furthermore, the rise time estimate from the distorted waveform would be much too long.

It would be dangerous to make a general statement regarding condenser microphone nonlinearity based solely on these observations of nonlinearity in the ½-in. microphone; however, the results above indicate that the 3% distortion specification commonly given for condenser microphones should not be interpreted as a 3% amplitude error in a peak-pressure measurement. The amplitude and rise time errors can be quite large for a peak pressure corresponding to the 3% distortion specification.* This distortion specification is not based on amplitude errors for sharp pulses; it is based on harmonic generation by sinusoidal signals.

While these results should be interpreted with caution, the shape of the distortion is particularly interesting. The apparent peak is lower in level than it should be, but the decay rate is slower, and the decay curve, rather

* The 3-percent distortion pressure for the GRAS 40AE is about 500 Pa-rms. For comparison, the 3-percent distortion pressure for the B&K 4938 (¼-in. pressure microphone) is about 8000 Pa-rms.

than being roughly exponential, is convex. This shape might be useful as a diagnostic tool for nonlinearity in time-domain blast-wave measurements for which there may be no undistorted reference waveform.

6.2 Wideband microphone and rise-time measurements

As discussed in Appendix G, an expression can be written for the product of rise time and peak pressure. For combined classical absorption and rotational relaxation, which should represent the minimum theoretical rise time, this product is:

$$t_{rise} \cdot p_{pk} = 0.15 \times 10^{-3} \left(\frac{T}{T_0} \right)^{1/2} \left(\frac{P_0}{P} \right) \qquad [\mathrm{Pa \cdot s}] \tag{14}$$

where:

T is the absolute temperature
P is the ambient atmospheric pressure
T_0 is the reference temperature (293.15 °K, which is 20 °C)
P_0 is the reference pressure (101325 Pa).

For shocks with peak pressures from 100 to 1000 Pa, the rise times could fall in a range as low as 1.5 to 0.15 microseconds.

If frequencies are sufficiently low (and humidity is sufficiently high) for vibrational relaxation of oxygen to be important, then the following expression should be used:

$$t_{rise} \cdot p_{pk} = 2.30 \times 10^{-3} \left(\frac{T}{T_0} \right)^{1/2} \left(\frac{P_0}{P} \right) \qquad [\mathrm{Pa \cdot s}] \tag{15}$$

Preliminary evidence suggests that this additional component is not significant for the peak pressures from C4 explosions in this investigation and for the range of humidity encountered in typical field measurements. Appendix G addresses nitrogen vibrational relaxation, but that mechanism is almost certainly negligible for the sorts of shocks considered here.

A recently developed wide-bandwidth sensor has been constructed specifically to resolve rise times of a few tenths of a microsecond. Several mechanisms can limit resolution of rise time in such a sensor:

- amplifier bandwidth
- mechanical resonance
- amplifier slew rate
- sensor tilt.

This sensor consists of a 16 by 16 mm square of 52 μm-thick PVDF (polyvinylidene difluoride, a piezoelectric polymer) bonded to the end of a 38-mm diameter cylindrical aluminum housing. The first thickness resonance of the PVDF should be about 10 MHz. The signal is amplified by a two OPA228-based non-inverting amplifier stages, the first with a voltage gain of 11, the second with a voltage gain of 7. The gain-bandwidth product of the OPA228 is 33 MHz so the bandwidth is limited to 3.3 MHz by the first stage. The ideal 10 to 90% rise-time resolution for step-function input* to a system with a single-pole low-pass characteristic frequency, f_1, is:

$$t_{rise} = \frac{2.2}{2\pi f_1} \tag{16}$$

For f_1 = 3.3 MHz, the theoretical rise-time resolution would be limited to no less than 0.11 μs.

The thickness-mode response coefficient for the PVDF film is 0.33 volts per meter of thickness per pascal of applied pressure. For the 52 μm-thick film, the intrinsic voltage response is about 17 μV/Pa. At the output of the second stage amplifier (after a total voltage gain of 77, that is), the response would be 1.3 mV/Pa. The OPA228 has a 10V/μs slew rate, which translates to 7700 Pa/μs at the output of the second stage. Consequently, a peak pressure of 1000 Pa would require 0.13 μs to slew the second-stage amplifier regardless of the actual pressure rise time.

For resolving sub-microsecond rise times, sensor orientation becomes critically important. A slight tilt with respect to the incoming shock front can artificially lengthen the apparent pressure rise. If the sensor disk is not parallel to the shock front, but is tilted by an angle, ϕ, then the front appears to sweep across the face of the sensor with a phase speed of $1/\sin\phi$ times the ordinary sound speed, c. Adapting the equation derived earlier for the effective rise time for a sensor face of radius, a, oriented perpendicular to the wave front (which would be equivalent to the ϕ = 90-degree case), the apparent rise time for an ideal step function is then:

$$t_{rise} = \frac{1.4\, a \sin\phi}{c} \tag{17}$$

* Determined from the Laplace-transform solution for step-function input to a simple resistor-capacitor low-pass filter.

Taking a = 9 mm (the radius that gives the same area as the square element of this sensor), the rise time of an ideal step function would appear to be 0.1 μs for a tilt of only 0.16 degrees. This is equivalent to a path misalignment of only 2.5 mm per meter.

This new wideband sensor was evaluated with balloon-burst shocks in the laboratory for peak pressures ranging from 20 to 1000 Pa. The sensor face was aligned with respect to the shock-tube axis using a laser that was bore-aligned with the shock tube. The sensor was mounted in a fixture that permitted adjustment of both horizontal and vertical angle and those adjustments were made until the reflection from the sensor face was within a centimeter of the outgoing beam. At the shortest test distance (1.3 m from the exit end of the shock tube or 2.6 m round trip for the alignment laser), this maintained the tilt error to less than 0.25 degrees or a limiting rise time of 0.15 μs. The shortest test distance represents the worst case for angular misalignment.

Figure 39 shows these measurements. The peak pressure was measured using a ⅛-in. pressure microphone in the 90-degree orientation; the wideband sensor was used only for the rise-time determination. The classical-plus-rotational absorption model (Equation 13) presents a reasonable lower bound to these measurements, whereas the addition of oxygen vibrational relaxation (Equation 14) predicts rise times considerably slower than observed. This supports the view that vibrational relaxation of oxygen (and certainly of nitrogen as well) should not be accounted for in a model for shock rise time at least for peak pressures greater than a 100 Pa, and that Equation 13 may be a reasonable lower bound for shock rise times.

The measured points show the same slope as the classical-plus-rotational model for rise times as short as 0.5 μs. The measurements for peak pressures near 1000 Pa show slower rise times than would be expected if the trend continued to these pressures. While individual rise-time limits by various mechanisms in the sensor do not strictly add up, an overall rise-time limit of 0.3 to 0.4 μs would not be unreasonable for this sensor so the 1000-Pa measurements may have reached the sensor limits; both angular misalignment and slew-rate limitations are of more consequence for the shorter-range, higher-amplitude measurements.

Figure 41. Measured rise times (red symbols) for shock waves from balloon bursts and the 3-m shock tube using the PVDF wideband microphone. Measurements were made at five distances from the exit end of the shock tube: 10.7 m, 7.6 m, 4.6 m, 2.4 m, and 1.3 m. The variation in pressure from individual balloon bursts spreads the clusters at any one distance. Predicted rise times according to classical-plus-rotational absorption (solid black curve, Equation 13), classical/rotational/oxygen-vibrational (black dashed curve, Equation 14) are also shown. The temperature in the laboratory was 20 °C, local atmospheric pressure was 97500 Pa, and the relative humidity was 60%.

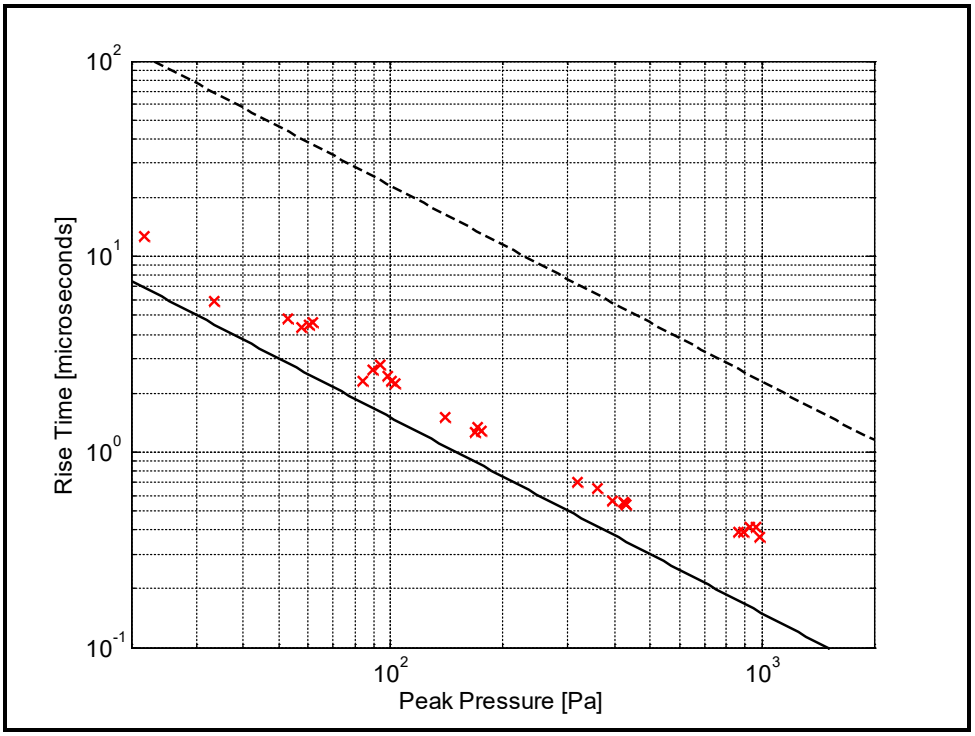

The next step in the development will be to replace the OPA228 with a faster amplifier. The rise-time limit will then be associated principally with misalignment although it is possible at the shorter ranges that there may be sufficient wave front curvature to further limit rise-time resolution. The effects of angular misalignment and wave front curvature can be reduced by using a smaller-diameter sense element.

For comparison, Figure 40 shows the data from Stoughton (1997) along with the measurements and model curves from Figure 39. Stoughton published measurements of shock-wave rise times for the Mach cones from supersonic bullets. He measured peak pressures at four distances: 520 Pa at 3.2 m, 220 Pa at 10 m, 120 Pa at 29 m, and 75 Pa at 53 m. Stoughton's equipment was capable of sub-microsecond resolution although his measurements were made outdoors (40 °C, no record of humidity) and may show the effects of turbulence at the longer ranges. The measurements from Figure 39 were made indoors at distances less than 11 m.

Figure 42. Measured rise times (blue symbols) for outdoor shock waves from supersonic-bullet Mach cones from Stoughton (1997) plotted with the results of Fig. 41 (red symbols – 60% relative humidity). Stoughton's measurements (unknown humidity) were made at 53 m, 29 m, 10 m, and 3.2 m corresponding to the blue circles from left to right. The two higher-amplitude points compare well to the rise times measured with the PVDF microphone. The rise-time increase for the two leftmost blue circles may indicate smearing from turbulence; however, this sort of transition has the same shape as that predicted by Bass, et al. (2002) when oxygen vibrational relaxation begins to become significant.

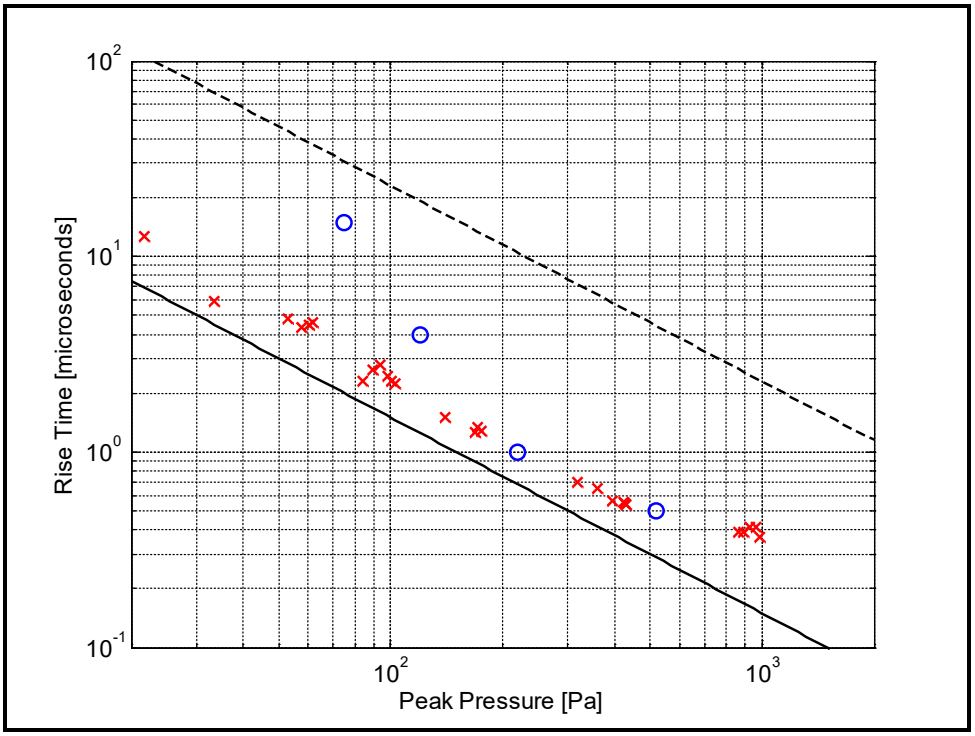

With regard to the influence of vibrational relaxation on the leading-edge shape, the worst case corresponds to the lowest peak pressure. The predicted rise time in the absence of vibrational relaxation for a pressure rise of 22 Pa is greater than 10 microseconds – a rise that would be resolved by the ⅛-in. microphone. If vibrational relaxation of oxygen were fully involved, the rise time would be an order of magnitude longer so the 22 Pa pulse presents an informative test of the rise time predictions (Figure 41). Also shown in Figure 41 is a hyperbolic tangent fit to the leading edge based on the expected rise time* with no vibrational relaxation:

$$p(t) = \frac{p_0}{2}\left[1 + \tanh\left(\frac{t}{t_{rise}/2}\right)\right] \quad (18)$$

* The rise time used in Equation 17 is actually the rise time based on maximum slope rather than 10- to 90-percent amplitude.

Figure 43. Measured rise phase (blue) for 22-Pa peak pressure shock. Also shown is a hyperbolic tangent fit (red) to the leading edge based on a rise time of 13 microseconds (comparable to that measured by the wideband microphone and shown as a red "x" in Fig. 42).

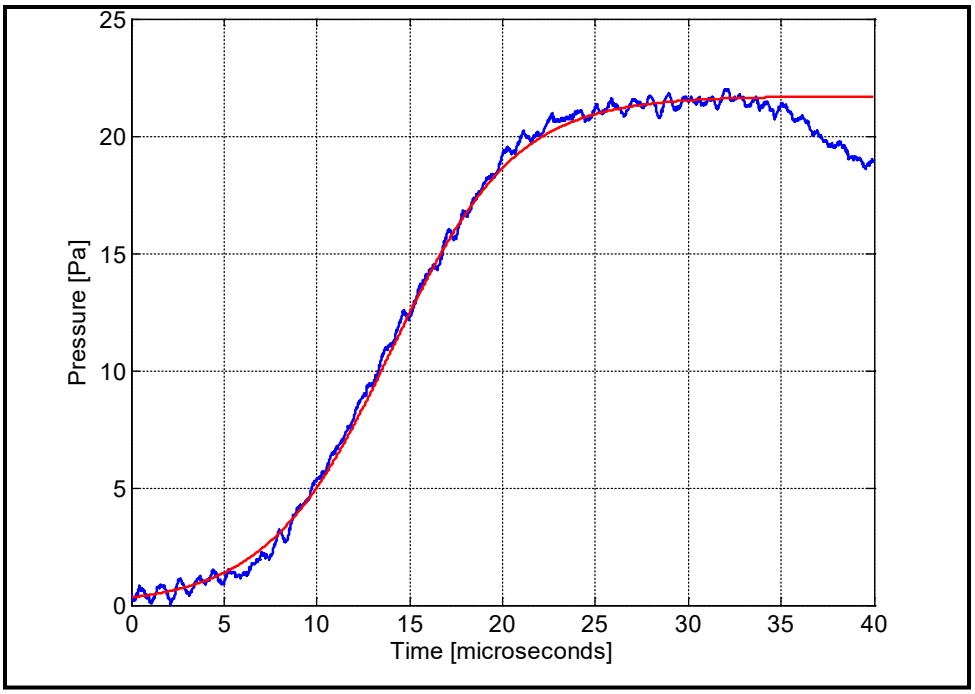

While this analysis seems to support the notion that vibrational relaxation can be neglected in the calculation of rise times, it is important to understand that these laboratory-generated waveforms are much shorter in duration than the C4 waveforms (which are, in turn, considerably shorter than typical sonic boom waveforms, for example). It is possible that the short overall duration of the laboratory-generated waveforms masks the effects of vibrational relaxation. It would be unlikely to see a predicted 100 microsecond rise time if the total time from initial rise to zero-crossing is only 100 microseconds; the rise-rate slowing that is characteristic of vibrational relaxation for a step change in pressure may be affecting the shorter waveform beyond the pressure peak so it does not appear as a lengthening of the rise time.

7 Conclusions

This work concludes that a model based on steady-state shocks with classical and rotational absorption (Equation 13) gives a reasonable lower bound for the rise time of shocks with peak pressures from 20 to 1000 (and perhaps higher) Pa at least for a relative humidity of 60%. Measured 10 to 90% rise times appear to be about 1.5 times the values predicted by Equation 13 (p 27).

This work also concludes that it should be possible to fabricate a field-hardened version of the PVDF wideband microphone with improved electronics suitable for measurement of rise times of outdoor explosions with peak pressures to 1000 Pa (0.2 microsecond rise time). If the peak pressure is less than 50 Pa, the conventional ⅛-in. condenser microphone should be able to resolve the rise time even if the rise time is near the theoretical minimum. For these weaker shocks, the lower noise floor of the condenser microphone would suggest its use over the wideband microphone.

References

American National Standards Institute (ANSI). 1983. *Estimating Airblast Characteristics for Single Point Explosions in Air*. ANSI S2.20-1983. New York, NY:ANSI.

ANSI. 1978. *Method for Calculation of the Absorption of Sound by the Atmosphere*. ANSI S1.26-1978. New York, NY:ANSI.

Bass, H. E., and R. Raspet. 1978. Vibrational relaxation effects on the atmospheric attenuation and rise times of explosive waves. *Journal of the Acoustical Society of America* 64:1208-1210.

Bass, H. E., J. Exell, and R. Raspet. 1983. Effects of vibrational relaxation effects on rise times of shock waves in the atmosphere. *Journal of the Acoustical Society of America* 74:1514-1517.

Bass, H. E., B. A. Layton, and L. N. Bolen. 1987. Propagation of medium strength shock waves through the atmosphere. *Journal of the Acoustical Society of America* 82:306-310.

Bass, H. E., R. Raspet, J. P. Chambers, and M. Kelly. 2002. Modification of sonic boom wave forms during propagation from the source to the ground. *Journal of the Acoustical Society of America* 111:81-486.

Bass, H. E., and R. Raspet. 1992. Comparison of sonic boom rise time prediction techniques. *Journal of the Acoustical Society of America* 91:1767-1768.

Chock, J. M. K., and R. K. Kapania. 2001. Review of two methods for calculating explosive air blast. *The Shock and Vibration Digest* 33:91-102.

Ford, R. D., D. J. Saunders, and G. Kerry. 1993. The acoustic pressure waveform from small unconfined charges of plastic explosive. *Journal of the Acoustical Society of America* 94:408-417.

Gabrielson, T. B., T. Marston, and A. Atchley. 2005. Nonlinear propagation modeling: Guidelines for supporting measurements. *NOISE-CON 2005* (*19th National Conference on Noise Control Engineering 2005*), Minneapolis, MN, 17-19 October 2005. Special Session on Advances in Military Jet Noise Modeling. *Journal of the Acoustical Society of America* 118:1873-1874.

Gabrielson, T. B., and T. Marston. 2007. Extraction of infrasonic waveforms from conventional condenser microphones. New Orleans, LA: 154th Meeting of Acoustical Society of America. *Journal of the Acoustical Society of America* 122:2958.

Gifford, C. M. 2005. *The Diffraction Correction for Small Microphones and Its Effect on the Measurement of High Frequency, High Amplitude Acoustic Pulses*. M.S. Thesis, Graduate Program in Acoustics, University Park, PA: Pennsylvania State University.

Ismail, M. M., and S. G. Murray. 1993. Study of blast wave parameters from small scale explosions. *Propellants, Explosives, Pyrotechnics* 18:11-17.

Jones, D. S. 1955. The scattering of a scalar wave by a semi-infinite rod of circular cross section. *Philosophical Transactions of the Royal Society of London* A247:499-528.

Landau, L. D., and E. M. Lifshitz. 1959. *Fluid Mechanics*, Eq. 87.9. Oxford, UK: Pergamon Press. p 340.

Linzer, M., and D. F. Hornig. 1963. Structure of shock fronts in Argon and Nitrogen. *Physics of Fluids* 6:1661- 1668.

Loubeau, A. 2006. *Nonlinear Propagation of High-Frequency Energy from Blast Waves as It Pertains to Bat Hearing*. Ph.D. Dissertation. Graduate Program in Acoustics, University Park, PA: Pennsylvania State University.

Loubeau, A., V. W. Sparrow, L. L. Pater, and W. M. Wright. 2006. High-frequency measurements of blast wave propagation. *Journal of the Acoustical Society of America* 120. Express Letters EL29-35.

Marston, T. M. 2006. *Diffraction Correction and Low-Frequency Response Extension for Condenser Microphones*. M.S. Thesis, Graduate Program in Acoustics, University Park, PA: Pennsylvania State University.

Pierce, A. 1989. *Acoustics – An Introduction to Its Physical Principles*. Eq. 11-6.13. Melville, NY: Acoustical Society of America. p 590.

Stoughton, R. 1997. Measurements of small-caliber ballistic shock waves in air. *Journal of the Acoustical Society of America* 102:781-787.

Acronyms and Abbreviations

Term	Definition
ANSI	American National Standards Institute
CA	Conditioning Amplifier
CERL	Construction Engineering Research Laboratory
COTR	Contracting Officer's Technical Representative
CR	Contract Report
DAQ	Data Acquisition Recorder
EQT	Environmental Quality Technology
ERDC	U.S. Army Engineer Research and Development Center
ESD	Energy Spectral Density
IC	Integrated Circuit
IP	Internet Protocol
LA	load allocation
MS	Millisecond
NOISE-CON	National Conference on Noise Control Engineering
PP	Post-Processing
PVC	Polyvinyl Chloride
PVDF	Polyvinylidene Difluoride
SF	Standard Form
UK	United Kingdom
USAPHC	U.S. Army Public Health Command

Appendix A: Sample Waveforms from C4 Explosions

Figure A-1. Pressure time histories for C4 explosions at 52 m. The sensor is a B&K 4138 ⅛-in. microphone in the 90-degree orientation. The charge weights are: top row, 0.071 kg (1/8 stick, two examples); middle row, 0.14 kg (1/4 stick); and bottom row, 0.28 kg (1/2 stick, two examples). The dashed red line is an analytical fit that includes a direct arrival and a ground bounce.

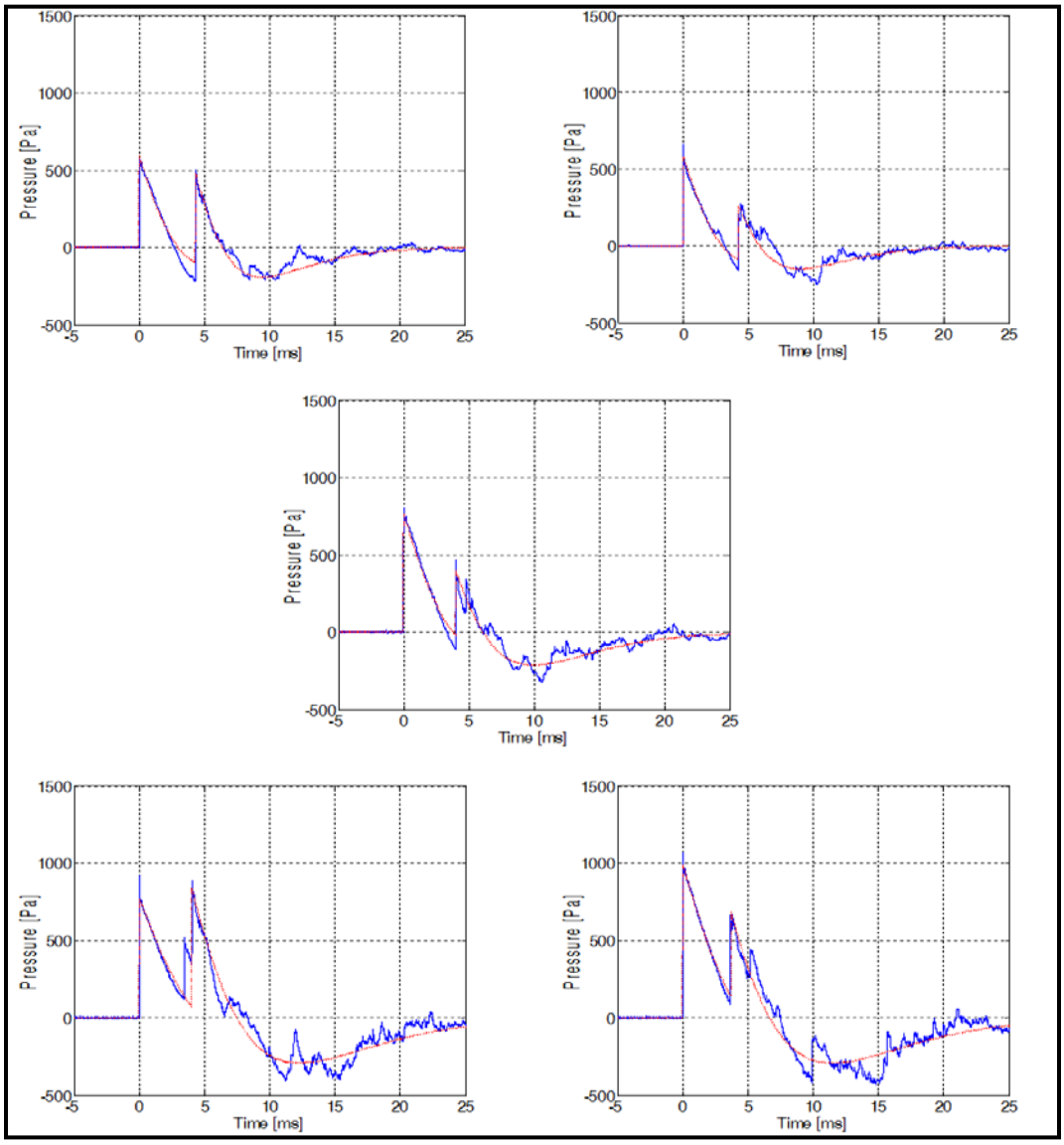

Figure A-2. Pressure time histories for C4 explosions at 52 m. The sensor is a B&K 4138 ⅛-in. microphone in the 90-degree orientation. The charge weights are: top row, 0.57 kg (full stick, two examples); and bottom row, 1.14 kg (two stick, two examples). The dashed red line is an analytical fit that includes a direct arrival and a ground bounce.

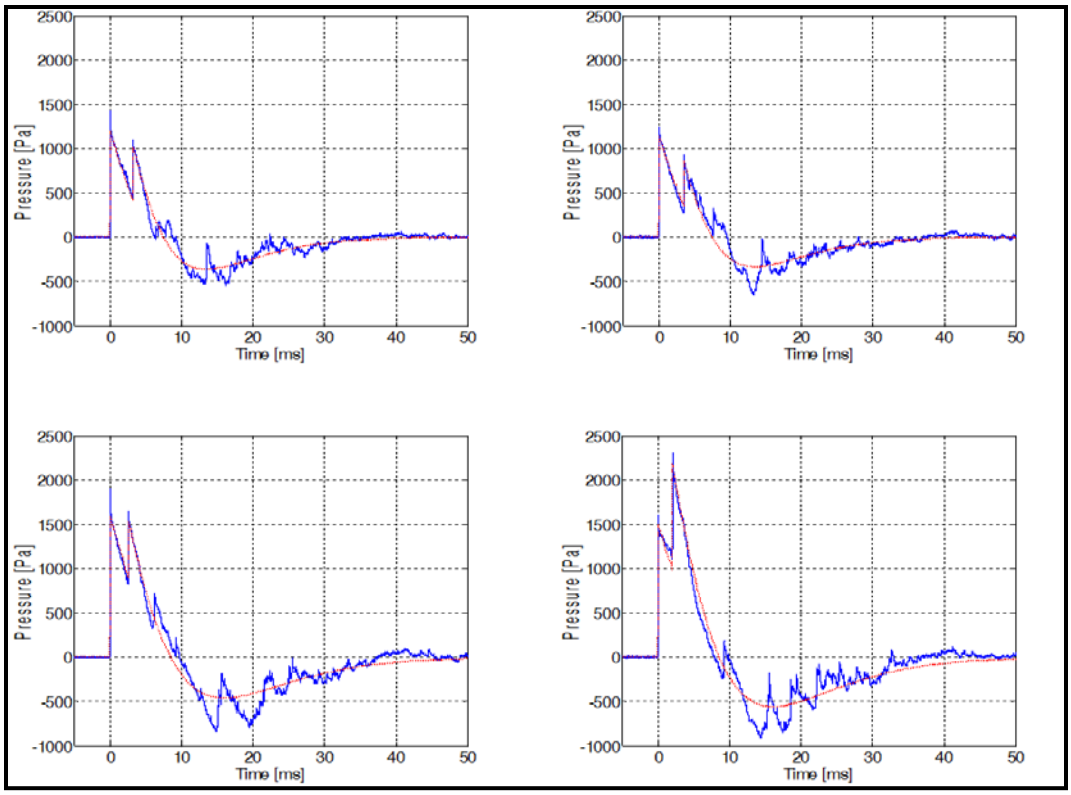

Appendix B: Variants of the Friedlander Pulse and Their Properties

The ordinary modified Friedlander function does not fit the negative phase of measured C4 waveforms well; however, a slight modification is significantly better:

$$p_{F2}(t) = p_0 \left[1 - (t/t_0)^2 \right] e^{-\alpha t/t_0} \quad \text{(B-1)}$$

For the measurements of C4 explosions made in this investigation, the ordinary Friedlander function produces a negative phase that is too long and, consequently, does not produce the proper low-frequency roll-off in the energy spectrum below the spectral peak. The simple modification above does not add any adjustable parameters, but the fit to the measurements is considerably better both in the time and frequency domains.

As in the ordinary Friedlander function, the peak pressure is p_o and the function crosses zero at $t = t_o$. The negative-pressure peak occurs at:

$$t = (t_0/\alpha)\left[1 + \sqrt{1 + \alpha} \right] \quad \text{(B-2)}$$

For energy calculations, the integral of pressure-squared is useful and this can be evaluated in closed form:

$$\int_0^\infty p_{F2}^2(t)\, dt = \frac{p_0^2\, t_0}{2\alpha}\left[1 - \frac{1}{\alpha^2} + \frac{3}{2\alpha^4} \right] \quad \text{(B-3)}$$

The "impulse" of both the positive and negative phases can be written in terms of Bessel functions of imaginary argument and Struve functions. Since one value for α suffices for all of the C4 explosions considered here, it is simpler to write the expressions for those impulses for the special case, $\alpha = 4/3$, as:

$$\int_0^{t_0} p_{F2}(t, \alpha = 4/3)\, dt = 0.425\, p_0\, t_0 \quad ; \quad [Pa \cdot s] \quad \text{(B-4)}$$

$$\int_{t_0}^\infty p_{F2}(t, \alpha = 4/3)\, dt = -0.52\, p_0\, t_0 \quad ; \quad [Pa \cdot s] \quad \text{(B-5)}$$

This variation on the Friedlander pulse can be made more general:

$$p_{Fb}(t) = p_0\left[1 - (t/t_0)^b\right]e^{-\alpha t/t_0} \tag{B-6}$$

The properties of this function can be examined by taking the Laplace transform:

$$\begin{aligned}\frac{P_{Fb}(s)}{p_0} &= t_0\left[\frac{1}{st_0 + \alpha} - \frac{\Gamma(b+1)}{(st_0 + \alpha)^{b+1}}\right] \\ &= t_0\left[\frac{(st_0 + \alpha)^b - \Gamma(b+1)}{(st_0 + \alpha)^{b+1}}\right]\end{aligned} \tag{B-7}$$

where Γ is the ordinary gamma function.

For large s (high frequency), this function approaches $1/s$. For small s, this function approaches zero only if α is chosen so that the constant term in the numerator vanishes:

$$\alpha_0 = \left[\Gamma(b+1)\right]^{1/b} \tag{B-8}$$

This is a reasonable choice from a physical point of view. If the spectrum goes to zero at zero frequency, that implies zero average value. Since the sensors used in the measurement of these waveforms are generally not DC coupled, the measured waveforms should have zero averages.

This approach introduces b as the adjustable parameter with α determined once b is selected. From a measurements point of view, this may be a more reasonable approach than selection of either *F1* or *F2* and adjusting α for the best fit; however, this choice for α_0 forces the positive impulse to equal the negative impulse, which may not be compatible with the actual explosion pressure pulse. Figure B-1 shows the waveforms produced for b = 0.5, 1.0, and 3.0.

Figure B-1. Waveform shapes for the generalized Friedlander function with $\alpha = \alpha_0$ and b = 0.5 (black), 1.0 (blue), and 3.0 (red).

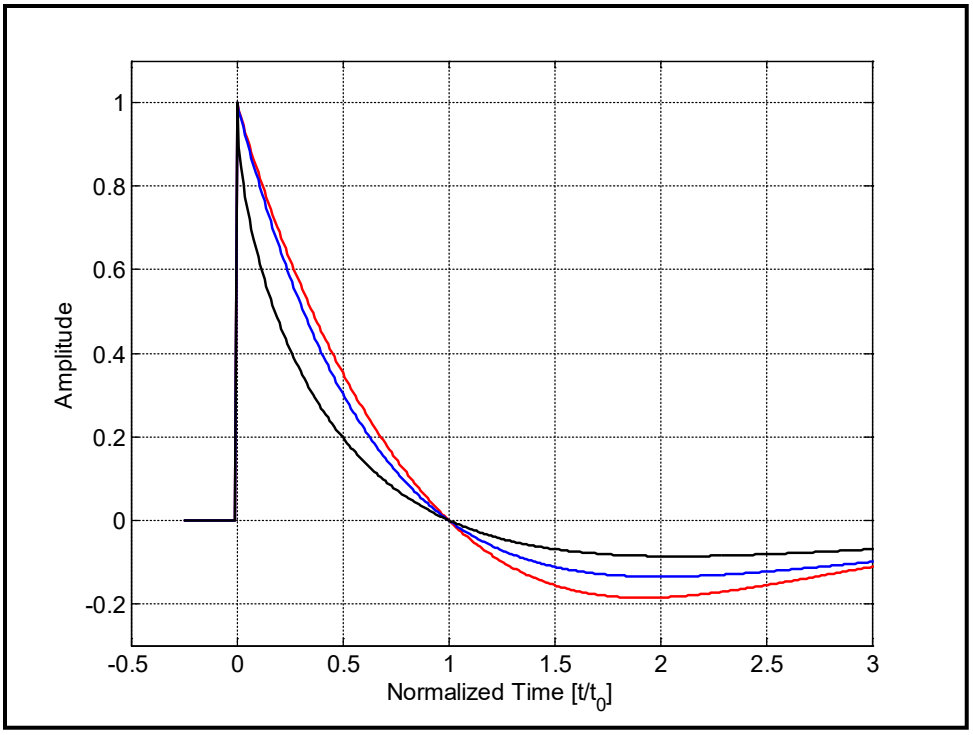

With this choice for α_0, the Laplace transform is:

$$\frac{P_{Fb}(s)}{p_0} = t_0 \left[\frac{(s t_0 + \alpha_0)^b - \alpha_0^b}{(s t_0 + \alpha_0)^{b+1}} \right] \tag{B-9}$$

Now, as s goes to zero, this function approaches zero as:

$$\frac{P_{Fb}(s)}{p_0} \rightarrow \frac{s t_0^2 b}{\alpha_0^2} \tag{B-10}$$

Since the high-frequency behavior is still $1/s$, the frequency of the spectral peak can be estimated by the intersection of the high- and low-frequency functions:

$$\frac{1}{s_{pk}} \approx \frac{s_{pk} t_0^2 b}{\alpha_0^2} \tag{B-11}$$

or:

$$s_{pk} \approx \frac{\alpha_0}{t_0 \sqrt{b}} \tag{B-12}$$

The Laplace transform expression can be converted to the frequency spectrum by substituting $j\omega$ for s:

$$\frac{P_{Fb}(\omega)}{p_0} = t_0 \left[\frac{(j\omega t_0 + \alpha_0)^b - \alpha_0^b}{(j\omega t_0 + \alpha_0)^{b+1}} \right] \quad \text{(B-13)}$$

with the spectral peak at:

$$\omega_{pk} \approx \frac{\alpha_0}{t_0 \sqrt{b}} \approx \frac{1}{t_0} \quad \text{(B-14)}$$

(The last approximation is reasonable for typical values of b.)

For integer values of b:

$$\alpha_0 = [b!]^{1/b} \quad \text{(B-15)}$$

Furthermore, if b is an integer, then the Laplace-domain response function is in the form of a numerator polynomial in s and a denominator polynomial in s. Consequently, time-domain filters can be derived for these cases. If one assumes that these responses are the responses to a step-function input, it is then possible to generate filter coefficients that, when applied to a step function, produce the explosion waveform.

Consider first the *F1* function – the ordinary modified Friedlander function. The s-domain response is:

$$\begin{aligned} P_{F1}(s) &= p_0 t_0 \left[\frac{s t_0}{(s t_0 + \alpha_0)^2} \right] \\ &= p_0 \left[\frac{s}{s^2 + 2 s \alpha_0 / t_0 + (\alpha_0 / t_0)^2} \right] \end{aligned} \quad \text{(B-16)}$$

The s-domain response for a step function with amplitude, p_0, is:

$$P_{step}(s) = \frac{p_0}{s} \quad \text{(B-17)}$$

so the effective filter function is:

$$H_{F1}(s) = \frac{P_{F1}(s)}{P_{step}(s)} = \frac{s^2}{s^2 + 2 s \alpha_0 / t_0 + (\alpha_0 / t_0)^2} \quad \text{(B-18)}$$

The *s*-domain expression is in the form of a numerator polynomial over a denominator polynomial so the bilinear transformation can be applied to generate the time-domain filter coefficients.

If the input to this filter is not an ideal step function, but rather a step with the leading edge having the rise shape of a step shock, then the filter will produce an approximation of the blast waveform that included a realistic rise phase. The simplest input for this purpose is the hyperbolic tangent "step", which would represent the shock rise phase if the only important absorption mechanisms were classical absorption and rotational relaxation. In this case, the input waveform would be:

$$p_{"step"}(t) = \frac{p_0}{2}\left[1 + \tanh\left(\frac{t}{t_{rise}/2}\right)\right] \quad \text{(B-19)}$$

where t_{rise} is the shock rise time.*

With a little more algebra, the equivalent filter for the *F2* function can be found:

$$H_{F2}(s) = \frac{s^3 + 2s^2\alpha_0/t_0}{s^3 + 3s^2\alpha_0/t_0 + 3s(\alpha_0/t_0)^2 + (\alpha_0/t_0)^3} \quad \text{(B-20)}$$

* In this form, the rise time is the maximum-slope rise time rather than the 10- to 90-percent rise time but, at this level of approximation, the distinction is unimportant.

Appendix C: Model Scaling for C4 Explosions

Assuming a pure traveling wave expanding spherically from the source explosion, the energy of the explosion can be related to the pressure-time waveform as follows. The acoustic intensity, I, is:

$$I(t) = \frac{p^2(t)}{\rho c} \quad ; \quad \left[\frac{W}{m^2}\right] \tag{C-1}$$

where ρ and c are the density and sound speed in the air and $p(t)$ is the pressure measured at some distance, R. The energy density, $\tilde{E}$, at the measurement distance, R, is:

$$\tilde{E} = \int_0^\infty I(t)\,dt = \frac{1}{\rho c}\int_0^\infty p^2(t)\,dt \quad ; \quad \left[\frac{J}{m^2}\right] \tag{C-2}$$

For a spherically spreading wave, the acoustic energy, E, would be:

$$E = 4\pi R^2 \tilde{E} \quad ; \quad [J] \tag{C-3}$$

In general, the integral of pressure-squared will be proportional to the peak pressure, p_0, times some characteristic time, t_0. Furthermore, the acoustic energy is expected to be proportional to the total stored chemical energy. Making the simplistic assumption that it is possible to use charge weight, W, as a measure of stored chemical energy,* the following proportionality is reasonable:

$$t_0\, p_0^2 \propto W \tag{C-4}$$

This proportionality suggests a plausible scaling relationship: the pressure scales as the one-third power of charge weight and all characteristic times scale as the one-third power of charge weight.

With this scaling law,† an expression that fits reasonably all of the C4 measurements made for this investigation is:

$$p(t) = p_A\left[1 - (t/t_A)^2\right]e^{-\alpha t/t_A} \tag{C-5}$$

* An assumption made reasonable by the use of TNT-equivalent charge weight. ANSI S2.20-1983 gives a factor of 1.37 for C4 – i.e., 1.37 kg of TNT is equivalent to 1.00 kg of C4.

† Commonly attributed to Hopkinson. Sachs scaling is also used but the difference is unimportant for the purposes of this Appendix.

with $\alpha = 4/3$:

$$p_A = p_0 \left(\frac{W}{W_0} \right)^{1/3} \left(\frac{R_0}{R} \right) \quad \text{(C-6)}$$

and

$$t_A = t_0 \left(\frac{W}{W_0} \right)^{1/3} \quad \text{(C-7)}$$

using the following reference values: R_0 = 50 m; p_0 = 1200 Pa; t_0 = 6.0 ms; and W_0 = 0.57 kg.

Note that nonlinearity in the propagation causes the time difference between the shock front and the zero crossing to increase with increasing range. This effect is not included in the model equations above; these model equations are only intended to be used in the vicinity of R_0 and for charge weights from one-eighth to twice W_0.

Appendix D: Low-Frequency Corrections

Microphones designed for extended high-frequency response often sacrifice very-low-frequency response – the roll-off at low frequency may start at several hertz. This is of no consequence with regard to measuring peak pressure or rise time, but other characteristics of the waveform are influenced by the low-frequency response. In general, the higher the charge energy (or charge weight), the longer the pulse and the greater the influence of a particular low-frequency roll-off. For the C4 charge weights (maximum of 1.14 kg) and for the microphones used in this investigation, the effects of the low-frequency roll-off are minor. In addition, there is a simple correction procedure that restores* the important part of the low-frequency response.

For the microphones used here, the low-frequency roll-off is the result of two mechanisms: (1) impedance loading of the microphone element by the preamplifier, and (2) the pressure-equalization leak. The pressure-equalization leak introduces a simple, single-pole, high-pass response that can be compensated by a filter that shifts that pole to lower frequency.† This compensation lacks precision because of the microphone-to-microphone variation in the characteristic leak frequency and because of the temperature dependence of the leak frequency. Notwithstanding the uncertainties, the compensation is still useful.

If the impedance loading of the preamplifier were simply the combination of microphone-element capacitance with the input resistance and capacitance of the preamplifier, compensation could be done in the same manner – by shifting the resultant pole lower in frequency. Microphone preamplifiers, however, are often "bootstrapped," which is a feedback configuration designed to raise the effective input impedance. While this makes the impedance loading more complicated than that of a simple pole, the effects of bootstrapping can be compensated with a relatively simple filter.‡

It is particularly convenient to implement these compensation filters as time-domain filters. MatLab functions for computing the filter coefficients

* This procedure moves the microphone's low-frequency roll-off lower in frequency. In effect, this flattens the low-end response. This response flattening comes at the expense of signal-to-noise ratio; however, the signal-to-noise ratio is only degraded over the low-frequency region where the correction takes effect.

† It is tempting to think that a filter that inverts the low-frequency roll-off would work; however, simply inverting the response roll-off leads to an extremely noisy and potentially unstable filter.

‡ These filter functions are developed in more detail in Gabrielson and Marston (2007).

are included below for the B&K 4138 (⅛-in.) microphone and for the B&K 4938 (¼-in.) microphone. As an example of the results of low-frequency compensation, Figure D-1 shows the waveform recorded from a B&K 4138 microphone in the 90-degree orientation before and after low-frequency compensation filtering. The corrected waveform is only slightly different. If the low-frequency correction was not done, the errors in estimation of the zero-crossing time and of the maximum negative pressure would be on the order of 10%. The errors would be less for the ¼-in. microphone (since it has better natural low-frequency response) and less for smaller charge weights (since there would be less low-frequency energy).

Figure D-1. Waveform (blue curve) for a 0.57 kg C4 charge at 52 m as recorded with a B&K 4138 (1/8-in.) microphone. The red dashed curve is the waveform produced by applying the low-frequency correction filter to the blue curve. The zero-crossing time is slightly later and the maximum negative pressure is slightly less negative after the low-frequency correction is applied.

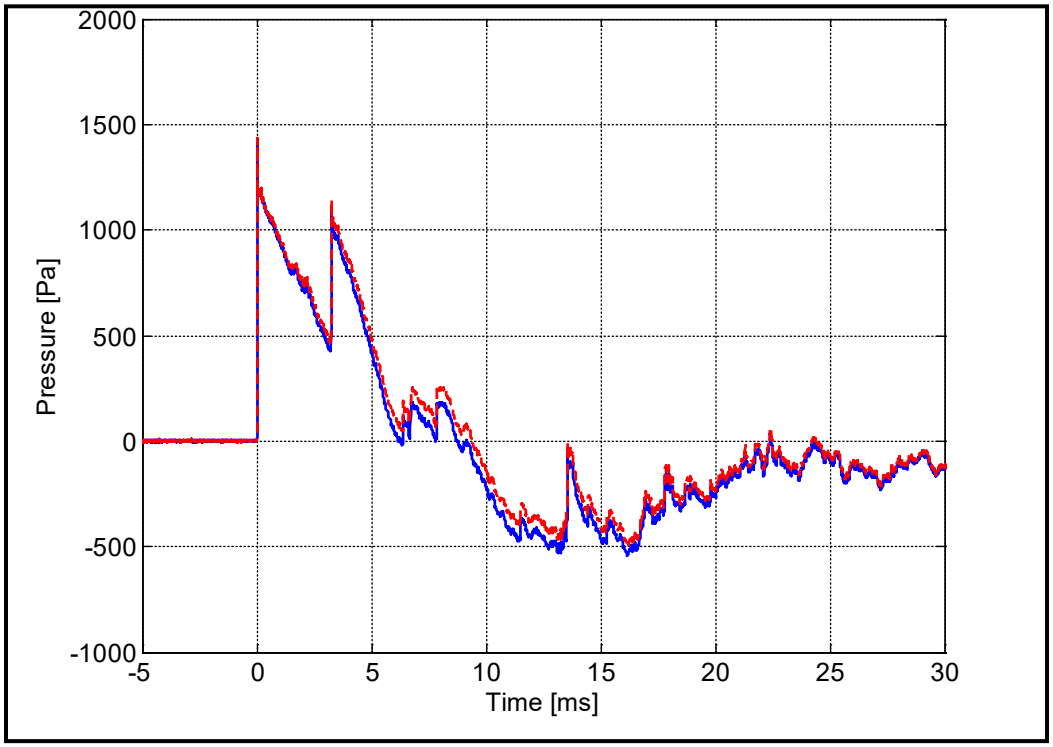

```
function [bb, aa] = BK4938_LF_correct(fs)
%  This function generates time-domain filter coefficients to reduce the
%  low-frequency pressure response of a B&K 1/4-in. microphone (BK 4938)
%  and 2670 preamplifier to that of a simple pole at 0.09 Hz.
%
%  USAGE:   [bb, aa] = BK4938_LF_correct(fs);
%  y_corrected = filter(bb, aa, y);
%
%  where fs is the sampling frequency and y is the original data.
%
%  Several parameters are required from the manufacturer's data sheet;
%  they are embedded in the first few lines of the function.
%
%  Microphone-element capacitance
Cmic = 6.1e-12;
%  Preamp values for bootstrapping (BK 2670)
R = 10e9; C = 6e-12;
%  Pressure-equalization leak - characteristic frequency
f_leak = 2.0;  w_leak = 2*pi*f_leak;
%  Simple pole at 0.09 Hz
w_pole = 0.09*2*pi;
%
%  The numerator and denominator polynomial coefficients (s-domain) are
%  constructed and passed to the bilinear transformation.
%
num_s_lk = [1, w_leak];
den_s_lk = [1, w_pole];
%
num_s_bt = [1, 2/(R*C), 1/(R*R*C*Cmic)];
den_s_bt = [1, 2/(R*C) + w_pole, 2*w_pole/(R*C)];
%
num_s = conv(num_s_lk, num_s_bt);
den_s = conv(den_s_lk, den_s_bt);
%
%  The 'bilinear' function from the MatLab Signal Processing Toolbox can
%  be used here if available. The 'bilinear_xform' function was written
%  to remove dependence on the special toolbox.
[bb, aa] = bilinear_xform(num_s, den_s, fs);
```

```
function [bb, aa] = BK4138_LF_correct(fs)
%  This function generates time-domain filter coefficients to reduce the
%  low-frequency pressure response of a B&K 1/8-in. microphone (BK 4138)
%  and 2670 preamplifier to that of a simple pole at 0.09 Hz.
%
%  USAGE:   [bb, aa] = BK4138_LF_correct(fs);
%  y_corrected = filter(bb, aa, y);
%
%  where fs is the sampling frequency and y is the original data.
%
%  Several parameters are required from the manufacturer's data sheet;
%  they are embedded in the first few lines of the function.
%
%  Microphone-element capacitance
Cmic = 3.5e-12;
%  Preamp values for bootstrapping (BK 2670)
R = 10e9; C = 6e-12;
%  Pressure-equalization leak - characteristic frequency
f_leak = 2.5;  w_leak = 2*pi*f_leak;
%  Simple pole at 0.09 Hz
w_pole = 0.09*2*pi;
%
%  The numerator and denominator polynomial coefficients (s-domain) are
%  constructed and passed to the bilinear transformation.
%
num_s_lk = [1, w_leak];
den_s_lk = [1, w_pole];
%
num_s_bt = [1, 2/(R*C), 1/(R*R*C*Cmic)];
den_s_bt = [1, 2/(R*C) + w_pole, 2*w_pole/(R*C)];
%
num_s = conv(num_s_lk, num_s_bt);
den_s = conv(den_s_lk, den_s_bt);
%
%  The 'bilinear' function from the MatLab Signal Processing Toolbox can
%  be used here if available. The 'bilinear_xform' function was written
%  to remove dependence on the special toolbox.
[bb, aa] = bilinear_xform(num_s, den_s, fs);
```

Appendix E: Model Function for Balloon-Burst Waveforms

Freely propagating shock waves with microsecond rise times can be produced in the laboratory by balloon-burst or small explosion inside one end of a several-meter long pipe. The pipe restricts spreading loss so the acoustic pressure remains high through the pipe. Nonlinearity in the propagation through the pipe sharpens the leading edge and the high-pass nature of the transmission coefficient of the open end of the pipe reduces the lower-frequency artifacts of the burst. In this investigation, both balloon-bursts and blank-firing pistol shots were used to generate free-field shocks with peak pressures ranging from 100 to 2000 Pa. A 3-m length of 6-in. PVC pipe was used to "shock up" the bursts.

The conventional modified Friedlander function (here denoted as F_1 in contrast to the F_2 function used for modeling C4 explosion waveforms) provides a reasonable fit for the balloon bursts:

$$p_{F1}(t) = p_A\left[1 - (t/t_A)\right]e^{-\alpha t/t_A} \quad \text{(E-1)}$$

for $t > 0$. Here, p_A is the peak pressure, t_A is the time of zero crossing, and α is a decay-rate parameter. Shot to shot, balloon bursts show considerably more variation in peak pressure than C4 explosions; however, a representative function for small balloons* and a 3-m pipe can be written using the following relations:

$$p_A = p_0\left(\frac{R_0}{R}\right) \quad \text{(E-2)}$$

and $\alpha = 1$; $R_0 = 3$ m; $p_0 = 400$ Pa; and $t_A = 125$ μs. [Note that R refers to the distance from the exit end of the pipe to the microphone and R_0 is a reference distance (not the pipe length). In practice, the peak pressure ranges from the full value shown to half that value.]

* In general, the smaller the balloon, the better the results. Balloons sold as "water balloons" seem to work well. They should be inflated until they burst naturally for the highest peak pressures.

Figure E-1 shows a typical waveform along with the modified Friedlander curve fit. The rise times of these waveforms are shorter than can be resolved by our laboratory microphones although one device is under development for this purpose.

Figure E-1. Typical waveform for a balloon burst in an open-ended 3-m pipe. The microphone (B&K 4138 ⅛-in. in the 90-degree orientation) was 3.25 m from the exit end (the far end with respect to the balloon location) of the pipe. The dashed red curve is the F1 fit described above (with p_A = 333 Pa).

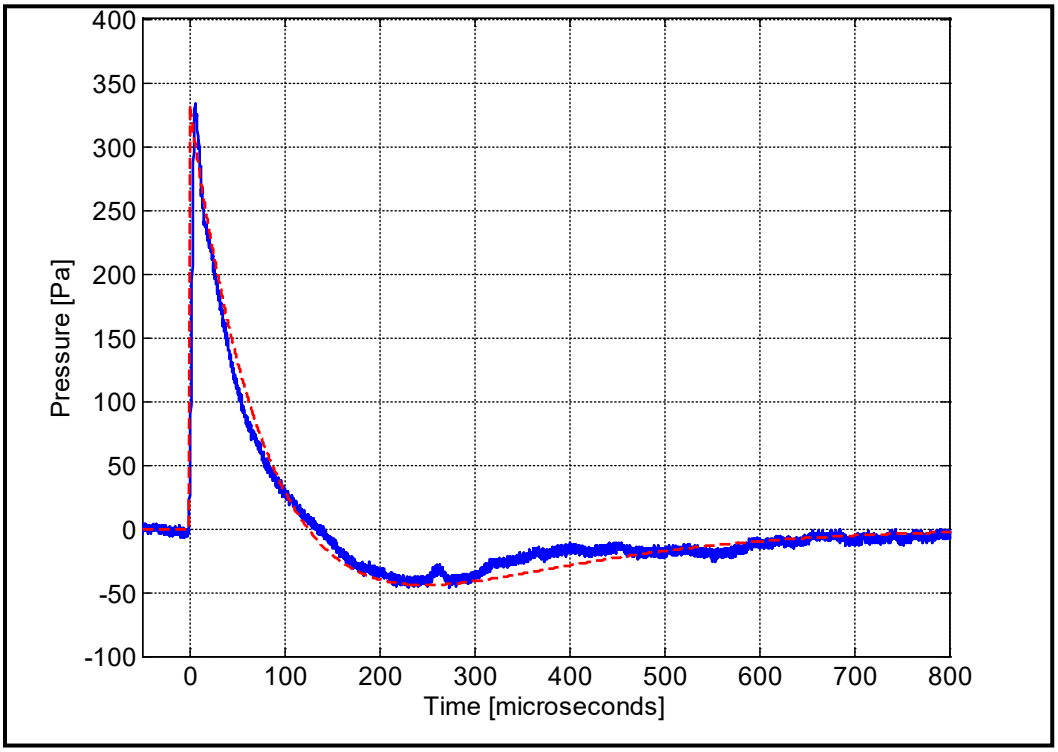

Note that nonlinearity in the propagation causes the time difference between the shock front and the zero crossing to increase with increasing range. This effect is not included in the model equations above; these model equations are only intended to be used in the vicinity of R_0 and for typical balloon bursts. Since the balloons are inflated until they burst (rather than inflating to a specific pressure, then piercing the balloon), there is scatter in the amplitudes obtained. For a particular variety of balloon, the scatter is surprisingly small (perhaps ± 30%) given the "random" nature of bursting under pressure.

Appendix F: Model Function for .38 Caliber Blank Waveforms

Two varieties of commercial .38 caliber rimmed (revolver) blank cartridges were used in this investigation: Fiocchi ("full" loads), and Sellier and Bellot. The Fiocchi cartridges are more readily available so the results give here are for those cartridges. They were fired with a Bruni Olympic blank-firing pistol. As is the case with most blank-firing pistols, the Olympic ports the explosion out to the side* (the "barrel" is permanently blocked). The pistol was inserted so that the explosion port was 15 to 20 cm into the "source" end of the 3-m length of 6-in. PVC pipe used to "shock up" the bursts.

Figure F-1 gives waveforms from six shots with the microphone place 3 m from the exit end of the pipe. These waveforms were recorded using a B&K 4138 ⅛-in. pressure microphone in the zero-degree orientation and sampled at 10 MS/s. The diffraction-correction filter has been applied to remove the diffraction overshoot. Figure F-2 also shows these same six waveforms on an expanded time scale to show the rise phase and peak pressure. The peak pressures range from 510 Pa to 625 Pa (average of 570 Pa) and the rise times range from 3.1 to 3.2 microseconds.

* Blank cartridges can also be fired from conventional revolvers in which case the explosion gases exit forward through the barrel. It is likely that the free-field peak pressure and waveform would be considerably different. Furthermore, there would be a high risk of microphone damage as the wadding used in the blank cartridges would be launched directly toward the microphone.

Figure F-1. Six waveforms recorded from Fiocchi .38 caliber blank cartridges in an open-ended 3-m pipe. The microphone (B&K 4138 ⅛-in. in the zero-degree orientation) was 3 m from the exit end of the pipe.

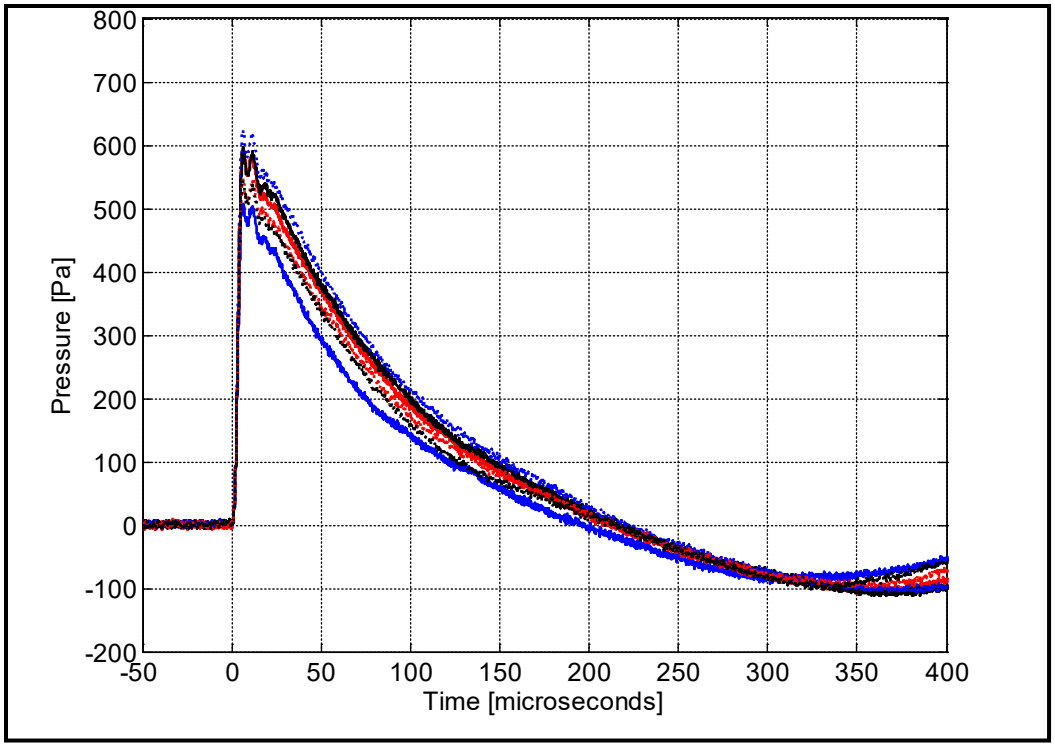

Figure F-2. The waveforms from Fig. F-1 on an expanded time scale to show the leading-edge behavior. The rise times are about 3 microseconds.

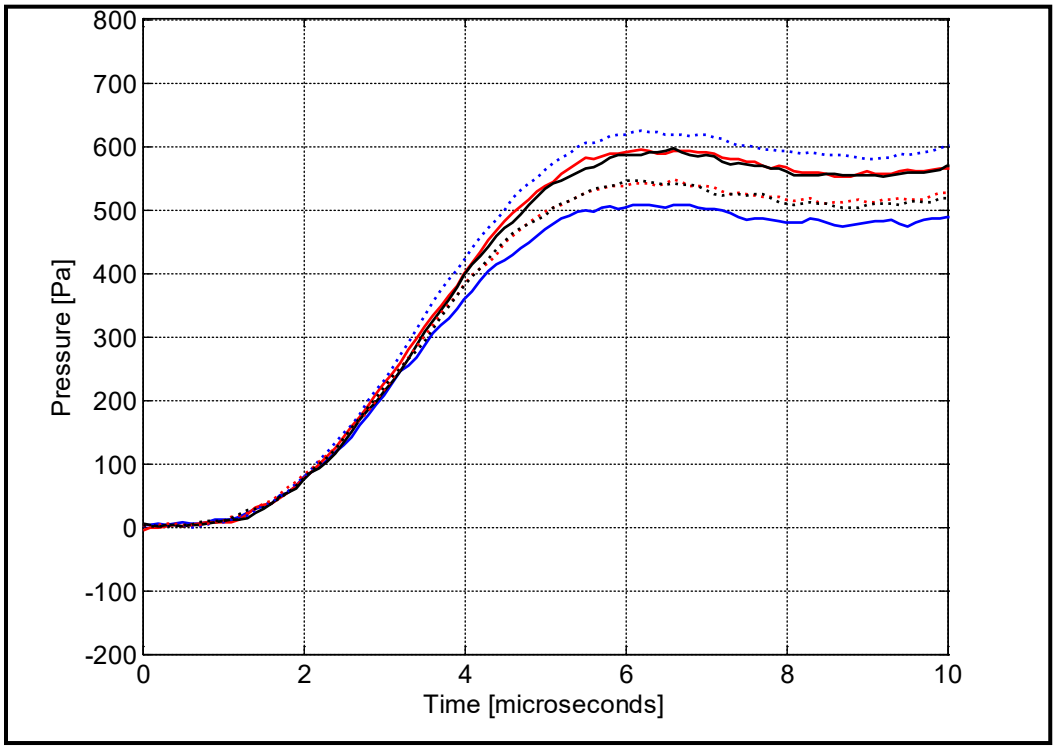

The conventional modified Friedlander function (here denoted as F_1 in contrast to the F_2 function used for modeling C4 explosion waveforms) provides a reasonable fit:

$$p_{F1}(t) = p_A\left[1 - (t/t_A)\right]e^{-\alpha t/t_A} \quad \text{(F-1)}$$

for $t > 0$.

Here, p_A is the peak pressure, t_A is the time of zero crossing, and α is a decay-rate parameter. Shot to shot, the blank cartridges show less variation in peak pressure than balloon bursts. A representative function for the Fiocchi cartridges, the Olympic blank-firing revolver, and a 3-m pipe can be written using the following relations:

$$p_A = p_0\left(\frac{R_0}{R}\right) \quad \text{(F-2)}$$

and $\alpha = 0.87$; $R_0 = 3$ m; $p_0 = 600$ Pa; and $t_A = 210$ μs. (Note that R refers to the distance from the exit end of the pipe to the microphone and R_0 is a reference distance (not the pipe length). In practice, the peak pressure ranges from the full value shown to half that value.) Figure F-3 shows a typical waveform along with the modified Friedlander curve fit.

Note that nonlinearity in the propagation causes the time difference between the shock front and the zero crossing to increase with increasing range. This effect is not included in the model equations above; these model equations are only intended to be used in the vicinity of R_0 and for the Fiocchi cartridges.

Figure F-3. One of the shot waveforms (red) and the modified Friedlander function fit (black) using a peak pressure of 594 Pa, a zero-crossing time of 210 microseconds and α = 0.87. The large feature from 400 to 700 microseconds is most likely a reflection from the transition cone in the microphone mount.

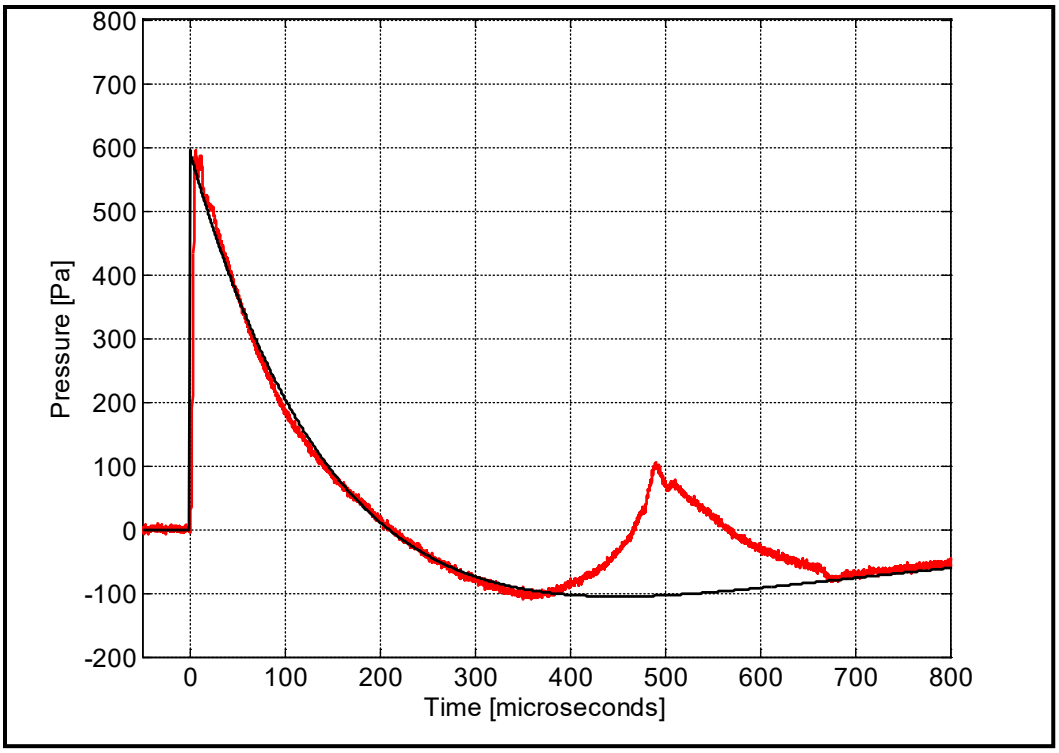

Of particular interest in Figure F-3 is the artifact in the vicinity of 500 microseconds. This artifact has not been identified definitively; however, it does not appear, except perhaps as a much smaller feature at 250 microseconds, in measurements made with the microphone in the 90-degree orientation. This suggests that it may be a reflection from the transition cone used in the microphone mount (Figure F-4). In the zero-degree orientation, a reflection path would extend from the microphone to the cone and back; whereas, in the 90-degree orientation, scatter from the cone would only travel half that distance (from the cone to the microphone) since, in that case, the cone and the microphone are in the same plane as the arriving wave front.

Figure F-4. Microphone holders used in laboratory and field measurements. Shown here are a ½-in. microphone (left) and a ¼-in. microphone (right). The ⅛-in. microphone fits in the same cone adapter as the ¼-in. microphone (the preamplifier diameter is the same for both). The tapered-cone (lighter part in right-hand assembly) is designed to reduce reflections whether used in zero-degree or 90-degree orientation. The front of the tapered cone sets back between 7 and 10 cm from the microphone element when used with the ⅛-in. microphone.

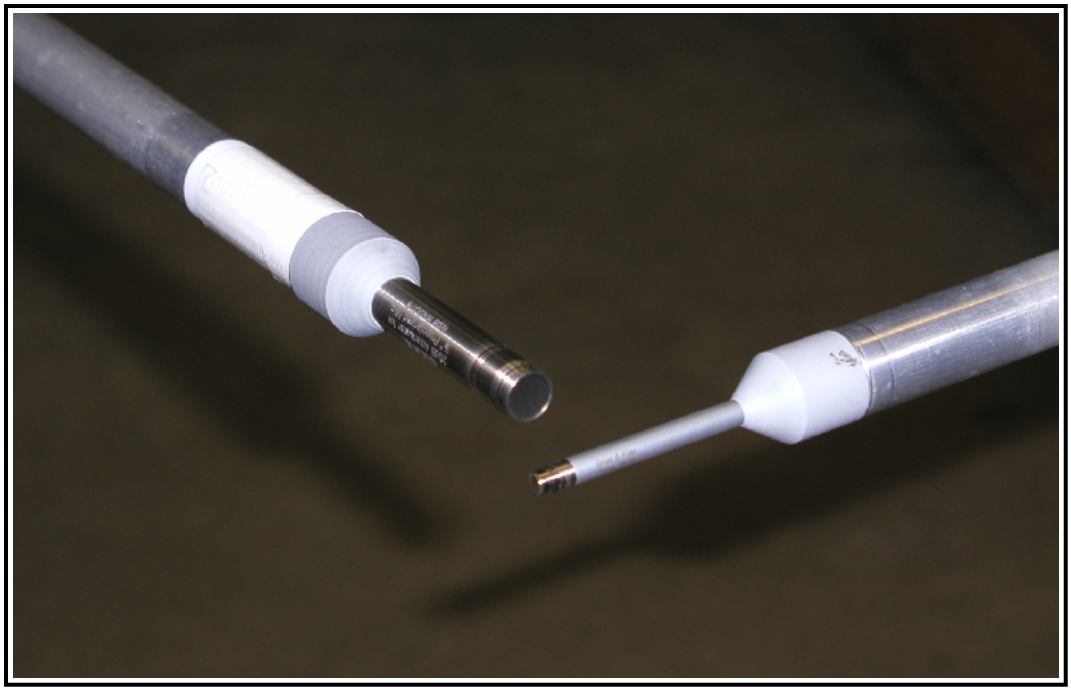

Figure F-5 shows the leading-edge behavior for the waveform from Figure F-2) on an expanded time scale. Also drawn are the 10 and 90% lines to illustrate the rise time calculation. The ⅛-in. microphone in the zero-degree orientation produces the best rise time estimate of all of the commercially available measurement microphones as long as the diffraction correction is done, the extended-bandwidth conditioning amplifier is used, and the output is sampled sufficiently fast (at least 1 MS/s).

Figure F-5. One of the shot waveforms (red) on a time scale expanded to show the detail of the apparent pressure rise at the shock front. The two blue dashed lines indicate the 10- and 90-percent amplitude values; the 10 to 90% rise time is 3.2 microseconds. This rise time is limited by the transducer and electronics response and it is the fastest rise time achievable with commercial, off-the-shelf measurement microphones.

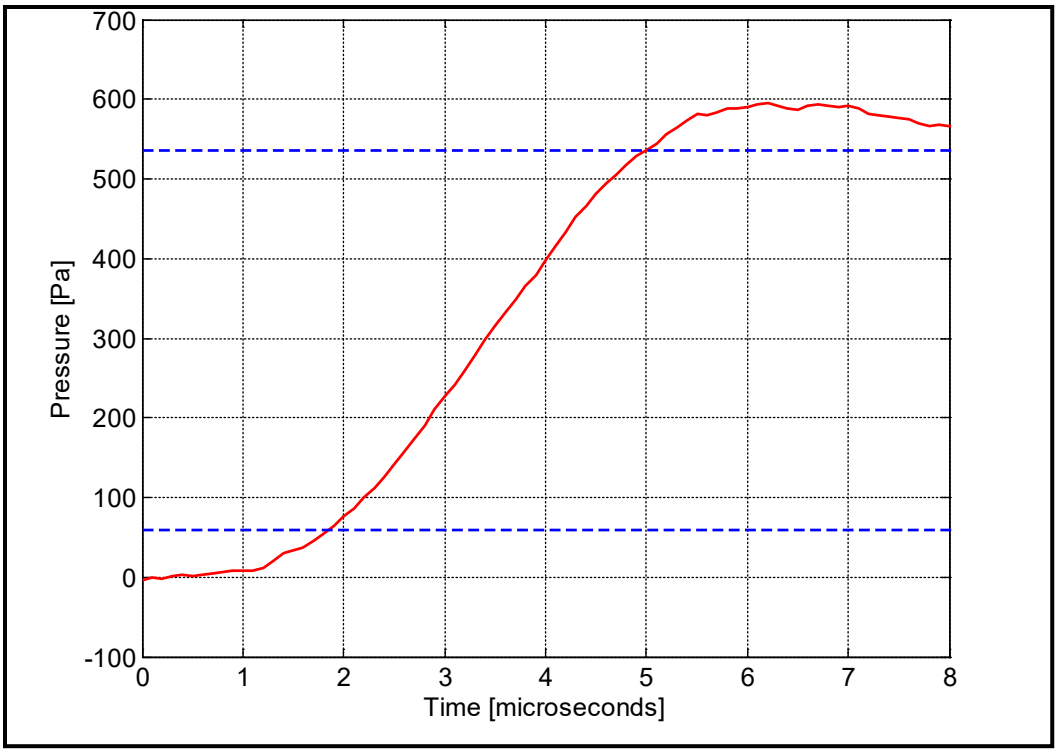

Appendix G: Predictions for Shock Rise Times

Reliable prediction of shock rise times has been hampered by the difficulty in implementing and running models that account for nonlinearity, absorption, and dispersion. The general discussion in Bass et al. (2002) is instructive for its summary of the important problems in modeling. They present a model (that has been used by other groups as well) that implements nonlinear effects in the time domain and absorption and dispersion in the frequency domain. In particular, they discuss the critical need for sufficient sampling of the shock rise phase with "... at least eight to ten sample points on the rise portion of the waveform." For a microsecond rise phase, the temporal sampling rate would need to be 10 Ms/s or more, which is equivalent to a sample spacing of less than 50 μm. Modeling the propagation of a C4 explosion waveform that might be 50 ms in duration would require 500,000 point Fourier transforms; propagation to 50 m distance would require several million transforms (one forward transform and one inverse transform per step). When the sampling is insufficient, the code still runs, but the rise time estimate then is limited by the numerical sampling rate rather than by physical processes. The problem is exacerbated by the scarcity of measurements capable of resolving the true rise time, especially measurements free from the effects of turbulence.

A simplification that may provide useful estimates of rise time is based on the assumptions that the shock has reached steady state and that the absorption is proportional to frequency squared. In that case, the rise time is given by (Bass et al., 2002; or Pierce, 1989, Eq. 11-6.13))

$$t_{rise} = \frac{8\rho_0 c^3}{\beta p_{pk}} \frac{\alpha}{\omega^2} \tag{G-1}$$

where:

ρ_0 and c are the equilibrium density and sound speed in the gas
β is the parameter of nonlinearity (1.2 for an ideal gas)
p_{pk} is the pressure jump at the shock
α is the absorption coefficient (in "nepers" per meter)
ω is the angular frequency (= $2\pi f$).

Even when relaxation processes contribute to the absorption, the absorption is proportional to frequency squared for frequencies sufficiently far

from the relaxation frequency. The simplification used in Equation G-1 amounts a limit on the rise time; the rise time would be no shorter than given by this equation if the mechanisms considered in the particular expression for α are all in effect.

Absorption of sound in the atmosphere can be modeled reasonably well with three components (ANSI S1.26-1978): (1) a combination of classical absorption and rotational relaxation,* (2) vibrational relaxation of oxygen, and (3) vibrational relaxation of nitrogen. The first component is proportional to frequency squared over the entire range of frequencies relevant here. The last two components are proportional to frequency squared only when the relevant frequency is less than the corresponding "relaxation" frequency. Well above the relaxation frequency, the corresponding vibrational-relaxation component is negligible.

Using the formulae in ANSI S1.26-1978 for the three components of the absorption model, α, the following expressions may be written for the product of rise time and peak pressure:

For combined classical absorption and rotational relaxation:

$$t_{rise} \cdot p_{pk} = 0.15 \times 10^{-3} \left(\frac{T}{T_0} \right)^{1/2} \left(\frac{P_0}{P} \right) \qquad [\mathrm{Pa \cdot s}] \tag{G-2}$$

where:

T is the absolute temperature
P is the ambient atmospheric pressure
T_0 is the reference temperature (293.15 °K, which is 20 °C)
P_0 is the reference pressure (101325 Pa).

For vibrational relaxation of oxygen, if the frequency of interest is below the relaxation frequency for oxygen:

$$t_{rise} \cdot p_{pk} = 2.15 \times 10^{-3} \left(\frac{T}{T_0} \right)^{1/2} \left(\frac{P_0}{P} \right) \qquad [\mathrm{Pa \cdot s}] \tag{G-3}$$

* Sometimes only classical absorption is used as the lower limit to losses by absorption. For the pressures and waveforms considered here, rotational relaxation should always be in effect; consequently, the lower limit for absorption is taken to be the combination of classical and rotational (as in ANSI S1.26). Rotational absorption is often "hidden" in the term, bulk viscosity.

For vibrational relaxation of nitrogen, if the frequency of interest is below the relaxation frequency for nitrogen:

$$t_{rise} \cdot p_{pk} = 35.3 \times 10^{-3} \left(\frac{T}{T_0} \right)^{1/2} \left(\frac{P_0}{P} \right) \qquad [\mathrm{Pa \cdot s}] \tag{G-4}$$

To reasonable approximation, the absorption coefficients add; consequently, so also do the rise times. If the frequency range of interest is well above both the nitrogen and the oxygen relaxation frequencies, then only the classical-plus-rotational component matters. In that case, a 100-Pa shock at the reference temperature and pressure would have a predicted rise time of 1.5 microseconds. If, however, the frequency range of interest* was above the relaxation frequency for nitrogen, but not above the relaxation frequency for oxygen, then a 100-Pa shock would have a rise time of 23 microseconds. If the nitrogen-relaxation process was also important, the 100-Pa shock would have a rise time of 375 microseconds.

The relaxation frequencies for vibrational excitation of either nitrogen or oxygen depend on relative humidity. Again, using formulae from ANSI S1.26-1978, Figure G-1 was generated to show the relationship between these vibrational relaxation frequencies and relative humidity.

In this investigation, both the C4 shots and the laboratory measurements showed rise times that were limited by the instrumentation. In no case were these apparent rise times greater than 10 microseconds and those larger values were obtained using measurement systems with less than 100 kHz bandwidth. If one considers that the important frequencies associated with the sudden pressure rise at the shock front are above 10 to 100 kHz, then one might conclude that nitrogen relaxation is never important although oxygen relaxation might enter for cases of higher humidity. The relative humidity measured at the Aberdeen test site during the C4 testing period ranged from 55 to 70%; the relative humidity in the laboratory would have been somewhat lower (normally in the range of 50 to 60%).

* The question, of course, is "What is the frequency range of interest?" For a shock with a rise time of one microsecond, it would be tempting to guess that the relevant frequencies extended from a decade below the reciprocal of the rise time to a decade above (100 kHz to 10 MHz), but this is by no means clear.

Figure G-1. Vibrational relaxation frequencies for oxygen (blue) and for nitrogen (red) as functions of percent relative humidity. If a frequency of interest is above the relaxation frequency, then that mode of vibrational relaxation is not excited. For the shocks considered in this investigation having rise times less than 3 microseconds, it is unlikely that vibrational relaxation of nitrogen is ever important. Furthermore, vibrational relaxation of oxygen may only enter to slow the rise time only for weak shocks and for conditions of high humidity.

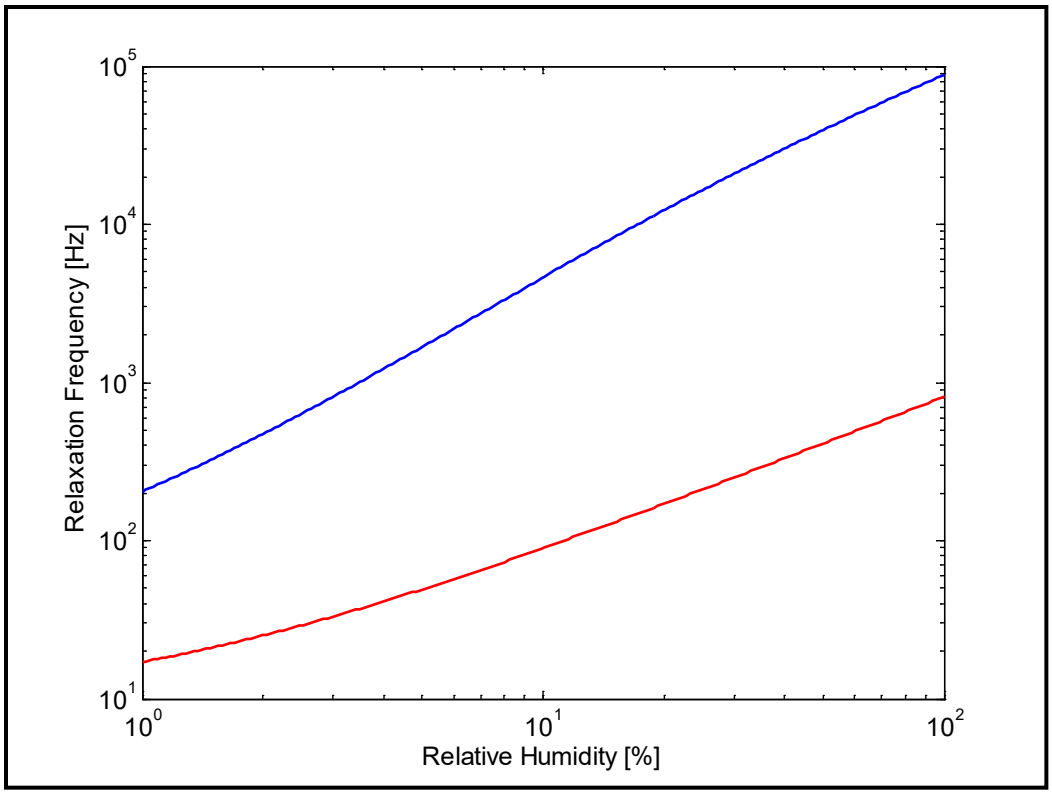

Figure G-2 shows the relationship between peak shock pressure and rise time for the two cases of importance: (1) for classical-plus-rotational absorption only, and (2) for classical-plus-rotational and oxygen-vibrational absorption.

These results have been developed for "weak shocks" – shock fronts that propagate at a speed within a few percent of the ordinary sound speed. Much of the literature on the physics of shocks is cast in terms of shock thickness. For weak shocks, the rise time is simply the shock thickness divided by the ordinary speed of sound. In fact, Equation G-2 (or G-3 or G-4) is more precise if multiplied through by the ordinary sound speed. Then the equation(s) expresses the product of shock thickness and pressure. However, for peak pressures below a few thousand pascals (a few percent of atmospheric pressure), the expressions and figures in this section are reasonable approximations.

Figure G-2. Predicted rise time as a function of pressure for a steady-state shock according to variants of Equation G-1. If the relevant frequencies are above the vibrational relaxation frequency for oxygen, then only classical and rotational absorption would be in effect (red curve – Equation G-2). If, however, vibrational relaxation of oxygen is important, then the rise times would be roughly an order of magnitude longer (blue dashed curve – Equation G-2 plus Equation G-3).

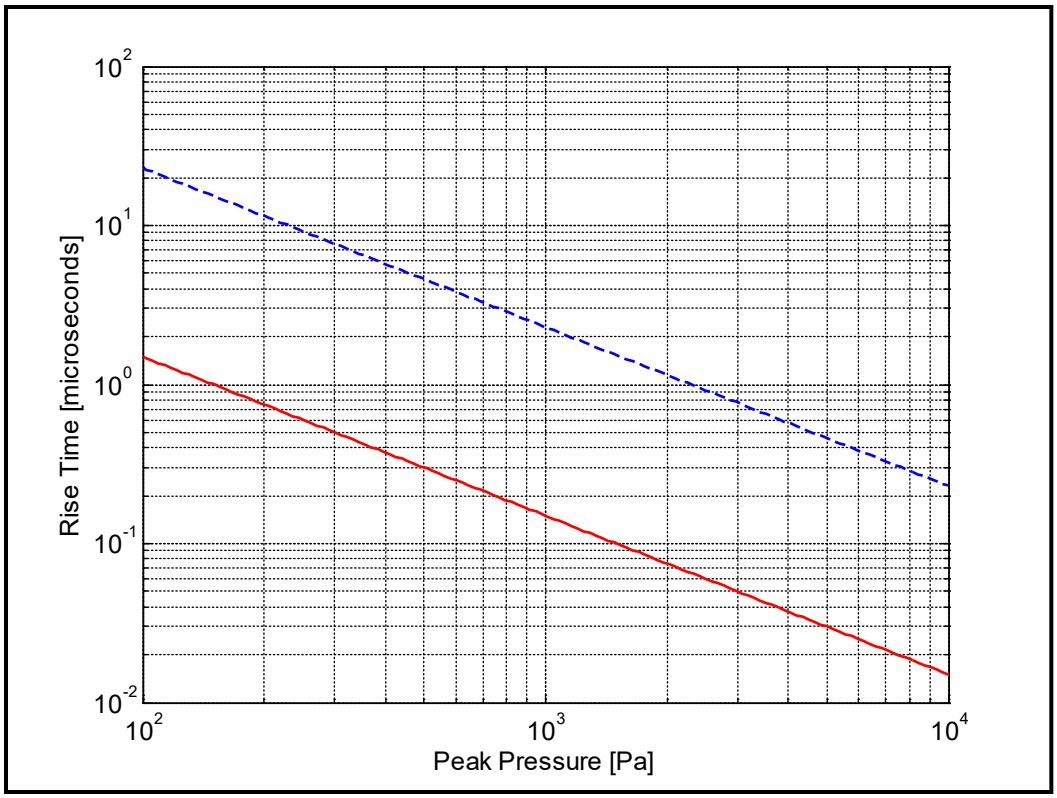

Note that there are at least three definitions for rise time in the literature. Two are based on the time required for the pressure rise from a low percentage of the peak to a higher percentage of the peak. In this section, the 10 to 90% rise time is used; in other literature, the 5 to 95% rise time is used though less frequently. The third common definition is the peak pressure divided by the maximum slope (the time rate of change of pressure).* The pressure rise for a steady-state shock dominated by simple f^2 absorption losses takes the form of a hyperbolic tangent. Compared to the 10 to 90% rise time for the hyperbolic tangent function, the peak pressure divided by the maximum slope gives a rise time 10% faster and the 5 to 95% rise time is 1.3 times longer. For the purposes of this report, the differences between these definitions would not change the conclusions.

* Or the time rate of change of pressure at the 50 percent point, which might be somewhat different depending on the shape of the rise phase.

Appendix H: Analog Bessel Filter Module

Figure H-1 shows the circuit diagram for an analog Bessel low-pass filter suitable for anti-alias filtering when recording explosive shocks. The filter's characteristic frequency is set by the resistor value, R. According to the datasheet for the LTC 1563-3, the maximum frequency is 256 kHz so this integrated circuit would be useful for measurement-microphone recordings, but not for special wideband microphones. If set to 80 kHz, the filter could be used in place of the internal anti-aliasing filter in the TEAC GX-1 instrumentation recorder at 200 kS/s; if set to 150 to 200 kHz and used with a higher-speed acquisition recorder at 400 to 500 kS/s, then the full bandwidth of the ⅛-in. measurement microphone would be preserved.

Figure H-1. Circuit diagram for 4th order Bessel filter module. The low-pass cutoff frequency is inversely proportional to the value of R. If R = 10 kΩ, then f_0 = 256 kHz; if R = 100 kΩ, then f_0 = 25.6 kHz. In all cases, C = 0.1 µF.

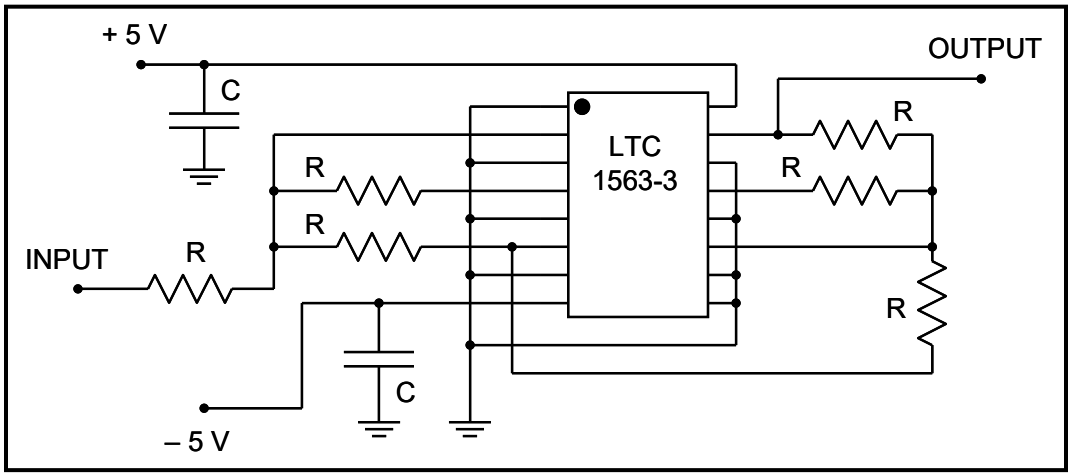

Figure H-2 shows a suggested circuit-board layout. The base provides input and output connections and supply voltages. Individual filter modules are assembled on smaller plug-in boards.

Figure H-2. Printed-circuit board layout for Bessel low-pass filter. The filter itself is assembled on a separate plug-in board shown on the left. The layout on the right contains positive- and negative-voltage regulators and connectors. The red traces and pads are areas of copper on the top surface of the boards; the green represents copper on the bottom surface. All holes are plated through from top to bottom.

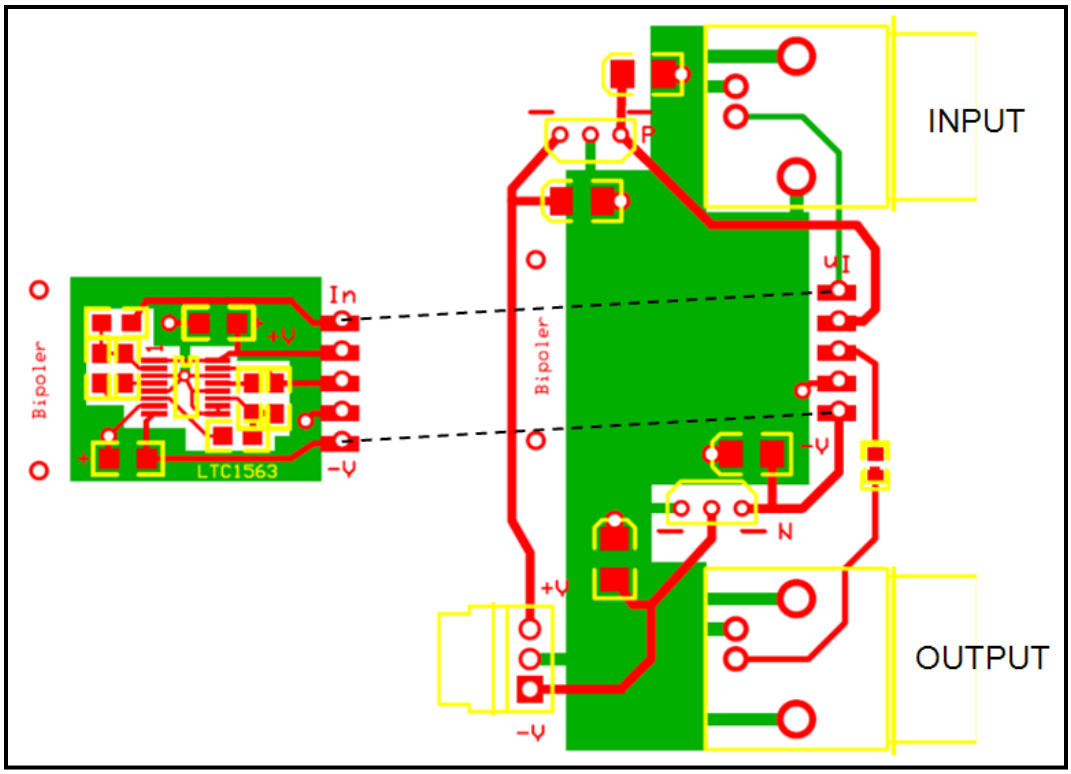

Appendix I: Time-Reversed Filtering to Shift Ringing of Anti-Aliasing Filter Response

Butterworth anti-aliasing filters introduce overshoot and ringing at the shock front. This ringing is difficult to remove while preserving the rise time; however, there is a technique whereby the ringing can be shifted to the region prior to arrival of the shock. This results in a clean rise and little overshoot or ringing at the pressure peak. The technique involves generating coefficients for a time-domain Butterworth filter of the same order as the anti-aliasing filter, but having a characteristic frequency 10% lower. Then the time series of the recorded waveform is reversed in time and filtered by this new filter. After filtering, the time series is restored to its original order with the result that the ringing has been shifted from after the sharp rise to before the rise. The following MatLab function performs this time-reversed filtering.

```
function y_filtered = Butterworth_artifact_shifter(y, fs, M, flpf);
%  This function applies a reverse-time filter to the input waveform, y,
%  that is designed to shift the overshoot and ringing from a Butterworth
%  low-pass filter to the region of the waveform before a sharp change.
%  This is particularly useful for cleaning up the rise phase and peak
%  pressure for shock front recordings made with acquisition systems that
%  use Butterworth anti-aliasing filters.
%
%  USAGE:   y_out = Butterworth_artifact_shifter(y_in, fs, M, flpf);
%
%  where fs is the sample rate and M and flpf are the order and 3-dB
%  frequency for the original Butterworth filter (that has already been
%  applied to y_in by the data acquisition system).
%
%  The first line finds the filter coefficients for the correction filter,
%  a Butterworth low-pass filter of the same order and a 10% lower 3-dB
%  frequency.

[bb, aa] = Butterworth_LP(M, flpf*0.9, fs);
%  Apply filter to time series reversed in time

yyrev = y(end:-1:1);
yyrevfilt = filter(bb, aa, yyrev);
y_filtered = yyrevfilt(end:-1:1);
%
%%%%%%%%%%%%%%%%%%%%%%%%%%%%%%%%%%%%%%%%%%%%%%%%%%%%%%%%%%%%%%%%%%%%%%%

function [bb,aa] = Butterworth_LP(N, f0_actual, fs);
%
%  This routine generates the 'filter' coefficients for IIR implementation
%  of a Butterworth low-pass filter of order, N, with 3-dB frequency, f0,
%  and for a sampling rate of fs. The frequencies entered are 'warped'
%  internal to the function so that the z-transform filter has the proper
%  frequencies; hence, the labels '_actual' on the input. Enter the
%  actual frequency you intend to be the 3-dB point.
%
%  Usage:
%  To produce a low-pass filter of order N with upper 3-dB edge at f0
%   (for use with data sampled at fs):
%   [bb,aa] = Butterworth_LP(N,f0,fs);
%   yfiltered = filter(bb,aa,yunfiltered);
%
```

```
if f0_actual > 0.45*fs
    warning('The sampling rate is too low; the 3-dB frequency has been changed');
    f0_actual = 0.45*fs;
end
f0 = fs*tan(pi*f0_actual/fs)/pi;
%  ... warp frequencies to account for bilinear transformation
%
%  Angular location of poles:

theta = pi/N;
angs = ((pi+theta)/2):theta:(3*pi/2);
%
%  LOW-PASS Filter
%
%  Radial location of poles:

w_crit = 2*pi*f0;
%  The poles:

roots = w_crit*exp(j*angs);
%
%  The low-pass filter is an all-pole filter; the denominator is simply the
%  polynomial with roots equal to the required poles:

dens = real(poly(roots));
mplus1 = length(dens);
%  The numerator is a constant to make the response one in the pass band:

nums = dens(mplus1);
%
%  Find the z-domain coefficients from the s-domain coefficients via the
%  bilinear transformation:

[bb,aa] = bilinear_xform(nums,dens,fs);
```

Appendix J: Diffraction-Function Calculation Used for Diffraction-Correction Filters for Baffled and Unbaffled Microphones

```
function avg_p = Jones_diffraction_function(ka_total, alpha, Nterms)
%
%  This routine calculates the average (complex) pressure on the face
% of a microphone in the zero-degree orientation. In this orientation, the
% incoming wave direction is along the cylindrical axis of the microphone
% (i.e., the wave front is parallel to the end face of the microphone).
%  The calculation is done for all values of ka included in ka_total where
% ka is the normalized frequency: 2*pi*f*a/c; f is the ordinary frequency,
% a is the face diameter, and c is the sound speed.
%
%  USAGE:   avg_p = Jones_diff_fn(ka_total, alpha, Nterms);
%
% where ka_total is the vector of ka values and alpha is a factor to
% account for an inactive outer ring as would be the case in a practical
% microphone. The factor, alpha, is the fraction of the diameter that
% represents active surface for the transducer. If alpha is not specified,
% a value of 0.85 typical of condenser microphones is assumed. Alpha must
% be positive, but not greater than one. If Nterms is not specified, then
% 5 terms are used;  the maximum value of Nterms is 13.
%
%  Reference: D. S. Jones, "The scattering of a scalar wave by a
%  semi-infinite rod of circular cross section," Phil. Trans.
%  Roy. Soc. London A247, 499-528, 1955.
%
%  Author: T. Gabrielson, Applied Research Lab - Penn State
%  tbg3@psu.edu
%
if nargin < 3; Nterms = 5; end
%
if nargin == 1;  alpha = 0.85; end
%
%  The alpha factor accounts for the non-responsive solid
% edge of the condenser microphone. Pressure for r > alpha
% is not considered in the sum over the face because it
% would have no effect on the diaphragm
%
if alpha > 1.0; error('Value of alpha cannot be greater than one.'); end
%
%  The table values of the "split function" only go to ka = 200. If
%  values greater than 200 are requested, a simple replacement value is
%  used (later).
ka_table_limit = 200;
nka = ka_total < ka_table_limit;
n1 = sum(nka); ka = ka_total(1:n1);
%
joo = 2.40483;
%  Find the gm constants, which are the coefficients of the
% Bessel series:
gms = Jones_rod_gms(ka, Nterms);
%
%  Prepare to do the integration only over the active surface (r < alpha)
dr = alpha/50;
r  = 0.0:dr:alpha;
%
%  The factor nfact adjusts the result to compensate for the
% Bessel weighting across the active area. The factor, 0.4318, is 2 times
% the integral of r*J0(joo*r)*dr from 0 to 1. (This factor is equivalent
% to 2*J1(joo)/joo.)
nfact = alpha^2*0.4318;
%
%  Implementation of a quasi-trapezoidal integration of
% the pressure over the active portion of the end face
%
```

```
avg_p = zeros(1, length(ka));
%
for kk = 1:length(ka)
    p_profile = Jones_p_profile(r,gms(1:Nterms, kk));
    %  Apply Bessel-function, J0, weighting appropriate for active membrane
    %  area
    p_profile = besselj(0,r*joo/alpha).*p_profile/nfact;
    int_sum = 0;
    for nn = 2:length(r)
        r1 = r(nn-1); p1 = p_profile(nn-1);
        r2 = r(nn)  ; p2 = p_profile(nn);
        %  Integration is performed as follows:  pressure is assumed to be
        %  linear between r1 and r2:  p(r) = p1 + bb*(r - r1)
        %  or  p(r) = p1 - bb*r1  +  bb*r
        %  then the integration (int(r*p(r)*dr) is done analytically,
        %  which leads to the r^2 and r^3 terms below.
        bb = (p2-p1)/(r2-r1); aa = p1-bb*r1;
        int_sum = int_sum + aa*(r2^2-r1^2)/2 + bb*(r2^3-r1^3)/3;
    end
    avg_p(kk) = int_sum*2;
end
%
%  Ad hoc extension if required since my tables of the split function
% only go to ka = 200. THIS NEEDS TO BE DONE BETTER.
%
if n1 < length(ka_total)
   ka1 = ka_total((n1 + 1):length(ka_total));
%  avgext = 2.00 + j*12.4028*exp(-ka1/1.9635);
   avgext = 2.00 + j*0.00*ka1;
   avg_p = [avg_p, avgext];
end
%=====================================================================
%
function gm = Jones_rod_gms(ka, Nterms)
%  Calculation of coefficients in Bessel series for
% pressure at rod end
%
%  Zeros of the derivative of the Bessel J-zero function
jom = [3.831707, 7.015587, 10.17347, 13.32369,...
        16.47063, 19.61586, 22.76008, 25.90367,...
        29.04683, 32.18968, 35.33231, 38.47477];
%
%  Calculate capital-K-sub-p functions by interpolating in
% the tables
%
KP = KP_fun_gen(ka, Nterms);
%
%  Construct kappa-a values for m = 0 to Nterms - 1
kk_a = zeros(Nterms, length(ka));
kk_a(1,:) = i*ka;
for ii = 2:Nterms
    kk_a(ii, :) = sqrt(jom(ii - 1)^2-ka.^2);
end
%
gm = zeros(Nterms, length(ka));
Q  = zeros(1, Nterms);
C  = zeros(Nterms, 1);
B  = zeros(Nterms, Nterms);
A  = zeros(Nterms, Nterms);
%
for ii = 1:length(ka)
    for im = 1:Nterms
        Q(im) = (kk_a(im, ii) + kk_a(1, ii))*KP(im, ii);
    end
    for ir = 1:Nterms
        for im = 1:Nterms
            Brm = kk_a(ir, ii) + kk_a(im, ii);
            A(ir, im) = Q(im)/Brm;
            B(ir, im) = Brm;
        end
    end
    for ir = 1:Nterms
        A(ir, ir) = A(ir, ir) + B(ir, ir)/Q(ir);
```

```
        C(ir) = -2*Q(1)/B(ir, 1);
    end
    gm(:, ii) = A\C;
end
%=================================================================
%
function p_profile = Jones_p_profile(x,gms_ka);
%  Calculation of pressure profile - Jones rod; normal incidence
%
%  This routine sums the Bessel series for the pressure
% as a function of radial coordinate, x. x = 0 at the center
% and x = 1 at the edge.
%
%  Zeros of the derivative of the Bessel J-zero function
jomm = [0.0, 3.831707, 7.015587, 10.17347, 13.32369,...
        16.47063, 19.61586, 22.76008, 25.90367,...
        29.04683, 32.18968, 35.33231, 38.47477];
%
Nterms = length(gms_ka);
%
bess = zeros(Nterms, length(x));
bess0 = zeros(Nterms, 1);
%
for ii = 1:Nterms
    bess(ii, :) = besselj(0, x*jomm(ii));
    bess0(ii)   = besselj(0,  jomm(ii));
end
%
%  Allocate space for summing vector
sum = x*0.0;
%
for ii = 1:Nterms
    sum = sum + gms_ka(ii)*bess(ii, :)/bess0(ii);
end
%
p_profile = 2 + sum;
%
%=================================================================
%
function kPP = KP_fun_gen(ka_array, Nterms)
%
%  This function interpolates a look-up table for values of the Jones
%  'split function' for orders from 0 to 12. These split functions have
%  'kinks' in them at the zeros of the derivative of the Bessel J-zero
%  function:
%  jom = [3.83171, 7.01559, 10.1735, 13.3237,...
%         16.4706, 19.6159, 22.7601, 25.9037,...
%         29.0468, 32.1897, 35.3323, 38.4748];
%  so the tables are constructed to be well-sampled in the vicinity of
%  these kinks. The interpolation is linear. A better approach might be
%  to use a separate spline interpolation over each interval between kinks
%  but that has not been implemented yet.
%
if Nterms > 13; error('Too many terms requested: Nterms <= 13.'); end
%
%  Breakpoints between table intervals
jom = [0.0, 3.83171, 7.01559, 10.1735, 13.3237,...
        16.4706, 19.6159, 22.7601, 25.9037,...
        29.0468, 32.1897, 35.3323, 38.4748, 40.0001, 200];
%
%  Table values for ka
ka_int=[0.00000, 0.25000, 0.50000, 0.75000,...
    1.00000, 1.25000, 1.50000, 1.75000,...
    2.00000, 2.25000, 2.50000, 2.75000,...
    3.00000, 3.25000, 3.50000, 3.70000,...
    3.75000, 3.79000, 3.81000, 3.82000,...
    3.83171, 3.84000, 3.85000, 3.87000,...
    3.90000, 4.00000, 4.25000, 4.50000,...
    4.75000, 5.00000, 5.25000, 5.50000,...
    5.75000, 6.00000, 6.25000, 6.50000,...
    6.75000, 6.90000, 6.95000, 6.98000,...
    7.00000, 7.01000, 7.01559, 7.02000,...
    7.03000, 7.04000, 7.06000, 7.09000,...
```

```
    7.25000, 7.50000, 7.75000, 8.00000,...
    8.25000, 8.50000, 8.75000, 9.00000,...
    9.25000, 9.50000, 9.75000, 10.00000,...
    10.10000, 10.13000, 10.15000, 10.16000,...
    10.17350, 10.18000, 10.19000, 10.21000,...
    10.25000, 10.50000, 10.75000, 11.00000,...
    11.25000, 11.50000, 11.75000, 12.00000,...
    12.25000, 12.50000, 12.75000, 13.00000,...
    13.25000, 13.27000, 13.30000, 13.31000,...
    13.32370, 13.33000, 13.34000, 13.37000,...
    13.40000, 13.45000, 13.50000, 13.75000,...
    14.00000, 14.25000, 14.50000, 14.75000,...
    15.00000, 15.25000, 15.50000, 15.75000,...
    16.00000, 16.25000, 16.30000, 16.35000,...
    16.40000, 16.45000, 16.47060, 16.50000,...
    17.00000, 17.50000, 18.00000, 18.50000,...
    19.00000, 19.50000, 19.61590, 20.00000,...
    20.50000, 21.00000, 21.50000, 22.00000,...
    22.50000, 22.76010, 23.00000, 23.50000,...
    24.00000, 24.50000, 25.00000, 25.50000,...
    25.90370, 26.00000, 26.50000, 27.00000,...
    27.50000, 28.00000, 28.50000, 29.04680,...
    29.50000, 30.00000, 30.50000, 31.00000,...
    31.50000, 32.00000, 32.18970, 32.50000,...
    33.00000, 33.50000, 34.00000, 34.50000,...
    35.00000, 35.33230, 35.50000, 36.00000,...
    36.50000, 37.00000, 37.50000, 38.00000,...
    38.47480, 39.00000, 39.50000, 40.00000,...
    50.00000, 75.00000, 100.00000, 200.00000];
%
kP0=[1.00000, 0.97394-0.14789i, 0.90558-0.27102i, 0.81628-0.36103i,...
    0.71950-0.41889i, 0.62483-0.44959i, 0.53776-0.45907i, 0.46100-0.45283i,...
    0.39540-0.43570i, 0.34083-0.41072i, 0.29675-0.38095i, 0.26225-0.34824i,...
    0.23649-0.31369i, 0.21898-0.27745i, 0.21019-0.23808i, 0.21242-0.19930i,...
    0.21571-0.18629i, 0.22044-0.17280i, 0.22445-0.16346i, 0.22754-0.15702i,...
    0.23777-0.13906i, 0.25230-0.14836i, 0.25891-0.15324i, 0.26719-0.16019i,...
    0.27507-0.16807i, 0.28795-0.18694i, 0.29182-0.21703i, 0.28131-0.23523i,...
    0.26519-0.24536i, 0.24703-0.24917i, 0.22877-0.24788i, 0.21156-0.24246i,...
    0.19615-0.23368i, 0.18305-0.22211i, 0.17265-0.20806i, 0.16552-0.19140i,...
    0.16295-0.17084i, 0.16560-0.15402i, 0.16824-0.14620i, 0.17098-0.13994i,...
    0.17404-0.13400i, 0.17676-0.12930i, 0.18151-0.12228i, 0.18751-0.12659i,...
    0.19211-0.13029i, 0.19499-0.13286i, 0.19898-0.13682i, 0.20295-0.14146i,...
    0.21136-0.15783i, 0.21089-0.17358i, 0.20440-0.18332i, 0.19531-0.18881i,...
    0.18517-0.19085i, 0.17489-0.19000i, 0.16510-0.18668i, 0.15624-0.18122i,...
    0.14866-0.17381i, 0.14275-0.16448i, 0.13912-0.15288i, 0.13943-0.13717i,...
    0.14229-0.12767i, 0.14409-0.12361i, 0.14597-0.12001i, 0.14737-0.11759i,...
    0.15285-0.11015i, 0.15766-0.11390i, 0.16045-0.11635i, 0.16376-0.11965i,...
    0.16760-0.12429i, 0.17394-0.14072i, 0.17180-0.15022i, 0.16667-0.15613i,...
    0.16017-0.15932i, 0.15312-0.16026i, 0.14606-0.15925i, 0.13938-0.15652i,...
    0.13337-0.15223i, 0.12832-0.14644i, 0.12460-0.13904i, 0.12289-0.12945i,...
    0.12594-0.11447i, 0.12683-0.11248i, 0.12888-0.10858i, 0.12999-0.10673i,...
    0.13426-0.10085i, 0.13803-0.10390i, 0.14019-0.10587i, 0.14364-0.10954i,...
    0.14567-0.11217i, 0.14781-0.11562i, 0.14911-0.11846i, 0.15032-0.12843i,...
    0.14765-0.13465i, 0.14331-0.13845i, 0.13820-0.14033i, 0.13281-0.14058i,...
    0.12750-0.13940i, 0.12253-0.13690i, 0.11813-0.13316i, 0.11457-0.12817i,...
    0.11221-0.12170i, 0.11195-0.11287i, 0.11238-0.11056i, 0.11312-0.10788i,...
    0.11439-0.10457i, 0.11699-0.09960i, 0.12094-0.09387i, 0.12750-0.09942i,...
    0.13362-0.11890i, 0.12708-0.12565i, 0.11852-0.12650i, 0.11044-0.12277i,...
    0.10453-0.11476i, 0.10448-0.09969i, 0.11152-0.08810i, 0.12244-0.10648i,...
    0.11829-0.11415i, 0.11138-0.11627i, 0.10434-0.11428i, 0.09867-0.10865i,...
    0.09642-0.09836i, 0.10365-0.08327i, 0.11285-0.09600i, 0.11104-0.10472i,...
    0.10550-0.10782i, 0.09935-0.10714i, 0.09398-0.10323i, 0.09086-0.09573i,...
    0.09734-0.07927i, 0.10364-0.08629i, 0.10483-0.09669i, 0.10052-0.10062i,...
    0.09515-0.10097i, 0.09013-0.09837i, 0.08662-0.09281i, 0.09179-0.07583i,...
    0.09932-0.08963i, 0.09619-0.09434i, 0.09154-0.09552i, 0.08689-0.09397i,...
    0.08324-0.08984i, 0.08241-0.08189i, 0.08749-0.07274i, 0.09417-0.08324i,...
    0.09231-0.08877i, 0.08834-0.09067i, 0.08407-0.08998i, 0.08047-0.08690i,...
    0.07864-0.08103i, 0.08347-0.07000i, 0.08909-0.07706i, 0.08882-0.08368i,...
    0.08553-0.08623i, 0.08163-0.08626i, 0.07806-0.08413i, 0.07574-0.07966i,...
    0.08019-0.06766i, 0.08550-0.07903i, 0.08291-0.08220i, 0.07940-0.08286i,...
    0.07071-0.07071i, 0.05774-0.05774i, 0.05000-0.05000i, 0.03536-0.03536i];
    %
kP1=[0.45340-0.00000i, 0.45562-0.00029i, 0.46190-0.00216i, 0.47152-0.00672i,...
```

```
    0.48373-0.01485i, 0.49773-0.02736i, 0.51261-0.04510i, 0.52718-0.06899i,...
    0.53966-0.09993i, 0.54789-0.13883i, 0.54834-0.18621i, 0.53595-0.24175i,...
    0.50312-0.30313i, 0.43801-0.36293i, 0.32073-0.39862i, 0.16358-0.35312i,...
    0.11007-0.30819i, 0.06091-0.24272i, 0.03342-0.18617i, 0.01867-0.14216i,...
    0.00270-0.00000i, 0.11763-0.00849i, 0.16519-0.01774i, 0.22097-0.03443i,...
    0.27033-0.05650i, 0.34420-0.11459i, 0.37667-0.20451i, 0.35608-0.25247i,...
    0.32335-0.27608i, 0.28927-0.28425i, 0.25776-0.28219i, 0.23031-0.27323i,...
    0.20743-0.25957i, 0.18919-0.24263i, 0.17557-0.22319i, 0.16678-0.20127i,...
    0.16394-0.17540i, 0.16726-0.15485i, 0.17040-0.14537i, 0.17359-0.13781i,...
    0.17714-0.13063i, 0.18026-0.12493i, 0.18569-0.11638i, 0.19306-0.12130i,...
    0.19874-0.12558i, 0.20233-0.12858i, 0.20731-0.13323i, 0.21232-0.13871i,...
    0.22313-0.15842i, 0.22294-0.17762i, 0.21526-0.18949i, 0.20445-0.19611i,...
    0.19247-0.19854i, 0.18048-0.19753i, 0.16920-0.19365i, 0.15912-0.18735i,...
    0.15063-0.17891i, 0.14410-0.16844i, 0.14015-0.15557i, 0.14054-0.13835i,...
    0.14364-0.12800i, 0.14558-0.12357i, 0.14759-0.11966i, 0.14909-0.11701i,...
    0.15496-0.10889i, 0.16023-0.11289i, 0.16330-0.11553i, 0.16695-0.11908i,...
    0.17120-0.12410i, 0.17831-0.14200i, 0.17603-0.15240i, 0.17046-0.15887i,...
    0.16340-0.16235i, 0.15578-0.16336i, 0.14817-0.16226i, 0.14101-0.15932i,...
    0.13460-0.15471i, 0.12925-0.14853i, 0.12533-0.14067i, 0.12354-0.13054i,...
    0.12675-0.11478i, 0.12768-0.11270i, 0.12981-0.10860i, 0.13097-0.10665i,...
    0.13542-0.10047i, 0.13939-0.10364i, 0.14167-0.10570i, 0.14532-0.10954i,...
    0.14747-0.11228i, 0.14974-0.11591i, 0.15112-0.11889i, 0.15244-0.12939i,...
    0.14965-0.13594i, 0.14510-0.13994i, 0.13973-0.14192i, 0.13408-0.14218i,...
    0.12853-0.14093i, 0.12335-0.13831i, 0.11878-0.13441i, 0.11509-0.12922i,...
    0.11265-0.12251i, 0.11239-0.11338i, 0.11283-0.11099i, 0.11360-0.10823i,...
    0.11491-0.10481i, 0.11759-0.09967i, 0.12164-0.09375i, 0.12843-0.09946i,...
    0.13481-0.11959i, 0.12806-0.12656i, 0.11923-0.12744i, 0.11092-0.12359i,...
    0.10486-0.11537i, 0.10482-0.09993i, 0.11199-0.08807i, 0.12320-0.10686i,...
    0.11896-0.11471i, 0.11189-0.11688i, 0.10471-0.11485i, 0.09892-0.10910i,...
    0.09665-0.09862i, 0.10398-0.08328i, 0.11336-0.09622i, 0.11152-0.10508i,...
    0.10589-0.10824i, 0.09963-0.10755i, 0.09420-0.10357i, 0.09103-0.09597i,...
    0.09758-0.07929i, 0.10398-0.08639i, 0.10519-0.09694i, 0.10082-0.10092i,...
    0.09538-0.10127i, 0.09030-0.09864i, 0.08675-0.09301i, 0.09197-0.07585i,...
    0.09959-0.08980i, 0.09643-0.09456i, 0.09173-0.09575i, 0.08703-0.09419i,...
    0.08335-0.09001i, 0.08251-0.08200i, 0.08763-0.07277i, 0.09438-0.08335i,...
    0.09250-0.08893i, 0.08850-0.09085i, 0.08419-0.09015i, 0.08057-0.08705i,...
    0.07872-0.08113i, 0.08359-0.07002i, 0.08925-0.07714i, 0.08897-0.08380i,...
    0.08566-0.08637i, 0.08173-0.08640i, 0.07815-0.08426i, 0.07581-0.07976i,...
    0.08028-0.06769i, 0.08563-0.07912i, 0.08302-0.08231i, 0.07949-0.08297i,...
    0.07071-0.07071i, 0.05774-0.05774i, 0.05000-0.05000i, 0.03536-0.03536i];
    %
kP2=[0.35274-0.00000i, 0.35368-0.00012i, 0.35633-0.00091i, 0.36033-0.00278i,...
    0.36533-0.00604i, 0.37098-0.01088i, 0.37692-0.01750i, 0.38276-0.02604i,...
    0.38787-0.03660i, 0.39201-0.04929i, 0.39432-0.06408i, 0.39390-0.08083i,...
    0.38957-0.09913i, 0.37957-0.11815i, 0.36082-0.13602i, 0.33391-0.14600i,...
    0.32343-0.14670i, 0.31218-0.14580i, 0.30434-0.14422i, 0.29896-0.14271i,...
    0.28442-0.13660i, 0.29006-0.12542i, 0.29282-0.12039i, 0.29661-0.11406i,...
    0.30080-0.10790i, 0.31087-0.09671i, 0.32951-0.08770i, 0.34540-0.08957i,...
    0.35965-0.09833i, 0.37189-0.11311i, 0.38107-0.13374i, 0.38551-0.16020i,...
    0.38271-0.19223i, 0.36899-0.22880i, 0.33880-0.26702i, 0.28352-0.29929i,...
    0.18819-0.30274i, 0.09948-0.25534i, 0.06145-0.21291i, 0.03557-0.16897i,...
    0.01651-0.11931i, 0.00618-0.07487i, 0.00190-0.00000i, 0.06584-0.00353i,...
    0.11181-0.01086i, 0.13940-0.01765i, 0.17594-0.03013i, 0.21063-0.04690i,...
    0.28056-0.11334i, 0.29224-0.17514i, 0.27532-0.20886i, 0.25123-0.22554i,...
    0.22659-0.23110i, 0.20397-0.22914i, 0.18437-0.22200i, 0.16818-0.21123i,...
    0.15549-0.19781i, 0.14642-0.18217i, 0.14137-0.16403i, 0.14217-0.14095i,...
    0.14616-0.12742i, 0.14859-0.12166i, 0.15107-0.11656i, 0.15291-0.11311i,...
    0.16007-0.10241i, 0.16708-0.10728i, 0.17121-0.11052i, 0.17616-0.11495i,...
    0.18201-0.12131i, 0.19218-0.14461i, 0.18951-0.15835i, 0.18239-0.16685i,...
    0.17336-0.17137i, 0.16373-0.17265i, 0.15427-0.17124i, 0.14550-0.16755i,...
    0.13781-0.16191i, 0.13150-0.15446i, 0.12698-0.14516i, 0.12498-0.13339i,...
    0.12866-0.11532i, 0.12970-0.11293i, 0.13209-0.10825i, 0.13339-0.10602i,...
    0.13833-0.09892i, 0.14292-0.10245i, 0.14556-0.10476i, 0.14981-0.10908i,...
    0.15233-0.11219i, 0.15500-0.11631i, 0.15665-0.11972i, 0.15830-0.13178i,...
    0.15516-0.13932i, 0.14997-0.14392i, 0.14386-0.14618i, 0.13748-0.14647i,...
    0.13124-0.14504i, 0.12546-0.14209i, 0.12040-0.13773i, 0.11635-0.13198i,...
    0.11370-0.12460i, 0.11344-0.11463i, 0.11392-0.11204i, 0.11475-0.10903i,...
    0.11616-0.10532i, 0.11904-0.09973i, 0.12339-0.09329i, 0.13081-0.09942i,...
    0.13791-0.12129i, 0.13059-0.12890i, 0.12103-0.12985i, 0.11210-0.12568i,...
    0.10565-0.11688i, 0.10562-0.10050i, 0.11316-0.08793i, 0.12513-0.10778i,...
    0.12065-0.11612i, 0.11318-0.11842i, 0.10560-0.11627i, 0.09954-0.11022i,...
    0.09717-0.09926i, 0.10479-0.08326i, 0.11462-0.09672i, 0.11272-0.10599i,...
    0.10684-0.10928i, 0.10034-0.10855i, 0.09470-0.10441i, 0.09143-0.09655i,...
```

```
    0.09817-0.07932i, 0.10480-0.08664i, 0.10606-0.09753i, 0.10155-0.10165i,...
    0.09594-0.10201i, 0.09072-0.09930i, 0.08707-0.09351i, 0.09243-0.07588i,...
    0.10025-0.09020i, 0.09701-0.09508i, 0.09219-0.09631i, 0.08738-0.09470i,...
    0.08362-0.09043i, 0.08276-0.08224i, 0.08798-0.07282i, 0.09488-0.08362i,...
    0.09297-0.08932i, 0.08888-0.09128i, 0.08448-0.09056i, 0.08079-0.08740i,...
    0.07892-0.08138i, 0.08386-0.07008i, 0.08963-0.07731i, 0.08935-0.08409i,...
    0.08598-0.08670i, 0.08199-0.08673i, 0.07834-0.08456i, 0.07597-0.07999i,...
    0.08050-0.06774i, 0.08594-0.07934i, 0.08330-0.08257i, 0.07971-0.08324i,...
    0.07071-0.07071i, 0.05774-0.05774i, 0.05000-0.05000i, 0.03536-0.03536i];
    %
kP3=[0.29902-0.00000i, 0.29957-0.00007i, 0.30111-0.00053i, 0.30344-0.00161i,...
    0.30633-0.00348i, 0.30959-0.00623i, 0.31301-0.00995i, 0.31638-0.01469i,...
    0.31928-0.02049i, 0.32180-0.02739i, 0.32342-0.03538i, 0.32373-0.04439i,...
    0.32215-0.05429i, 0.31781-0.06477i, 0.30907-0.07521i, 0.29569-0.08228i,...
    0.29023-0.08345i, 0.28420-0.08385i, 0.27989-0.08365i, 0.27688-0.08328i,...
    0.26847-0.08119i, 0.27066-0.07460i, 0.27179-0.07164i, 0.27342-0.06791i,...
    0.27531-0.06427i, 0.28012-0.05761i, 0.28955-0.05194i, 0.29771-0.05222i,...
    0.30500-0.05590i, 0.31131-0.06222i, 0.31632-0.07083i, 0.31959-0.08148i,...
    0.32054-0.09392i, 0.31841-0.10774i, 0.31215-0.12232i, 0.30022-0.13650i,...
    0.27957-0.14778i, 0.25916-0.15017i, 0.24915-0.14890i, 0.24114-0.14683i,...
    0.23366-0.14405i, 0.22787-0.14136i, 0.21954-0.13639i, 0.22395-0.12950i,...
    0.22752-0.12423i, 0.22991-0.12090i, 0.23349-0.11623i, 0.23760-0.11142i,...
    0.25226-0.09928i, 0.26874-0.09463i, 0.28253-0.09765i, 0.29436-0.10610i,...
    0.30387-0.11939i, 0.31008-0.13734i, 0.31149-0.15977i, 0.30581-0.18615i,...
    0.28970-0.21508i, 0.25812-0.24299i, 0.20299-0.26066i, 0.10937-0.23677i,...
    0.05385-0.18449i, 0.03384-0.15206i, 0.01923-0.11828i, 0.01141-0.09290i,...
    0.00490-0.00002i, 0.06568-0.00432i, 0.09904-0.01038i, 0.13694-0.02140i,...
    0.17872-0.04064i, 0.24767-0.12018i, 0.24633-0.16354i, 0.22982-0.18722i,...
    0.20961-0.19844i, 0.18973-0.20131i, 0.17181-0.19845i, 0.15651-0.19158i,...
    0.14409-0.18184i, 0.13464-0.16988i, 0.12837-0.15586i, 0.12593-0.13910i,...
    0.13097-0.11457i, 0.13231-0.11138i, 0.13535-0.10511i, 0.13697-0.10210i,...
    0.14313-0.09249i, 0.14942-0.09688i, 0.15309-0.09979i, 0.15907-0.10534i,...
    0.16266-0.10940i, 0.16652-0.11485i, 0.16894-0.11940i, 0.17172-0.13575i,...
    0.16768-0.14603i, 0.16083-0.15224i, 0.15282-0.15524i, 0.14455-0.15559i,...
    0.13661-0.15372i, 0.12939-0.14995i, 0.12321-0.14449i, 0.11836-0.13742i,...
    0.11527-0.12854i, 0.11502-0.11674i, 0.11559-0.11369i, 0.11655-0.11018i,...
    0.11818-0.10583i, 0.12148-0.09930i, 0.12641-0.09174i, 0.13520-0.09871i,...
    0.14394-0.12431i, 0.13541-0.13328i, 0.12434-0.13437i, 0.11415-0.12956i,...
    0.10693-0.11959i, 0.10692-0.10137i, 0.11515-0.08746i, 0.12861-0.10933i,...
    0.12369-0.11861i, 0.11543-0.12114i, 0.10713-0.11877i, 0.10056-0.11216i,...
    0.09803-0.10033i, 0.10614-0.08313i, 0.11679-0.09753i, 0.11479-0.10752i,...
    0.10848-0.11106i, 0.10151-0.11028i, 0.09552-0.10585i, 0.09206-0.09751i,...
    0.09915-0.07933i, 0.10617-0.08701i, 0.10755-0.09852i, 0.10279-0.10288i,...
    0.09687-0.10325i, 0.09139-0.10040i, 0.08758-0.09433i, 0.09315-0.07594i,...
    0.10134-0.09086i, 0.09797-0.09596i, 0.09294-0.09723i, 0.08794-0.09556i,...
    0.08404-0.09111i, 0.08316-0.08264i, 0.08854-0.07290i, 0.09571-0.08405i,...
    0.09373-0.08996i, 0.08951-0.09198i, 0.08502-0.09119i, 0.08116-0.08798i,...
    0.07923-0.08178i, 0.08430-0.07016i, 0.09024-0.07758i, 0.08997-0.08456i,...
    0.08650-0.08725i, 0.08240-0.08728i, 0.07866-0.08504i, 0.07623-0.08035i,...
    0.08086-0.06782i, 0.08644-0.07968i, 0.08374-0.08300i, 0.08007-0.08368i,...
    0.07071-0.07071i, 0.05774-0.05774i, 0.05000-0.05000i, 0.03536-0.03536i];
    %
kP4=[0.26424+0.00000i, 0.26461-0.00005i, 0.26565-0.00036i, 0.26721-0.00108i,...
    0.26916-0.00233i, 0.27134-0.00416i, 0.27363-0.00662i, 0.27589-0.00974i,...
    0.27777-0.01354i, 0.27950-0.01804i, 0.28069-0.02324i, 0.28106-0.02910i,...
    0.28028-0.03555i, 0.27778-0.04245i, 0.27249-0.04950i, 0.26412-0.05463i,...
    0.26063-0.05563i, 0.25671-0.05617i, 0.25388-0.05624i, 0.25188-0.05615i,...
    0.24623-0.05517i, 0.24737-0.05070i, 0.24800-0.04869i, 0.24892-0.04615i,...
    0.25003-0.04367i, 0.25297-0.03911i, 0.25897-0.03511i, 0.26424-0.03507i,...
    0.26899-0.03722i, 0.27313-0.04100i, 0.27650-0.04617i, 0.27888-0.05255i,...
    0.27997-0.05999i, 0.27937-0.06828i, 0.27652-0.07716i, 0.27053-0.08612i,...
    0.25951-0.09413i, 0.24799-0.09721i, 0.24208-0.09738i, 0.23722-0.09691i,...
    0.23257-0.09599i, 0.22889-0.09496i, 0.22343-0.09280i, 0.22542-0.08824i,...
    0.22710-0.08475i, 0.22826-0.08255i, 0.23004-0.07946i, 0.23213-0.07627i,...
    0.24002-0.06812i, 0.24922-0.06458i, 0.25695-0.06559i, 0.26354-0.06949i,...
    0.26891-0.07566i, 0.27276-0.08376i, 0.27470-0.09354i, 0.27418-0.10464i,...
    0.27049-0.11661i, 0.26262-0.12864i, 0.24898-0.13931i, 0.22576-0.14507i,...
    0.21045-0.14318i, 0.20392-0.14116i, 0.19823-0.13883i, 0.19446-0.13698i,...
    0.18342-0.12942i, 0.18842-0.12259i, 0.19152-0.11861i, 0.19553-0.11380i,...
    0.20099-0.10799i, 0.22076-0.09517i, 0.23474-0.09403i, 0.24647-0.09848i,...
    0.25621-0.10732i, 0.26347-0.12020i, 0.26728-0.13694i, 0.26612-0.15724i,...
    0.25775-0.18036i, 0.23888-0.20443i, 0.20444-0.22494i, 0.14604-0.22944i,...
    0.04585-0.16170i, 0.03472-0.14421i, 0.01647-0.10382i, 0.00984-0.08179i,...
```

```
    0.00232-0.00001i, 0.05662-0.00367i, 0.08637-0.00902i, 0.13173-0.02328i,...
    0.15722-0.03581i, 0.18329-0.05407i, 0.19914-0.06986i, 0.22256-0.12522i,...
    0.21475-0.15634i, 0.19874-0.17300i, 0.18109-0.18019i, 0.16434-0.18093i,...
    0.14956-0.17718i, 0.13716-0.17023i, 0.12732-0.16093i, 0.12017-0.14968i,...
    0.11600-0.13641i, 0.11593-0.11973i, 0.11674-0.11553i, 0.11806-0.11072i,...
    0.12022-0.10480i, 0.12447-0.09592i, 0.13067-0.08554i, 0.14301-0.09440i,...
    0.15634-0.12920i, 0.14494-0.14153i, 0.13036-0.14296i, 0.11741-0.13670i,...
    0.10863-0.12427i, 0.10869-0.10241i, 0.11820-0.08587i, 0.13465-0.11161i,...
    0.12888-0.12271i, 0.11915-0.12571i, 0.10951-0.12291i, 0.10202-0.11529i,...
    0.09921-0.10190i, 0.10818-0.08264i, 0.12028-0.09865i, 0.11809-0.10988i,...
    0.11104-0.11386i, 0.10331-0.11297i, 0.09671-0.10808i, 0.09296-0.09895i,...
    0.10059-0.07921i, 0.10826-0.08748i, 0.10982-0.09999i, 0.10466-0.10473i,...
    0.09826-0.10513i, 0.09237-0.10204i, 0.08832-0.09552i, 0.09419-0.07596i,...
    0.10298-0.09180i, 0.09939-0.09724i, 0.09405-0.09860i, 0.08875-0.09682i,...
    0.08464-0.09212i, 0.08373-0.08320i, 0.08935-0.07297i, 0.09691-0.08466i,...
    0.09485-0.09087i, 0.09041-0.09300i, 0.08570-0.09217i, 0.08167-0.08881i,...
    0.07967-0.08234i, 0.08493-0.07025i, 0.09113-0.07795i, 0.09086-0.08522i,...
    0.08725-0.08803i, 0.08299-0.08806i, 0.07911-0.08573i, 0.07660-0.08088i,...
    0.08137-0.06792i, 0.08716-0.08017i, 0.08436-0.08360i, 0.08058-0.08431i,...
    0.07071-0.07071i, 0.05774-0.05774i, 0.05000-0.05000i, 0.03536-0.03536i];
    %
kP5=[0.23935+0.00000i, 0.23962-0.00004i, 0.24039-0.00026i, 0.24153-0.00079i,...
    0.24295-0.00170i, 0.24454-0.00303i, 0.24622-0.00481i, 0.24787-0.00707i,...
    0.24917-0.00980i, 0.25045-0.01304i, 0.25136-0.01676i, 0.25170-0.02097i,...
    0.25124-0.02560i, 0.24959-0.03060i, 0.24597-0.03576i, 0.24010-0.03967i,...
    0.23761-0.04050i, 0.23481-0.04101i, 0.23276-0.04115i, 0.23131-0.04114i,...
    0.22718-0.04061i, 0.22787-0.03732i, 0.22827-0.03584i, 0.22887-0.03397i,...
    0.22962-0.03214i, 0.23165-0.02876i, 0.23590-0.02575i, 0.23968-0.02562i,...
    0.24311-0.02706i, 0.24611-0.02966i, 0.24860-0.03322i, 0.25042-0.03763i,...
    0.25138-0.04276i, 0.25123-0.04852i, 0.24959-0.05472i, 0.24586-0.06111i,...
    0.23870-0.06712i, 0.23095-0.06985i, 0.22689-0.07029i, 0.22350-0.07024i,...
    0.22022-0.06988i, 0.21759-0.06938i, 0.21364-0.06819i, 0.21478-0.06487i,...
    0.21577-0.06233i, 0.21646-0.06072i, 0.21755-0.05846i, 0.21887-0.05613i,...
    0.22401-0.05011i, 0.23023-0.04732i, 0.23552-0.04774i, 0.24007-0.05013i,...
    0.24383-0.05401i, 0.24665-0.05913i, 0.24832-0.06530i, 0.24853-0.07233i,...
    0.24688-0.07997i, 0.24281-0.08785i, 0.23530-0.09529i, 0.22175-0.10068i,...
    0.21230-0.10093i, 0.20811-0.10032i, 0.20438-0.09944i, 0.20187-0.09867i,...
    0.19420-0.09505i, 0.19670-0.09025i, 0.19829-0.08745i, 0.20041-0.08407i,...
    0.20339-0.07998i, 0.21478-0.07078i, 0.22302-0.06940i, 0.22988-0.07139i,...
    0.23555-0.07572i, 0.23988-0.08197i, 0.24260-0.08982i, 0.24331-0.09900i,...
    0.24147-0.10912i, 0.23639-0.11963i, 0.22704-0.12959i, 0.21160-0.13714i,...
    0.18371-0.13618i, 0.17998-0.13491i, 0.17280-0.13171i, 0.16946-0.12990i,...
    0.15943-0.12277i, 0.16433-0.11660i, 0.16734-0.11302i, 0.17270-0.10717i,...
    0.17642-0.10357i, 0.18127-0.09951i, 0.18529-0.09672i, 0.20058-0.09107i,...
    0.21253-0.09230i, 0.22250-0.09790i, 0.23044-0.10720i, 0.23577-0.11998i,...
    0.23745-0.13603i, 0.23391-0.15492i, 0.22285-0.17563i, 0.20086-0.19573i,...
    0.16256-0.20918i, 0.09844-0.19740i, 0.08097-0.18703i, 0.06133-0.17065i,...
    0.03896-0.14348i, 0.01276-0.08804i, 0.00002-0.00380i, 0.09959-0.01401i,...
    0.20152-0.12800i, 0.17541-0.16216i, 0.14539-0.16543i, 0.12272-0.15382i,...
    0.10952-0.13381i, 0.10995-0.10258i, 0.12225-0.07977i, 0.14642-0.11439i,...
    0.13878-0.12988i, 0.12574-0.13395i, 0.11323-0.13021i, 0.10390-0.12050i,...
    0.10060-0.10413i, 0.11108-0.08105i, 0.12596-0.09995i, 0.12348-0.11351i,...
    0.11509-0.11827i, 0.10598-0.11721i, 0.09834-0.11148i, 0.09411-0.10101i,...
    0.10261-0.07871i, 0.11137-0.08794i, 0.11326-0.10210i, 0.10744-0.10746i,...
    0.10026-0.10791i, 0.09373-0.10443i, 0.08927-0.09723i, 0.09563-0.07585i,...
    0.10535-0.09309i, 0.10144-0.09906i, 0.09561-0.10054i, 0.08986-0.09859i,...
    0.08544-0.09351i, 0.08447-0.08394i, 0.09045-0.07299i, 0.09860-0.08547i,...
    0.09641-0.09214i, 0.09166-0.09442i, 0.08663-0.09353i, 0.08235-0.08995i,...
    0.08024-0.08310i, 0.08577-0.07034i, 0.09235-0.07844i, 0.09208-0.08613i,...
    0.08827-0.08909i, 0.08377-0.08912i, 0.07970-0.08667i, 0.07707-0.08157i,...
    0.08205-0.06802i, 0.08813-0.08082i, 0.08521-0.08441i, 0.08125-0.08515i,...
    0.07071-0.07071i, 0.05774-0.05774i, 0.05000-0.05000i, 0.03536-0.03536i];
    %
kP6=[0.22041+0.00000i, 0.22062-0.00003i, 0.22121-0.00020i, 0.22209-0.00061i,...
    0.22319-0.00131i, 0.22442-0.00234i, 0.22571-0.00370i, 0.22698-0.00543i,...
    0.22792-0.00752i, 0.22892-0.00999i, 0.22964-0.01283i, 0.22994-0.01603i,...
    0.22964-0.01958i, 0.22844-0.02340i, 0.22577-0.02741i, 0.22136-0.03050i,...
    0.21948-0.03118i, 0.21734-0.03164i, 0.21577-0.03179i, 0.21466-0.03181i,...
    0.21146-0.03150i, 0.21193-0.02895i, 0.21220-0.02780i, 0.21263-0.02634i,...
    0.21317-0.02492i, 0.21468-0.02229i, 0.21790-0.01991i, 0.22079-0.01976i,...
    0.22342-0.02082i, 0.22574-0.02275i, 0.22767-0.02540i, 0.22912-0.02868i,...
    0.22994-0.03252i, 0.22996-0.03683i, 0.22889-0.04150i, 0.22630-0.04637i,...
    0.22116-0.05108i, 0.21547-0.05341i, 0.21244-0.05390i, 0.20990-0.05399i,...
```

```
    0.20741-0.05385i, 0.20541-0.05358i, 0.20237-0.05284i, 0.20310-0.05028i,...
    0.20376-0.04832i, 0.20423-0.04708i, 0.20497-0.04533i, 0.20589-0.04352i,...
    0.20960-0.03882i, 0.21419-0.03656i, 0.21813-0.03675i, 0.22156-0.03839i,...
    0.22442-0.04114i, 0.22662-0.04480i, 0.22801-0.04921i, 0.22840-0.05426i,...
    0.22752-0.05979i, 0.22496-0.06556i, 0.21999-0.07120i, 0.21067-0.07576i,...
    0.20395-0.07650i, 0.20092-0.07632i, 0.19819-0.07592i, 0.19633-0.07553i,...
    0.19055-0.07339i, 0.19207-0.06975i, 0.19307-0.06762i, 0.19442-0.06505i,...
    0.19637-0.06193i, 0.20415-0.05479i, 0.20995-0.05349i, 0.21482-0.05463i,...
    0.21888-0.05741i, 0.22206-0.06148i, 0.22421-0.06661i, 0.22510-0.07261i,...
    0.22443-0.07927i, 0.22181-0.08628i, 0.21657-0.09318i, 0.20750-0.09907i,...
    0.18998-0.10093i, 0.18751-0.10048i, 0.18265-0.09916i, 0.18034-0.09833i,...
    0.17314-0.09474i, 0.17573-0.09024i, 0.17737-0.08763i, 0.18036-0.08337i,...
    0.18250-0.08075i, 0.18535-0.07778i, 0.18774-0.07573i, 0.19702-0.07132i,...
    0.20426-0.07151i, 0.21023-0.07429i, 0.21498-0.07903i, 0.21833-0.08536i,...
    0.22000-0.09302i, 0.21958-0.10171i, 0.21654-0.11099i, 0.21016-0.12022i,...
    0.19932-0.12825i, 0.18165-0.13248i, 0.17674-0.13230i, 0.17101-0.13144i,...
    0.16395-0.12943i, 0.15366-0.12465i, 0.14266-0.11704i, 0.15256-0.10495i,...
    0.18632-0.08780i, 0.20506-0.09723i, 0.21499-0.11977i, 0.20877-0.15310i,...
    0.16937-0.18783i, 0.05354-0.15479i, 0.00405-0.00002i, 0.18666-0.09943i,...
    0.17125-0.14535i, 0.14303-0.15504i, 0.11998-0.14773i, 0.10525-0.13139i,...
    0.10090-0.10713i, 0.11472-0.07506i, 0.13651-0.10035i, 0.13358-0.11941i,...
    0.12218-0.12599i, 0.11015-0.12452i, 0.10048-0.11708i, 0.09536-0.10405i,...
    0.10539-0.07713i, 0.11616-0.08799i, 0.11872-0.10512i, 0.11176-0.11161i,...
    0.10321-0.11212i, 0.09555-0.10802i, 0.09045-0.09967i, 0.09757-0.07536i,...
    0.10880-0.09483i, 0.10438-0.10164i, 0.09780-0.10332i, 0.09136-0.10111i,...
    0.08646-0.09543i, 0.08541-0.08489i, 0.09190-0.07287i, 0.10096-0.08650i,...
    0.09857-0.09386i, 0.09341-0.09631i, 0.08786-0.09539i, 0.08322-0.09148i,...
    0.08096-0.08408i, 0.08687-0.07036i, 0.09398-0.07903i, 0.09372-0.08732i,...
    0.08963-0.09051i, 0.08480-0.09053i, 0.08045-0.08790i, 0.07767-0.08248i,...
    0.08292-0.06811i, 0.08941-0.08166i, 0.08632-0.08548i, 0.08213-0.08626i,...
    0.07071-0.07071i, 0.05774-0.05774i, 0.05000-0.05000i, 0.03536-0.03536i];
    %
kP7=[0.20537+0.00000i, 0.20554-0.00002i, 0.20601-0.00016i, 0.20672-0.00049i,...
    0.20760-0.00105i, 0.20858-0.00187i, 0.20962-0.00296i, 0.21064-0.00434i,...
    0.21132-0.00600i, 0.21213-0.00797i, 0.21272-0.01023i, 0.21298-0.01278i,...
    0.21277-0.01560i, 0.21186-0.01865i, 0.20978-0.02187i, 0.20632-0.02440i,...
    0.20482-0.02497i, 0.20312-0.02537i, 0.20187-0.02552i, 0.20098-0.02556i,...
    0.19841-0.02535i, 0.19875-0.02330i, 0.19895-0.02238i, 0.19928-0.02120i,...
    0.19969-0.02005i, 0.20086-0.01793i, 0.20341-0.01599i, 0.20572-0.01585i,...
    0.20782-0.01666i, 0.20968-0.01816i, 0.21124-0.02024i, 0.21242-0.02281i,...
    0.21313-0.02582i, 0.21321-0.02921i, 0.21246-0.03290i, 0.21053-0.03678i,...
    0.20661-0.04061i, 0.20220-0.04259i, 0.19983-0.04306i, 0.19782-0.04321i,...
    0.19585-0.04317i, 0.19426-0.04301i, 0.19183-0.04251i, 0.19234-0.04046i,...
    0.19280-0.03888i, 0.19314-0.03789i, 0.19369-0.03648i, 0.19437-0.03502i,...
    0.19720-0.03122i, 0.20078-0.02934i, 0.20389-0.02941i, 0.20660-0.03064i,...
    0.20888-0.03272i, 0.21066-0.03551i, 0.21184-0.03889i, 0.21227-0.04277i,...
    0.21174-0.04703i, 0.20996-0.05153i, 0.20636-0.05602i, 0.19941-0.05987i,...
    0.19428-0.06072i, 0.19193-0.06072i, 0.18981-0.06053i, 0.18836-0.06031i,...
    0.18378-0.05891i, 0.18480-0.05601i, 0.18549-0.05432i, 0.18644-0.05227i,...
    0.18783-0.04977i, 0.19362-0.04399i, 0.19803-0.04283i, 0.20177-0.04356i,...
    0.20491-0.04554i, 0.20742-0.04850i, 0.20918-0.05226i, 0.21005-0.05667i,...
    0.20981-0.06158i, 0.20818-0.06682i, 0.20470-0.07208i, 0.19842-0.07683i,...
    0.18578-0.07922i, 0.18394-0.07905i, 0.18029-0.07838i, 0.17853-0.07792i,...
    0.17297-0.07573i, 0.17461-0.07222i, 0.17567-0.07019i, 0.17766-0.06685i,...
    0.17910-0.06479i, 0.18106-0.06245i, 0.18273-0.06082i, 0.18934-0.05720i,...
    0.19458-0.05705i, 0.19893-0.05881i, 0.20243-0.06195i, 0.20499-0.06618i,...
    0.20646-0.07131i, 0.20660-0.07714i, 0.20510-0.08342i, 0.20153-0.08981i,...
    0.19513-0.09571i, 0.18421-0.09983i, 0.18106-0.10014i, 0.17732-0.10010i,...
    0.17261-0.09947i, 0.16549-0.09737i, 0.15748-0.09346i, 0.16296-0.08449i,...
    0.18364-0.07121i, 0.19509-0.07594i, 0.20141-0.08738i, 0.20061-0.10309i,...
    0.18877-0.11957i, 0.15531-0.12544i, 0.12975-0.11069i, 0.16474-0.08501i,...
    0.18445-0.08955i, 0.19643-0.10700i, 0.19601-0.13499i, 0.17081-0.16805i,...
    0.09195-0.17378i, 0.00249-0.00001i, 0.16521-0.06840i, 0.16754-0.12859i,...
    0.14185-0.14522i, 0.11856-0.14219i, 0.10255-0.12909i, 0.09533-0.10905i,...
    0.10873-0.07127i, 0.12437-0.08559i, 0.12882-0.10956i, 0.11930-0.11866i,...
    0.10786-0.11932i, 0.09798-0.11390i, 0.09170-0.10333i, 0.10015-0.07379i,...
    0.11418-0.09714i, 0.10888-0.10545i, 0.10097-0.10746i, 0.09337-0.10481i,...
    0.08770-0.09816i, 0.08654-0.08605i, 0.09382-0.07236i, 0.10432-0.08779i,...
    0.10168-0.09617i, 0.09575-0.09903i, 0.08949-0.09797i, 0.08432-0.09357i,...
    0.08184-0.08535i, 0.08828-0.07023i, 0.09619-0.07972i, 0.09596-0.08888i,...
    0.09145-0.09241i, 0.08615-0.09243i, 0.08141-0.08954i, 0.07840-0.08364i,...
    0.08403-0.06814i, 0.09111-0.08273i, 0.08777-0.08686i, 0.08325-0.08770i,...
    0.07071-0.07071i, 0.05774-0.05774i, 0.05000-0.05000i, 0.03536-0.03536i];
```

```
    %
kP8=[0.19305+0.00000i, 0.19319-0.00002i, 0.19358-0.00013i, 0.19416-0.00040i,...
    0.19489-0.00087i, 0.19570-0.00154i, 0.19655-0.00244i, 0.19740-0.00357i,...
    0.19790-0.00493i, 0.19857-0.00655i, 0.19906-0.00840i, 0.19928-0.01049i,...
    0.19913-0.01281i, 0.19841-0.01532i, 0.19674-0.01798i, 0.19392-0.02010i,...
    0.19270-0.02059i, 0.19130-0.02093i, 0.19027-0.02107i, 0.18954-0.02111i,...
    0.18742-0.02098i, 0.18767-0.01928i, 0.18783-0.01852i, 0.18808-0.01754i,...
    0.18841-0.01659i, 0.18936-0.01482i, 0.19144-0.01321i, 0.19334-0.01307i,...
    0.19507-0.01372i, 0.19660-0.01494i, 0.19790-0.01662i, 0.19889-0.01871i,...
    0.19950-0.02116i, 0.19961-0.02391i, 0.19906-0.02693i, 0.19755-0.03011i,...
    0.19443-0.03330i, 0.19088-0.03500i, 0.18896-0.03544i, 0.18732-0.03561i,...
    0.18571-0.03562i, 0.18440-0.03552i, 0.18240-0.03517i, 0.18277-0.03348i,...
    0.18311-0.03217i, 0.18337-0.03135i, 0.18379-0.03018i, 0.18433-0.02897i,...
    0.18658-0.02581i, 0.18948-0.02422i, 0.19201-0.02424i, 0.19423-0.02519i,...
    0.19611-0.02684i, 0.19759-0.02907i, 0.19860-0.03177i, 0.19902-0.03488i,...
    0.19869-0.03831i, 0.19737-0.04196i, 0.19460-0.04564i, 0.18914-0.04893i,...
    0.18505-0.04978i, 0.18316-0.04985i, 0.18145-0.04977i, 0.18027-0.04964i,...
    0.17652-0.04866i, 0.17725-0.04628i, 0.17776-0.04489i, 0.17846-0.04320i,...
    0.17952-0.04114i, 0.18405-0.03633i, 0.18756-0.03529i, 0.19057-0.03579i,...
    0.19312-0.03731i, 0.19517-0.03959i, 0.19665-0.04251i, 0.19745-0.04596i,...
    0.19741-0.04981i, 0.19630-0.05395i, 0.19377-0.05818i, 0.18907-0.06212i,...
    0.17930-0.06452i, 0.17785-0.06447i, 0.17495-0.06412i, 0.17355-0.06384i,...
    0.16905-0.06237i, 0.17019-0.05952i, 0.17094-0.05786i, 0.17238-0.05514i,...
    0.17344-0.05346i, 0.17490-0.05154i, 0.17616-0.05020i, 0.18123-0.04714i,...
    0.18530-0.04687i, 0.18871-0.04810i, 0.19149-0.05040i, 0.19357-0.05354i,...
    0.19486-0.05737i, 0.19517-0.06174i, 0.19431-0.06648i, 0.19194-0.07138i,...
    0.18751-0.07606i, 0.17967-0.07970i, 0.17736-0.08012i, 0.17459-0.08032i,...
    0.17105-0.08015i, 0.16561-0.07903i, 0.15933-0.07662i, 0.16292-0.06950i,...
    0.17772-0.05860i, 0.18620-0.06158i, 0.19109-0.06936i, 0.19130-0.08009i,...
    0.18447-0.09171i, 0.16319-0.09820i, 0.14487-0.09085i, 0.16625-0.07119i,...
    0.17858-0.07311i, 0.18598-0.08229i, 0.18729-0.09598i, 0.17948-0.11145i,...
    0.15614-0.12176i, 0.11945-0.10599i, 0.14579-0.08421i, 0.16704-0.08371i,...
    0.18055-0.09682i, 0.18425-0.12019i, 0.16906-0.15044i, 0.11450-0.17012i,...
    0.00297-0.00001i, 0.12356-0.03184i, 0.16321-0.11098i, 0.14138-0.13540i,...
    0.11813-0.13684i, 0.10101-0.12684i, 0.09168-0.10996i, 0.10306-0.06812i,...
    0.12400-0.09997i, 0.11682-0.11170i, 0.10611-0.11443i, 0.09616-0.11086i,...
    0.08906-0.10231i, 0.08775-0.08735i, 0.09634-0.07073i, 0.10948-0.08922i,...
    0.10632-0.09954i, 0.09916-0.10302i, 0.09170-0.10172i, 0.08566-0.09652i,...
    0.08284-0.08700i, 0.09010-0.06972i, 0.09928-0.08045i, 0.09909-0.09096i,...
    0.09394-0.09501i, 0.08792-0.09502i, 0.08260-0.09175i, 0.07927-0.08515i,...
    0.08544-0.06801i, 0.09337-0.08409i, 0.08969-0.08867i, 0.08471-0.08959i,...
    0.07071-0.07071i, 0.05774-0.05774i, 0.05000-0.05000i, 0.03536-0.03536i];
    %
kP9=[0.18272+0.00000i, 0.18283-0.00002i, 0.18316-0.00011i, 0.18366-0.00034i,...
    0.18427-0.00073i, 0.18495-0.00130i, 0.18567-0.00206i, 0.18639-0.00301i,...
    0.18674-0.00415i, 0.18731-0.00550i, 0.18773-0.00706i, 0.18793-0.00882i,...
    0.18781-0.01076i, 0.18722-0.01288i, 0.18584-0.01512i, 0.18349-0.01693i,...
    0.18246-0.01735i, 0.18129-0.01766i, 0.18043-0.01778i, 0.17981-0.01782i,...
    0.17802-0.01773i, 0.17822-0.01630i, 0.17834-0.01565i, 0.17855-0.01483i,...
    0.17882-0.01402i, 0.17960-0.01252i, 0.18135-0.01115i, 0.18294-0.01102i,...
    0.18440-0.01156i, 0.18569-0.01257i, 0.18679-0.01397i, 0.18764-0.01571i,...
    0.18817-0.01775i, 0.18829-0.02005i, 0.18787-0.02257i, 0.18665-0.02525i,...
    0.18409-0.02796i, 0.18115-0.02944i, 0.17955-0.02984i, 0.17818-0.03001i,...
    0.17683-0.03005i, 0.17573-0.02999i, 0.17404-0.02973i, 0.17432-0.02830i,...
    0.17459-0.02720i, 0.17479-0.02650i, 0.17513-0.02552i, 0.17556-0.02449i,...
    0.17741-0.02180i, 0.17982-0.02044i, 0.18193-0.02042i, 0.18380-0.02119i,...
    0.18538-0.02254i, 0.18664-0.02437i, 0.18752-0.02660i, 0.18791-0.02917i,...
    0.18770-0.03201i, 0.18668-0.03505i, 0.18447-0.03815i, 0.18003-0.04100i,...
    0.17666-0.04180i, 0.17510-0.04191i, 0.17367-0.04189i, 0.17268-0.04181i,...
    0.16954-0.04109i, 0.17009-0.03909i, 0.17047-0.03791i, 0.17103-0.03649i,...
    0.17186-0.03475i, 0.17553-0.03066i, 0.17843-0.02974i, 0.18092-0.03010i,...
    0.18305-0.03130i, 0.18477-0.03314i, 0.18604-0.03551i, 0.18676-0.03830i,...
    0.18682-0.04145i, 0.18602-0.04484i, 0.18408-0.04834i, 0.18037-0.05168i,...
    0.17250-0.05396i, 0.17131-0.05397i, 0.16893-0.05379i, 0.16777-0.05361i,...
    0.16403-0.05256i, 0.16487-0.05018i, 0.16543-0.04879i, 0.16652-0.04651i,...
    0.16735-0.04509i, 0.16849-0.04348i, 0.16949-0.04234i, 0.17355-0.03971i,...
    0.17686-0.03940i, 0.17965-0.04032i, 0.18194-0.04210i, 0.18369-0.04457i,...
    0.18482-0.04760i, 0.18519-0.05106i, 0.18465-0.05485i, 0.18295-0.05881i,...
    0.17962-0.06267i, 0.17359-0.06587i, 0.17178-0.06630i, 0.16960-0.06658i,...
    0.16678-0.06661i, 0.16240-0.06597i, 0.15727-0.06434i, 0.15982-0.05848i,...
    0.17121-0.04925i, 0.17794-0.05133i, 0.18197-0.05718i, 0.18253-0.06533i,...
    0.17791-0.07438i, 0.16233-0.08042i, 0.14798-0.07602i, 0.16319-0.05995i,...
    0.17238-0.06090i, 0.17804-0.06720i, 0.17956-0.07666i, 0.17515-0.08753i,...
```

```
    0.16050-0.09602i, 0.13462-0.08879i, 0.15085-0.07202i, 0.16441-0.07072i,...
    0.17276-0.07779i, 0.17578-0.08965i, 0.17113-0.10396i, 0.15425-0.11598i,...
    0.11127-0.10160i, 0.12724-0.08666i, 0.15185-0.07942i, 0.16660-0.08867i,...
    0.17329-0.10797i, 0.16535-0.13502i, 0.12773-0.15977i, 0.00001-0.00283i,...
    0.15686-0.09159i, 0.14126-0.12511i, 0.11847-0.13140i, 0.10042-0.12451i,...
    0.08938-0.11028i, 0.08780-0.08837i, 0.09912-0.06512i, 0.11864-0.09020i,...
    0.11456-0.10484i, 0.10478-0.10965i, 0.09488-0.10786i, 0.08720-0.10107i,...
    0.08380-0.08917i, 0.09243-0.06814i, 0.10386-0.08094i, 0.10381-0.09383i,...
    0.09757-0.09877i, 0.09035-0.09877i, 0.08407-0.09486i, 0.08025-0.08715i,...
    0.08722-0.06748i, 0.09652-0.08583i, 0.09231-0.09111i, 0.08662-0.09216i,...
    0.07071-0.07071i, 0.05774-0.05774i, 0.05000-0.05000i, 0.03536-0.03536i];
%
kP10=[0.17389+0.00000i, 0.17399-0.00001i, 0.17427-0.00010i, 0.17470-0.00029i,...
    0.17522-0.00063i, 0.17581-0.00111i, 0.17643-0.00176i, 0.17704-0.00258i,...
    0.17729-0.00356i, 0.17778-0.00471i, 0.17814-0.00604i, 0.17832-0.00754i,...
    0.17822-0.00921i, 0.17773-0.01102i, 0.17656-0.01295i, 0.17456-0.01451i,...
    0.17369-0.01488i, 0.17268-0.01515i, 0.17194-0.01527i, 0.17141-0.01531i,...
    0.16988-0.01525i, 0.17003-0.01401i, 0.17014-0.01346i, 0.17031-0.01275i,...
    0.17053-0.01205i, 0.17120-0.01076i, 0.17269-0.00958i, 0.17405-0.00946i,...
    0.17530-0.00991i, 0.17641-0.01076i, 0.17736-0.01196i, 0.17810-0.01343i,...
    0.17856-0.01517i, 0.17869-0.01713i, 0.17835-0.01928i, 0.17734-0.02158i,...
    0.17520-0.02392i, 0.17271-0.02522i, 0.17134-0.02558i, 0.17018-0.02574i,...
    0.16902-0.02580i, 0.16808-0.02576i, 0.16663-0.02557i, 0.16685-0.02434i,...
    0.16707-0.02339i, 0.16723-0.02279i, 0.16751-0.02194i, 0.16787-0.02106i,...
    0.16942-0.01874i, 0.17146-0.01755i, 0.17327-0.01751i, 0.17486-0.01815i,...
    0.17622-0.01929i, 0.17731-0.02082i, 0.17808-0.02270i, 0.17845-0.02487i,...
    0.17830-0.02728i, 0.17749-0.02987i, 0.17567-0.03253i, 0.17197-0.03502i,...
    0.16912-0.03577i, 0.16780-0.03589i, 0.16659-0.03590i, 0.16575-0.03585i,...
    0.16306-0.03531i, 0.16349-0.03359i, 0.16379-0.03258i, 0.16423-0.03136i,...
    0.16492-0.02987i, 0.16797-0.02633i, 0.17041-0.02550i, 0.17253-0.02578i,...
    0.17434-0.02676i, 0.17582-0.02829i, 0.17692-0.03025i, 0.17758-0.03259i,...
    0.17768-0.03522i, 0.17708-0.03808i, 0.17553-0.04105i, 0.17251-0.04393i,...
    0.16597-0.04605i, 0.16498-0.04609i, 0.16297-0.04600i, 0.16199-0.04588i,...
    0.15881-0.04510i, 0.15945-0.04307i, 0.15989-0.04188i, 0.16075-0.03993i,...
    0.16141-0.03872i, 0.16234-0.03733i, 0.16315-0.03635i, 0.16652-0.03406i,...
    0.16928-0.03373i, 0.17163-0.03445i, 0.17357-0.03589i, 0.17507-0.03790i,...
    0.17607-0.04038i, 0.17646-0.04323i, 0.17611-0.04637i, 0.17481-0.04966i,...
    0.17220-0.05293i, 0.16734-0.05576i, 0.16587-0.05617i, 0.16408-0.05648i,...
    0.16176-0.05660i, 0.15811-0.05624i, 0.15380-0.05508i, 0.15572-0.05011i,...
    0.16487-0.04215i, 0.17043-0.04369i, 0.17385-0.04833i, 0.17454-0.05487i,...
    0.17116-0.06227i, 0.15897-0.06775i, 0.14721-0.06488i, 0.15883-0.05130i,...
    0.16617-0.05177i, 0.17079-0.05652i, 0.17230-0.06377i, 0.16940-0.07224i,...
    0.15876-0.07942i, 0.13858-0.07549i, 0.15016-0.06170i, 0.16033-0.06018i,...
    0.16669-0.06505i, 0.16932-0.07332i, 0.16684-0.08339i, 0.15633-0.09255i,...
    0.12621-0.08654i, 0.13603-0.07494i, 0.15194-0.06886i, 0.16118-0.07389i,...
    0.16560-0.08402i, 0.16347-0.09713i, 0.15132-0.10970i, 0.10443-0.09836i,...
    0.13815-0.07657i, 0.15409-0.08216i, 0.16301-0.09783i, 0.16041-0.12161i,...
    0.13501-0.14749i, 0.05973-0.13837i, 0.00222-0.00001i, 0.14597-0.06940i,...
    0.14098-0.11397i, 0.11932-0.12569i, 0.10052-0.12204i, 0.08803-0.11027i,...
    0.08338-0.09219i, 0.09490-0.06264i, 0.11171-0.07977i, 0.11223-0.09801i,...
    0.10366-0.10494i, 0.09396-0.10489i, 0.08586-0.09972i, 0.08116-0.08995i,...
    0.08949-0.06591i, 0.10124-0.08810i, 0.09614-0.09459i, 0.08927-0.09585i,...
    0.07071-0.07071i, 0.05774-0.05774i, 0.05000-0.05000i, 0.03536-0.03536i];
%
kP11=[0.16624+0.00000i, 0.16633-0.00001i, 0.16657-0.00008i, 0.16694-0.00026i,...
    0.16740-0.00055i, 0.16791-0.00097i, 0.16845-0.00153i, 0.16898-0.00224i,...
    0.16914-0.00309i, 0.16957-0.00409i, 0.16988-0.00525i, 0.17004-0.00655i,...
    0.16997-0.00800i, 0.16954-0.00957i, 0.16854-0.01125i, 0.16681-0.01262i,...
    0.16605-0.01295i, 0.16518-0.01319i, 0.16454-0.01330i, 0.16408-0.01334i,...
    0.16274-0.01329i, 0.16287-0.01222i, 0.16296-0.01173i, 0.16310-0.01111i,...
    0.16329-0.01051i, 0.16387-0.00938i, 0.16515-0.00834i, 0.16634-0.00823i,...
    0.16743-0.00862i, 0.16840-0.00936i, 0.16922-0.01038i, 0.16987-0.01166i,...
    0.17029-0.01316i, 0.17040-0.01486i, 0.17013-0.01672i, 0.16928-0.01872i,...
    0.16745-0.02076i, 0.16530-0.02192i, 0.16412-0.02225i, 0.16311-0.02240i,...
    0.16211-0.02246i, 0.16129-0.02245i, 0.16003-0.02229i, 0.16021-0.02122i,...
    0.16039-0.02039i, 0.16052-0.01987i, 0.16076-0.01913i, 0.16106-0.01836i,...
    0.16238-0.01633i, 0.16415-0.01528i, 0.16571-0.01523i, 0.16709-0.01578i,...
    0.16828-0.01675i, 0.16924-0.01806i, 0.16992-0.01968i, 0.17025-0.02154i,...
    0.17016-0.02362i, 0.16949-0.02586i, 0.16796-0.02817i, 0.16481-0.03038i,...
    0.16237-0.03107i, 0.16123-0.03120i, 0.16018-0.03122i, 0.15945-0.03120i,...
    0.15712-0.03077i, 0.15746-0.02928i, 0.15771-0.02840i, 0.15807-0.02734i,...
    0.15864-0.02603i, 0.16123-0.02293i, 0.16333-0.02219i, 0.16516-0.02240i,...
    0.16673-0.02323i, 0.16802-0.02452i, 0.16899-0.02619i, 0.16958-0.02818i,...
```

```
    0.16971-0.03043i, 0.16924-0.03288i, 0.16797-0.03545i, 0.16545-0.03797i,...
    0.15990-0.03992i, 0.15905-0.03997i, 0.15733-0.03994i, 0.15648-0.03986i,...
    0.15373-0.03927i, 0.15424-0.03750i, 0.15459-0.03647i, 0.15529-0.03478i,...
    0.15584-0.03372i, 0.15660-0.03251i, 0.15729-0.03166i, 0.16013-0.02963i,...
    0.16249-0.02931i, 0.16451-0.02988i, 0.16618-0.03108i, 0.16749-0.03277i,...
    0.16838-0.03485i, 0.16877-0.03726i, 0.16853-0.03991i, 0.16751-0.04273i,...
    0.16538-0.04555i, 0.16135-0.04806i, 0.16012-0.04845i, 0.15862-0.04876i,...
    0.15666-0.04893i, 0.15355-0.04873i, 0.14985-0.04787i, 0.15135-0.04359i,...
    0.15893-0.03662i, 0.16365-0.03780i, 0.16661-0.04161i, 0.16734-0.04705i,...
    0.16474-0.05328i, 0.15481-0.05823i, 0.14489-0.05626i, 0.15417-0.04454i,...
    0.16026-0.04475i, 0.16418-0.04853i, 0.16561-0.05438i, 0.16354-0.06132i,...
    0.15527-0.06752i, 0.13873-0.06525i, 0.14760-0.05354i, 0.15575-0.05200i,...
    0.16094-0.05566i, 0.16326-0.06203i, 0.16175-0.06989i, 0.15417-0.07739i,...
    0.13068-0.07454i, 0.13766-0.06496i, 0.14959-0.05963i, 0.15664-0.06304i,...
    0.16021-0.07017i, 0.15933-0.07942i, 0.15183-0.08868i, 0.11912-0.08483i,...
    0.14064-0.06766i, 0.15081-0.07057i, 0.15642-0.07906i, 0.15635-0.09092i,...
    0.14786-0.10342i, 0.12470-0.10906i, 0.09854-0.09439i, 0.12535-0.07520i,...
    0.14268-0.07703i, 0.15332-0.08941i, 0.15470-0.11000i, 0.13833-0.13510i,...
    0.08485-0.14510i, 0.00000-0.00140i, 0.12463-0.04270i, 0.14002-0.10151i,...
    0.12052-0.11945i, 0.10124-0.11931i, 0.08747-0.10993i, 0.08064-0.09456i,...
    0.09189-0.06050i, 0.10964-0.09100i, 0.10267-0.10017i, 0.09334-0.10187i,...
    0.07071-0.07071i, 0.05774-0.05774i, 0.05000-0.05000i, 0.03536-0.03536i];
%
kP12=[0.15952+0.00000i, 0.15960-0.00001i, 0.15981-0.00007i, 0.16014-0.00022i,...
    0.16054-0.00048i, 0.16099-0.00085i, 0.16147-0.00135i, 0.16194-0.00197i,...
    0.16202-0.00272i, 0.16240-0.00360i, 0.16268-0.00461i, 0.16282-0.00576i,...
    0.16276-0.00703i, 0.16239-0.00841i, 0.16151-0.00990i, 0.16000-0.01111i,...
    0.15934-0.01140i, 0.15857-0.01162i, 0.15801-0.01172i, 0.15760-0.01175i,...
    0.15642-0.01172i, 0.15653-0.01078i, 0.15660-0.01035i, 0.15673-0.00980i,...
    0.15689-0.00927i, 0.15739-0.00827i, 0.15852-0.00735i, 0.15957-0.00725i,...
    0.16052-0.00758i, 0.16138-0.00823i, 0.16211-0.00913i, 0.16268-0.01025i,...
    0.16305-0.01156i, 0.16317-0.01305i, 0.16294-0.01468i, 0.16221-0.01644i,...
    0.16062-0.01825i, 0.15875-0.01928i, 0.15772-0.01958i, 0.15683-0.01973i,...
    0.15595-0.01979i, 0.15523-0.01979i, 0.15412-0.01966i, 0.15427-0.01872i,...
    0.15441-0.01799i, 0.15453-0.01753i, 0.15473-0.01687i, 0.15499-0.01619i,...
    0.15614-0.01440i, 0.15768-0.01346i, 0.15905-0.01341i, 0.16027-0.01388i,...
    0.16131-0.01472i, 0.16216-0.01586i, 0.16277-0.01727i, 0.16308-0.01890i,...
    0.16302-0.02071i, 0.16246-0.02267i, 0.16115-0.02472i, 0.15842-0.02668i,...
    0.15630-0.02732i, 0.15530-0.02745i, 0.15438-0.02749i, 0.15375-0.02748i,...
    0.15169-0.02714i, 0.15197-0.02582i, 0.15218-0.02505i, 0.15248-0.02411i,...
    0.15297-0.02296i, 0.15520-0.02021i, 0.15703-0.01954i, 0.15863-0.01971i,...
    0.16001-0.02041i, 0.16115-0.02152i, 0.16201-0.02297i, 0.16255-0.02469i,...
    0.16269-0.02665i, 0.16232-0.02878i, 0.16125-0.03103i, 0.15910-0.03326i,...
    0.15431-0.03505i, 0.15357-0.03512i, 0.15207-0.03512i, 0.15133-0.03507i,...
    0.14892-0.03460i, 0.14933-0.03305i, 0.14962-0.03214i, 0.15020-0.03065i,...
    0.15066-0.02972i, 0.15131-0.02865i, 0.15190-0.02790i, 0.15435-0.02609i,...
    0.15640-0.02578i, 0.15815-0.02625i, 0.15962-0.02727i, 0.16078-0.02871i,...
    0.16157-0.03049i, 0.16194-0.03256i, 0.16179-0.03486i, 0.16096-0.03730i,...
    0.15918-0.03977i, 0.15577-0.04202i, 0.15471-0.04239i, 0.15342-0.04269i,...
    0.15174-0.04288i, 0.14905-0.04278i, 0.14582-0.04212i, 0.14702-0.03838i,...
    0.15344-0.03220i, 0.15752-0.03314i, 0.16013-0.03635i, 0.16086-0.04097i,...
    0.15879-0.04634i, 0.15046-0.05082i, 0.14193-0.04943i, 0.14957-0.03916i,...
    0.15475-0.03920i, 0.15814-0.04231i, 0.15948-0.04720i, 0.15794-0.05306i,...
    0.15123-0.05849i, 0.13727-0.05719i, 0.14436-0.04703i, 0.15113-0.04552i,...
    0.15552-0.04842i, 0.15761-0.05359i, 0.15663-0.06005i, 0.15076-0.06641i,...
    0.13149-0.06513i, 0.13681-0.05696i, 0.14635-0.05221i, 0.15210-0.05473i,...
    0.15515-0.06025i, 0.15480-0.06748i, 0.14944-0.07495i, 0.12394-0.07383i,...
    0.13980-0.05940i, 0.14758-0.06124i, 0.15199-0.06725i, 0.15243-0.07566i,...
    0.14727-0.08474i, 0.13204-0.09019i, 0.11286-0.08243i, 0.13010-0.06731i,...
    0.14137-0.06783i, 0.14802-0.07471i, 0.14964-0.08530i, 0.14410-0.09738i,...
    0.12708-0.10594i, 0.09345-0.09167i, 0.11256-0.07582i, 0.13211-0.07312i,...
    0.14415-0.08244i, 0.14854-0.10000i, 0.13895-0.12338i, 0.10099-0.14128i,...
    0.00256-0.00001i, 0.13763-0.08704i, 0.12202-0.11226i, 0.10265-0.11602i,...
    0.07071-0.07071i, 0.05774-0.05774i, 0.05000-0.05000i, 0.03536-0.03536i];
%
kP = [kP0; kP1; kP2; kP3;  kP4;  kP5; kP6;...
      kP7; kP8; kP9; kP10; kP11; kP12];
%
kPP = zeros(Nterms, length(ka_array));
% ==================================
% %  Linear-Interpolation VERSION
% %  Simple linear interpolation in the table isn't too bad in practice
% %  even though the kPP samples aren't very smooth
```

```
% for ii = 1:Nterms
%  kPP(ii, :)  = interp1(ka_int, kP(ii, :),  ka_array);
% end
% %  END Linear-Interpolation VERSION
% ================================
%  VERSION WITH CURVE-FIT INTERPOLATION
%  This version uses curve-fit interpolation and produces smoother
%  sampling of the kPP function. The curve-fit interpolation is
%  complicated by the fact that the kPP functions have "kinks" in
%  the vicinity of zeros of J1. Consequently, the interpolation
%  is performed section by section where each section is bounded
%  by two adjacent zeros of J1
%
%  If there are ka values > 100, do them separately by linear
%  interpolation
nka_lessthan_100 = sum(ka_array < 100);
ka_array_lt = ka_array(1:nka_lessthan_100);
%  Find index values for interval breakpoints for table values and for
%  input values
ntable(1) = 1;  ninput(1) = 1;
for ii = 2:length(jom)
    ntable(ii) = sum(ka_int < jom(ii) + 0.0001);
    if sum(ka_array_lt < jom(ii)) == 0;
        ninput(ii) = 1;
    else
        ninput(ii) = sum(ka_array_lt < jom(ii));
    end
end
%
%  Determine the intervals required based on span of input ka vector
m_lower_interval = sum(jom <= min(ka_array_lt));
m_upper_interval = sum(jom <  max(ka_array_lt));
%
ninput(m_lower_interval) = ninput(m_lower_interval) - 1;
%
for ii = m_lower_interval:m_upper_interval
    m_ka_int = ntable(ii):ntable(ii+1);
    m_ka_arr = (ninput(ii)+1):ninput(ii+1);
    %  Perform the table interpolation. Note:  'spline' interpolation tends
    %  to overshoot too much; 'pchip' is better in that regard.
    for jj = 1:Nterms
        kPP(jj, m_ka_arr) = interp1(ka_int(m_ka_int), kP(jj, m_ka_int),...
            ka_array_lt(m_ka_arr), 'pchip');
    end
end
%
%  If there are values of ka > 100, do those by linear interpolation here
if nka_lessthan_100 < length(ka_array)
    nnka = (nka_lessthan_100 + 1):length(ka_array);
    for jj = 1:Nterms
        kPP(jj, nnka) = interp1(ka_int((end-1):end), kP(jj, (end-1):end),...
            ka_array(nnka), 'linear');
    end
end
%
% END Curve-fit VERSION
%=================================================================
```

Appendix K: Frequency-Domain Filter for Diffraction Correction of a Pressure Microphone Used in the Zero-Degree Orientation

```
function filtered_signal =...
    frequency_domain_diffraction_filter(signal, fs, mic_diameter_inches)
%
%  This function filters the input signal to remove the effects of
%  zero-degree-incidence diffraction. The filter function is computed
%  from the "exact" diffraction solution and is applied in the frequency
%  domain. The sampling frequency, fs, and the microphone diameter must
%  be specified.
%
%  USAGE:  filt_sig = frequency_domain_diffraction_filter(sig, fs, D_inches);
%
%  This function requires the m-function, Jones_diffraction_function.
%
%  Author: T. Gabrielson, Applied Research Lab - Penn State
%  tbg3@psu.edu
%
dt = 1/fs;
%
%  Set up frequency-domain parameters
c_air = 345;  %  sound-speed in air [meters per second]
%  Microphone radius in meters
mic_a_meters = (mic_diameter_inches/2)*25.4e-3;
%  Frequency at which ka  =  1:
f_ka_1 = c_air/(2*pi*mic_a_meters);
%  Signal parameters and frequencies of the linear spectrum of the signal
NN = length(signal);  TT = NN*dt;  df = 1/TT;
nfreqs = 1 + NN/2;
ffrqs  = ((1:nfreqs) - 1)*df;
ffrqs(1)  =  df/1000;
%  Generate the normalized-frequency vector
ka_array = ffrqs/f_ka_1;
%  Calculate the diffraction response using default values acceptable for
% condenser microphones
diff_fn = Jones_diffraction_function(ka_array, 0.85, 4);
%  Generate the inverse filter (frequency domain)
diff_fn = (1./diff_fn).';
%  Find the linear spectrum of the input signal
specsig = ffttime(signal)*dt;
%  Apply inverse filter to spectrum of pulse
modspecsig = (specsig.*diff_fn).';
%  Transform the result back to the time domain
filtered_signal = iffthalf(modspecsig)/dt;
```

Appendix L: Time-Domain Filter Coefficients for Diffraction Correction of a Pressure Microphone Used in the Zero-Degree Orientation

```
function [bb, aa] = Time_domain_diffraction_filter(mic_diameter_inches, fs, QB)
%
%  This function generates time-domain filter coefficients for a filter
%  that removes the effects of microphone diffraction for a microphone
%  oriented at zero degrees to the incoming wave. The sampling frequency,
%  fs, and the microphone diameter must be specified.
%
%  USAGE:  [bb, aa] = Time_domain_diffraction_filter(mic_diameter_inches, fs);
%  corr_wave = filter(bb, aa, uncorr_wave);
%
%  QB is an optional input. It defaults to 1.0, but can be changed to
%  modify the sharpness of the diffraction peak.
%
%  This function requires an m-function for implementation of the
%  bilinear transformation. 'bilinear_xform' is referenced here, which is
%  a custom routine that is appended to this function. The 'bilinear'
%  m-function in the MatLab Signal Processing Toolbox will also work.
%
%  Author: T. Gabrielson, Applied Research Lab - Penn State
%  tbg3@psu.edu
%
if nargin < 3; QB = 1.0; end
%
c_air = 345;  %  sound-speed in air [meters per second]
%  Microphone radius in meters
mic_a_meters = (mic_diameter_inches/2)*25.4e-3;
%  Frequency at which ka  =  1:
f_ka_1 = c_air/(2*pi*mic_a_meters);
%
fmid = 1.0*f_ka_1;
%
fpk = 2.5*f_ka_1;
%
if (fpk*1.05) > (fs/2)
    warning(' Filter may be erratic; sampling rate is too low');
end
A2 = 0.5;
%
%  Set up numerator and denominator polynomials in s ( = j*omega) for
%  first and second factors in response approximation.
%
%  First-stage response (with pre-warped frequencies)
fmid_warped = tan(fmid*pi/fs)/(pi/fs);
f1_warped = fmid_warped/sqrt(2);  f2_warped = 2*f1_warped;
w1 = 2*pi*f1_warped;  w2 = 2*pi*f2_warped;
A1 = w2/w1;
densA = [1, w1]*A1;
numsA = [1, w2];
%
%  Second-stage response (with pre-warped frequencies)
w0 = 2*pi*tan(fpk*pi/fs)/(pi/fs);
densB = [(1/w0)^2, (1 + A2)/(QB*w0), 1];
numsB = [(1/w0)^2, 1/(QB*w0), 1];
%
%  Combine the stages
dens = conv(densA, densB);
nums = conv(numsA, numsB);
%
%  Convert from s-domain to filter coefficients (z-domain)
[bb, aa] = bilinear_xform(nums, dens, fs);
%
```

```
%=========================================================
%
function [numz, denz] = bilinear_xform(nums, dens, fs);
%  This routine performs a bilinear transformation from the s-domain
%  expression given by the numerator, nums, and denominator, dens, polynomial
%  coefficient vectors (in order from highest power of s to the constant)
%  to the z-domain expression given by the numerator, bb, and denominator,
%  aa, polynomial coefficient vectors (in order from constant to highest
%  power of z^-1) for the specified sampling rate, fs. The coefficient
%  orders are chosen to conform to the MatLab conventions.
%
%  Typical usage:
%
%  [bb, aa] = bilinear_xform(nums, dens, fs);
%
%  This bilinear transformation produces results equivalent to the MatLab
%  Signal-Processing-Toolbox routine 'bilinear' when that routine is used
%  in the transfer function mode. However, bilinear_xform does not first convert
%  to state-space as does 'bilinear'; this routine uses the more conventional
%  (though perhaps less efficient) direct transformation.
%
%  In typical use, this routine would be used to find the coefficients for
%  a time-domain filter:
%
%  [bb,aa] = bilinear_xform(nums, dens, fs);
%  yfiltered = filter(bb,aa,yunfiltered);
%
[dc, nn] = size(nums);
%  Check dimensions and force into row vectors
if dc ~= 1
    nums = nums.';  nn = dc;
end
[dc, mm] = size(dens);
if dc ~= 1
    dens = dens.';  mm = dc;
end
%
%  Check for proper relative order of numerator compared to denominator
if nn > mm
    error(' Order of numerator cannot exceed order of denominator')
end
%
%  Zero fill numerator, if necessary, to make it the same length as the
%  denominator vector. This is done simply to save some logic in the code
%  below.
if nn < mm
    padz = zeros(1,(mm-nn));  nums = [padz,nums];
end
%
%  The bilinear transformation is produced by taking the response
%  expression in the s-domain and replacing s with the quantity,
%  (2*fs)*(1 - z^-1)/(1 + z^-1). Here, fs is the sampling rate
%  (inexplicably written as 1/T in most texts) and z^-1 is
%
%  z^-1  =  exp(-j*pi*f/fs)
%
%  When this substitution is made, the numerator and denominator are no
%  longer proper polynomials (in z^-1). Multiply numerator and denominator
%  by (1 + z^-1)^m (where m is the highest power of s in the original
%  denominator) to put them into a form that can be simplified to
%  coefficients of ascending powers of z^-1. (In this code, m would be
%  mm - 1.)
%
%  The key to understanding the code below is that, after the substitution
%  of (2*fs)*(1 - z^-1)/(1 + z^-1) for s and the subsequent multiplication
%  by (1 + z^-1)^m, every term has the form of ((1 + z^-1)^ma)*((1 - z^-1)^mb)
%  where ma+mb = m. So the roots of the resulting polynomial (for that
%  particular term) are ma negative ones and mb positive ones.
%
%  Set up polynomial root vector, initially to all negative ones; note
% that the order is mm-1:  mm is the number of terms in the original vector
% of the denominator polynomial in the s-domain; if that polynomial were
% second order (a quadratic), then mm would be 3 and m, the order notation
```

```
% used above, would be 2.
rootv = - ones(1,mm-1);
%  Set up accumulators for numerator and denominator coefficients
numz = zeros(1,mm) ; denz = numz;
%  Initialize leading factor
fsfact = 1;
%
%  Develop polynomial coefficients term by term. Note that in MatLab, the
%  assumed order for values in polynomial coefficient vectors in the
%  s-domain is in decreasing powers of s while the assumed order for values
%  in polynomial coefficient vectors in the z-domain is in increasing
%  powers of z^-1. This accounts for the reversed indexing between nums
%  and numz or between dens and denz. The MatLab order is preserved so
%  that this routine is compatible with other MatLab routines.
for ii=1:mm
    basepoly = poly(rootv)*fsfact;
    numz = numz + basepoly*nums(mm-ii+1);  %  (nums values stored in opposite or-
der)
    denz = denz + basepoly*dens(mm-ii+1);  %  (dens values stored in opposite or-
der)
    %  Modify fsfact and rootv except on final pass through loop
    if ii<mm
        fsfact = fsfact*2*fs;
        rootv(ii) = rootv(ii) + 2;  % Add 2 to change -1 to +1
    end
end
%
%  Normalize coefficients (not necessary, but done for compatibility with
%  other MatLab routines)
numz = numz/denz(1); denz = denz/denz(1);
```

REPORT DOCUMENTATION PAGE

Form Approved
OMB No. 0704-0188

1. REPORT DATE (DD-MM-YYYY)	2. REPORT TYPE	3. DATES COVERED (From - To)
07/02/2018	Final	

4. TITLE AND SUBTITLE
Measurement of Blast Waveforms with Condenser Microphones: Measurement Interpretation and Correction

5a. CONTRACT NUMBER
W9132T-07-2-0011.

5b. GRANT NUMBER

5c. PROGRAM ELEMENT

6. AUTHOR(S)
Thomas B. Gabrielson

5d. PROJECT NUMBER
622720D048

5e. TASK NUMBER

5f. WORK UNIT NUMBER

7. PERFORMING ORGANIZATION NAME(S) AND ADDRESS(ES)
U.S. Army Engineer Research and Development Center (ERDC)
Construction Engineering Research Laboratory (CERL)
PO Box 9005,
Champaign, IL 61826-9005

8. PERFORMING ORGANIZATION REPORT NUMBER
ERDC/CERL CR-18-2

9. SPONSORING / MONITORING AGENCY NAME(S) AND ADDRESS(ES)
U.S. Army Public Health Command (USAPHC)
5158 Blackhawk Rd
Aberdeen Proving Ground (APG), MD 21010-5403

10. SPONSOR/MONITOR'S ACRONYM(S)
MCHB-IP-EON

11. SPONSOR/MONITOR'S REPORT NUMBER(S)

12. DISTRIBUTION / AVAILABILITY STATEMENT
Approved for public release; distribution is unlimited.

13. SUPPLEMENTARY NOTES

14. ABSTRACT

This work evaluated the accuracy of blast-wave measurements using commercial measurement-grade condenser microphones. The principal advantages of measurement microphones are their ease of calibration and wide acceptance as measurement standards in acoustics. A number of special techniques are discussed for improving the results obtained with these microphones. Of particular importance are: (1) the desired resolutions for the measured parameters (peak pressure, rise time, time to zero-crossing, peak under-pressure); (2) the sensors and data-acquisition equipment used; (3) post-measurement corrections and digital correction filters; and, (4) laboratory evaluation compared to field measurements.

15. SUBJECT TERMS
Scientific apparatus and instruments--Evaluation, Electrostatic microphone, Sound, Detonation waves, Blast effect

16. SECURITY CLASSIFICATION OF:			17. LIMITATION OF ABSTRACT	18. NUMBER OF PAGES	19a. NAME OF RESPONSIBLE PERSON
a. REPORT	b. ABSTRACT	c. THIS PAGE			19b. TELEPHONE NUMBER (include area code)
Unclassified	Unclassified	Unclassified	SAR	126	